/
Article / Book Information

( )	
Title(English)	Passivity-based Visual Feedback Pose Synchronization in Three Dimensions
( )	
Author(English)	Tatsuya Ibuki
( )	: ( ), : , : 9286 , :2013 9 25 , : , : , , , ,
Citation(English)	Degree:Doctor (Engineering), Conferring organization: Tokyo Institute of Technology, Report number: 9286 , Conferred date:2013/9/25, Degree Type:Course doctor, Examiner:,,,,
( )	
Type(English)	Doctoral Thesis

Doctoral Dissertation

Passivity-based Visual Feedback Pose Synchronization in Three Dimensions

Advisor: Professor Masayuki Fujita
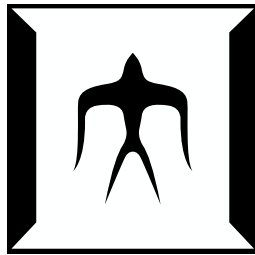
Tokyo Institute of Technology

Graduate School of Science and Engineering

Department of Mechanical and Control Engineering

Tatsuya Ibuki

September, 2013

Abstract

This dissertation investigates visual feedback attitude/pose synchronization on the Special Euclidean group $SE(3)$ for a group of rigid bodies equipped with vision sensors. The objective of attitude synchronization is to lead orientations of all the bodies with the same linear body velocity to a common value. Therefore, all the bodies move in the same direction when attitude synchronization is achieved. On the other hand, the goal of pose synchronization is to drive orientations and virtual positions to common values. Here, a virtual position is the position with a desired position bias to guarantee collision avoidance and visibility to neighbor bodies when synchronization is achieved.

We first introduce a notion of visual robotic networks to be controlled throughout this work. Visual robotic networks consist of multiple rigid bodies with kinematic models, visibility structures representing visual information flows between bodies and measured output, called visual measurements, extracted by monocular cameras which bodies equip. We next define visual feedback attitude/pose synchronization as the goals of this work. The definitions require each body to utilize only visual measurements for the implementation of control laws in addition to achieve synchronization, which is the main feature of this work. We then propose visual feedback attitude/pose synchronization laws consisting of vision-based observers to estimate relative poses of visible bodies and relative pose information-based synchronization laws. Here, passivity of the kinematic models plays a central role for the design of the present estimation and control mechanisms.

We next give convergence and performance analysis for the visual robotic network with the present estimation and control schemes. In the analysis, we focus mainly on leader-following visibility structures. It is first shown via Lyapunov methods that the present laws achieve visual feedback attitude/pose synchronization under leader-following type visibility structures. Then, for the leader moving independently, we analyze the tracking performance of the network by employing the theory of input-to-state stability or input-to-output stability. Here, we regard the individual velocity of the leader as an external disturbance to the network and evaluate the total estimation and control errors in the network.

We also give some further developments on visual feedback attitude/pose synchronization in regard to (i) linear velocity observers for visual feedback attitude synchronization, (ii) ring-type visibility structures which does not require the existence of a leader, (iii) extension from velocity laws to force and torque ones by integrating Newton-Euler equations as rigid body dynamics, and (iv) collision avoidance and visibility maintenance. The effectiveness and validity of the present estimation and control strategies and the convergence and performance analysis are demonstrated through simulation in three dimensions and experiments on a planar testbed.

Acknowledgment

I would like to express sincere gratitude to my advisor, Masayuki Fujita, whose experience and motivation were instrumental for this dissertation. As an advisor, he provided guidance in my research and encouragement in developing my own ideas. The international cultures he has introduced to our laboratory has encouraged and facilitated my learning. Also, I would like to thank him for giving me many chances to work in a professional environment by exposing me to various professional activities such as journal/conference reviews, proposal writing, teaching classroom lectures, societal outreach activity, etc. I feel fortunate to have had the opportunity to work with him and would like to thank him for all the technical as well as non-technical knowledge he has given me.

I am deeply indebted Takeshi Hatanaka for his suggestions and technical discussions during various occasions over my graduate school career. Co-work with him greatly improved my writing and presentation skills. Also, I received not only a training about technical matters but also a training on questioning each and every step. This has played a crucial role for the technical development in this dissertation.

I would also like to thank the secretary of our laboratory, Yoko Nishiyama, my co-workers, and friends for their support and encouragement. Thanks to her various support, I have got everything done all right. Technical discussions with my co-workers have helped me learn and understand the subject in detail, and I had a lot of great help for conducting various experiments. Also, I appreciate my friends for giving me a fun life.

Finally, I would like to thank my parents for their love and support, and my brother for his support to my higher education.

Contents

iii

List of Figures

Chapter 1

Introduction

1.1 Motivation

Large-scale persistent *environmental monitoring* has been an urgent need due to recent serious natural disasters including earthquakes, tsunamis, nuclear meltdowns, hurricanes, floods, large forest fires, volcanic eruptions or oil spills [1, 2]. In fact, the Great East Japan Earthquake has wreaked severe damage to Japan on March 11th, 2011, and the radioactive contamination caused by the damage of nuclear power plants threatens health of organism. The objective of the environmental monitoring is to reveal and understand the states of the environment. However, it is hard for existing technologies using static sensors to monitor them efficiently since such damage spreads through a wide area and the measurement in general requires a large amount of sensing data.

For these kinds of issues, a solution to efficient data collection is a new technology called *mobile sensor network*, and a large amount of research works have been devoted to mobile sensor networks [3, 4, 5, 6]. The networks consist of collections of interconnected multiple mobile sensors with appropriate data processing and sampling techniques. Therefore, this technique has potential advantages in performances and robustness against sensor failures especially in dynamical environments. In practice, each mobile sensor is often required to behave cooperatively each other by using only limited information so that the group achieves specified behavior.

Cooperative control [7, 8, 9] gives fundamentals to meet the requirement of mobile sensor networks. Early works of cooperative control are motivated by scientific interests in cooperative behavior in nature like flocking of birds [10, 11, 12] and schooling of fish [13, 14]. Its objective is to design a distributed control strategy using only local information so that the aggregate system achieves specified behavior such as *consensus* [15, 16], *flocking* [10, 11, 12, 17, 18, 19, 20], *synchronization* [21, 22], *coordination* [23, 24, 25, 26, 27, 28] or *coverage* [29, 30]. In cooperative control problems, two distinctly different approaches have emerged. One is to employ an agent taking on *leader* roles, and the other is to handle the case that all the agent are fully autonomous. We focus mainly on the former case in

this dissertation. Among such cooperative behavior, control problems for mobile sensor networks have been formulated as two dimensional (2D) or three dimensional (3D) pose (position and attitude) coordination problems [3, 4, 5, 6].

In the stage of implementation, it is unavoidable to consider how to acquire necessary information for cooperative control laws. In multi-agent systems, agents might be capable of communicating with neighbor agents, where measurements on global information might be assumed, or measuring relative information with respect to neighbors via relative sensors without communication. This dissertation addresses the latter scenario for ease of implementation and cost reduction. In such situations, it would be useful for agents to estimate their necessary information from relative measurements [31]. Among relative sensors, a *vision sensor* brings rich information including 3D poses of other agents compressed into 2D image plane [32]. A vision sensor is also a powerful tool to grasp what is going on in the environment [33, 34]. Furthermore, vision is considered to play a central role in cooperative behavior in nature [35]. Due to this nature, we use only vision as a tool to obtain necessary information for control strategies.

Numerous research works have been devoted to fusion of control theory and computer vision so-called *visual feedback control* or *visual servoing* [36, 37]. Whereas early works are mainly motivated by robot control as in [38], the motivating scenarios of the integration have currently spread over the robotic systems into security and surveillance systems [39], medical imaging procedures [40] and even understanding biological perceptual processing [41]. Furthermore, a lot of researchers have recently gained attention to *visual feedback cooperative control* not only for implementation of motion coordination but also for camera/visual sensor networks to monitor environments [39, 42, 43]. Visual feedback control is generally classified as *image-based* or *position-based* control [36, 37]. In image-based control, 2D visual information is directly fedback, which might reduce the degree of freedom to be controlled and have difficulties in convergence analysis such as existence of local minima or singularities. On the other hand, position-based control requires feedback of a 3D target object pose relative to a vision camera. Therefore, it is often necessary for a vision camera to estimate the relative pose from visual information, which makes convergence analysis hard and the analysis for cooperative control much more difficult. Due to this nature, not a few works propose only control schemes without theoretical guarantees and experimental verifications, or tackle estimation and control problems separately. In this dissertation, we propose a novel pose estimation mechanism for cooperative control laws based on [44, 45] and give convergence and performance analysis for the integrated systems.

1.2   Problem Statement and Overview

In view of the motivation, this dissertation studies *visual feedback attitude/pose synchronization* on the Special Euclidean group $SE(3)$ for a group of rigid bodies equipped with
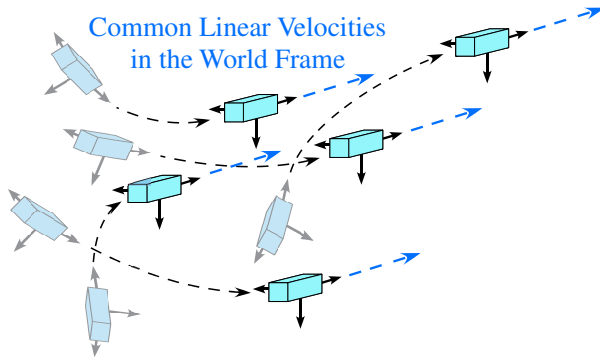
Figure 1.1: Attitude Synchronization   Figure 1.2: Pose Synchronization
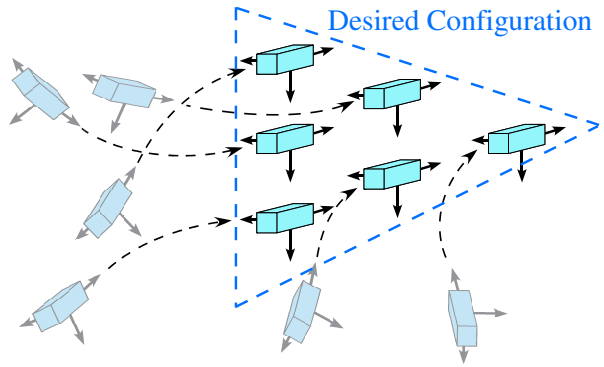
vision sensors. The objective of *attitude synchronization* is to drive the orientations of all the bodies with the same linear body velocity to a common value. Therefore, all the bodies move in the same direction when attitude synchronization is achieved (see Fig. 1.1). On the other hand, the goal of *pose synchronization* is to lead orientations and virtual positions of all the bodies to common values. Here, a virtual position is the position with a desired position bias to guarantee collision avoidance and visibility to neighbor bodies when synchronization is achieved (see Fig. 1.2). Although we have already proposed relative pose information-based attitude/pose synchronization laws in [46, 47, 48], the way to obtain relative poses of neighbor bodies necessary for the present laws has not been mentioned. Thus, in this dissertation, we newly propose visual feedback attitude/pose synchronization laws using only visual measurements extracted by a monocular camera and prove that the present estimation and control mechanisms achieve the same goals as in [46, 47, 48] under leader-following type or ring-type interconnection topologies between bodies. Moreover, we show that even if the leader moves independently in leader-following type rigid body networks, the present laws work successfully and flocking-like behavior is achieved.

We first introduce a notion of *visual robotic networks* to be controlled throughout this dissertation. Here, visual robotic networks consist of multiple rigid bodies with kinematic models called *rigid body motion*, *visibility structures* representing visual information flows between bodies and measured output, called *visual measurements*, extracted by monocular cameras which bodies equip. Then, the visual robotic network becomes the robotic network [7] regarding interconnection topologies between bodies as visibility structures and adding explicit formulation of measured output. This setting enables each body to be fully autonomous. We next define visual feedback attitude/pose synchronization as the goals of this work. The definitions require each body to utilize only visual measurements for control laws in addition to those in [46, 47, 48]. We then propose visual feedback attitude/pose synchronization laws consisting of visual feedback observers based on [44, 45]

3

and the synchronization laws presented in [46, 47, 48]. Here, *passivity* of rigid body motion plays crucial roles for the design of the present estimation and control strategies.

We next give convergence and performance analysis for the visual robotic network with the present estimation and control schemes. In the analysis, we focus mainly on leader-following visibility structures. We first prove via *Lyapunov methods* that the present protocols achieve attitude/pose synchronization under leader-following type visibility structures, where passivity of rigid body motion also plays a central role. However, in the present control scheme, the leader does not rotate/move, and as a result, the network cannot rotate/move after attitude/pose synchronization. In order to overcome these issues, we next consider the case that the leader rotates/moves independently. In this situation, we analyze the tracking performance of the network for the leader by employing the theory of *input-to-state stability* and *input-to-output stability* [49, 50, 51]. Here, we regard the individual velocity of the leader as an external disturbance to the network and evaluate the total estimation and control errors in the network.

We moreover give some further developments on visual feedback attitude/pose synchronization in regard to (i) linear velocity observers for attitude synchronization, (ii) ring-type visibility structures which does not require the existence of a leader, (iii) consideration of rigid body dynamics, i.e. extension from velocity laws to force and torque ones, and (iv) *visibility maintenance* and *collision avoidance*. The effectiveness and validity of the present estimation and control schemes and the convergence and performance analysis are demonstrated through simulation in three dimensions and experiments on a planar testbed.

1.3 Literature Review

Attitude/Pose Synchronization

Synchronization on the Special Orthogonal group $SO(3)$ or $SE(3)$ is investigated in [8, 24, 46, 47, 48, 52, 53, 54, 55, 56, 57]. Here, the papers [46, 47, 48, 52] handle kinematic models of rigid body motion, [8, 24, 53, 54, 55] consider attitude dynamics represented by Euler-Lagrange equations, and [56, 57] deal with general Lagrangian systems. [8, 52] propose attitude synchronization laws on $SO(3)$ based only on relative attitude information, but they assume that information exchanges between agents are modeled by undirected graphs. On the other hand, [53, 54, 55, 56, 57] present synchronization laws with milder assumptions of topologies. However, the present laws feedback information other than relative attitudes. [24] tackles pose synchronization problems on $SE(3)$, but it considers undirected topologies. Inspired by [9, 58], our group has proposed passivity-based synchronization laws on $SO(3)$ [46] and $SE(3)$ [47], where the notion of passivity plays a central role in proving synchronization. However, while the control law in [46] is based only on relative attitude information, [47] partially requires absolute pose information to cancel the coupling term between a position and an orientation. These works have proved

synchronization under milder topology assumptions than [8, 24, 52], but the assumptions are still more restrictive than consensus/synchronization on vector space [16] where the interconnection topology is assumed to contain a spanning tree. Based on these facts, we have also proposed relative pose information-based pose synchronization protocols and given a necessary and sufficient condition of fixed directed graphs in [48] by employing the theory of perturbed systems [49] to prove synchronization. However, all these works do not consider how to get information necessary for implementation of control laws.

Visual Feedback Motion Coordination

Vision-based motion coordination problems are tackled in [59, 60, 61, 62, 63, 64, 65, 66, 67, 68, 69]. [59] proposes vision-based control laws using only monocular vision images to achieve 2D flocking for nonholonomic robots. It shows for complete or ring-type graphs that the present control laws achieving some formation patterns are implementable by using information extracted from the images. Also, [60] addresses 2D attitude alignment problems by using epipoles computed from pairs of images to estimate the misalignment between neighbor agents. However, these approaches deeply rely on complicated image processing techniques which might yield long sampling time. [61] tackles vision-based connectivity maintenance problems. The authors propose a two level control framework for connectivity maintenance and cooperation of multi-agent systems, and image feedback is used to maintain connectivity. However, they assume the usage of partial communication. On the other hand, most of current works on visual feedback motion coordination handle leader-following type formation control problems on 2D plane [62, 63, 64, 65, 66, 67, 68, 69]. [62] tackles the formation control problem via input-output feedback linearization to design control laws and a vision-based extended Kalman filter to get relative information. The authors in [63, 64, 65] make use of a range estimator for leader-follower type formation control. Although [63, 64] show stability of the closed-loop system via Lyapunov arguments, the present control scheme premises communication between the leader and follower. The range estimator proposed in [65] is based on the extended Kalman filter and the validity is given through simulation results. The works in [66, 67, 68, 69] also address the formation problem. In [66], the follower vehicle tracks the trajectory of the leader delayed by constant time. The approaches in [67, 68] are based on visual servoing control techniques, where the authors translate the problem from the configuration space into a separate visual servoing control task for each follower and design a control law by feedback linearization. [69] presents a new observability condition based on the extended output Jacobian, and the state of the leader-follower system is estimated via the extended Kalman filter. In summary, to the best of our knowledge, there exists no visual feedback observer-based control law which guarantees achievement of 3D pose coordination in the absence of communication.

1.4   Contributions

The main contribution of this work is to give theoretical guarantees of visual feedback 3D attitude/pose synchronization for the total system integrating estimation and control systems of multiple rigid bodies. Indeed, most of related works take one of the following three approaches as mentioned in Section 1.3. One is that they assume acquisition of information other than visual measurements for control laws. Another is to utilize extended Kalman filters in order to estimate necessary information and show the validity through simulation or experimental results. The other is to consider only one leader and one follower formation problems and give no stability analysis for the cascade connection of the frameworks.

The other contributions are listed as follows.

- We propose a novel robotic network explicitly formalizing measured output of rigid bodies. In fact, the visual robotic network is the network regarding interconnection topologies as visibility structures and adding measured output extracted by vision sensors to the robotic network defined in [7].

- We present a novel structure incorporating both attitude/pose synchronization laws and visual feedback pose estimation mechanisms into a feedback loop, which enables each rigid body to be fully autonomous.

- The present estimation and control laws achieve the same goals as in [46, 47, 48] in spite of requiring each body to utilize only visual measurements for the protocols.

- In addition to 3D simulation, we perform experiments in order to confirm the effectiveness and validity of the present control scheme and the convergence and performance analysis.

1.5   Dissertation Outline

In Chapter 2, we formalize visual feedback attitude/pose synchronization problems in three dimensions. We introduce a notion of visual robotic networks to be controlled throughout this dissertation. We then define visual feedback attitude/pose synchronization as the goals of this work. Finally, we introduce passivity properties which play a crucial role to propose control laws, some stability concepts of dynamical systems for the main analysis, and review of previous results related to this work.

We first investigate visual feedback attitude synchronization in Chapter 3. We propose a synchronization law based on the passivity-based attitude synchronization law and the vision-based observer introduced in Chapter 2. In the present control law, we assume that all the rigid bodies have a common linear velocity, and relative orientations necessary for attitude synchronization laws are estimated by a vision-based observer. The

present scheme is hence almost completely constructed by visual measurements extracted by vision. We then prove synchronization for the case that there exists a leader in visual robotic networks. However, in the present control strategy, the leader does not rotate, and as a result, the network cannot change the direction of the movement. In order to overcome this issue, we next consider the case that the leader rotates independently. In this situation, we give tracking performance analysis of the network for the leader by employing the theory of input-to-state stability and input-to-output stability. Here, we regard the angular velocity of the leader as an external disturbance to the network. The effectiveness of the present control scheme is demonstrated through simulation in three dimensions and experiments on a planar testbed.

We next study visual feedback pose synchronization in Chapter 4. We first propose a synchronization law based on the passivity-based pose synchronization law and the vision-based observer introduced in Chapter 2. In the present control scheme, relative poses necessary for pose synchronization laws are estimated by a vision-based observer. The present mechanism is hence completely constructed by visual measurements extracted by vision. This is the main point of this dissertation. We next prove pose synchronization where passivity of rigid body motion plays a central role. Since the leader does not move in the present control law similarly to the visual feedback attitude synchronization law, the network cannot move after synchronization. In order to work out this problem, we moreover consider the situation that the leader moves independently. In this case, we analyze the tracking performance of the network by taking the same approaches as in Chapter 3. The effectiveness of the present control protocol is also demonstrated through simulation in three dimensions and experiments on a planar testbed.

Chapter 5 gives some further developments on visual feedback attitude/pose synchronization in regard to (i) linear velocity observers for attitude synchronization, (ii) ring-type visibility structures which does not require the existence of a leader, (iii) consideration of rigid body dynamics by integrating Newton-Euler equations, i.e. extension from velocity laws to force and torque ones, and (iv) collision avoidance and visibility maintenance. Here, we not only propose new visual feedback synchronization protocols but also give convergence analysis.

Finally, Chapter 6 concludes this dissertation.

NOTATION: The following notations are to be used through this dissertation.

$\mathbb{N}$	set of natural numbers
$\mathbb{R}$	set of real numbers
$\mathbb{C}$	set of imaginary numbers
$\mathbb{R}_+$	set of positive real numbers
$\mathbb{R}^n$	n-dimensional Euclidean space
$\mathbb{R}^{m \times n}$	set of $m \times n$ matrices with real entries
$so(3)$	set of 3×3 skew-symmetric matrices: $so(3) = \{\Omega \in \mathbb{R}^{3\times3} \mid \Omega^T = -\Omega\}$
$SO(3)$	special orthogonal group in 3 dimensions: $SO(3) = \{R \in \mathbb{R}^{3\times3} \mid RR^T = I_3, \ \det(R) = 1\}$
$se(3)$	product space of $\mathbb{R}^3$ with $so(3)$: $se(3) = \{(v, \Omega) \mid v \in \mathbb{R}^3, \ \Omega \in so(3)\}$
$SE(3)$	product space of $\mathbb{R}^3$ with $SO(3)$ (special Euclidean group): $SE(3) = \{(p, R) \mid p \in \mathbb{R}^3, \ R \in SO(3)\}$
$\lvert x \rvert$	absolute value of a scalar x
$\lVert x \rVert_2$	Euclidean norm of a vector x
$\lVert x \rVert_{\mathcal{L}_2}$	$\mathcal{L}_2$ norm of a signal x
$\lVert A \rVert_F$	Frobenius matrix norm of a matrix A
$\mathbf{1}$	column vector with corresponding dimensions whose entries are all 1
I_n	n-dimensional identity matrix
$A^{\mathrm{T}} \ (x^{\mathrm{T}})$	transpose of a matrix A (vector x)
A^{-1}	inverse matrix of a matrix A
$A^{\dagger}$	pseudo inverse matrix of a matrix A
$A > 0 \ (A \geq 0)$	positive definite (semidefinite) matrix A
$\mathrm{tr}(A)$	trace of a square matrix A
$\det(A)$	determinant of a square matrix A
$\mathrm{diag}\{a_1, \cdots, a_n\}$	diagonal matrix with diagonal elements a_1 to a_n
$\lvert \mathcal{V} \rvert$	cardinality of a set $\mathcal{V}$
$p_{ab} \in \mathbb{R}^3$	position of a frame Σ_b relative to a frame Σ_a
$e^{\hat{\xi}_{ab}\theta_{ab}} \in SO(3)$	rotation matrix of a frame Σ_b relative to a frame Σ_a ($\xi_{ab} \in \mathbb{R}^3$ ($\lVert \xi \rVert_2 = 1$) and $\theta_{ab} \in \mathbb{R}$ represent the rotation axis and the rotation angle, respectively)
$\hat{\cdot} \ (\cdot^{\wedge})$	operator $\mathbb{R}^3 \mapsto so(3)$ or $\mathbb{R}^6 \mapsto se(3)$: for $a = [a_1 \ a_2 \ a_3]^{\mathrm{T}} \in \mathbb{R}^3$, $V = (v, \omega) \in \mathbb{R}^6$, $v, \omega \in \mathbb{R}^3$, $\hat{a} = \begin{bmatrix} 0 & -a_3 & a_2 \\ a_3 & 0 & -a_1 \\ -a_2 & a_1 & 0 \end{bmatrix} \in so(3)$, $\hat{V} = \begin{bmatrix} \hat{\omega} & v \\ 0 & 0 \end{bmatrix} \in se(3)$
$\cdot^{\vee}$	inverse operator to $\wedge$

$g_{ab} \in \mathbb{R}^{4 \times 4}$ homogeneous representation of a pose $(p_{ab}, e^{\hat{\xi}_{ab}\theta_{ab}}) \in SE(3)$:

$$g_{ab} = \begin{bmatrix} e^{\hat{\xi}_{ab}\theta_{ab}} & p_{ab} \\ 0 & 1 \end{bmatrix} \in \mathbb{R}^{4 \times 4}$$

$V_{ab}^b = (v_{ab}^b, \omega_{ab}^b) \in \mathbb{R}^6$ body velocity of a frame Σ_b relative to a frame Σ_a:

$$V_{ab}^b = (g_{ab}^{-1} \dot{g}_{ab})^\vee = \begin{bmatrix} v_{ab}^b \\ \omega_{ab}^b \end{bmatrix} \in \mathbb{R}^6$$

$\hat{V}_{ab}^b \in \mathbb{R}^{4 \times 4}$ homogeneous representation of a body velocity $V_{ab}^b \in \mathbb{R}^6$:

$$\hat{V}_{ab}^b = g_{ab}^{-1} \dot{g}_{ab} = \begin{bmatrix} \hat{\omega}_{ab}^b & v_{ab}^b \\ 0 & 0 \end{bmatrix} \in \mathbb{R}^{4 \times 4}$$

$\mathrm{Ad}_{(g_{ab})} \in \mathbb{R}^{6 \times 6}$ adjoint transformation associated with $g_{ab} \in SE(3)$:

$$\mathrm{Ad}_{(g_{ab})} = \begin{bmatrix} e^{\hat{\xi}_{ab}\theta_{ab}} & \hat{p}_{ab} e^{\hat{\xi}_{ab}\theta_{ab}} \\ 0 & e^{\hat{\xi}_{ab}\theta_{ab}} \end{bmatrix} \in \mathbb{R}^{6 \times 6}$$

$\mathrm{Ad}_{(p_{ab})} \in \mathbb{R}^{6 \times 6}$ adjoint transformation associated with $p_{ab} \in \mathbb{R}^3$:

$$\mathrm{Ad}_{(p_{ab})} = \begin{bmatrix} I_3 & \hat{p}_{ab} \\ 0 & I_3 \end{bmatrix} \in \mathbb{R}^{6 \times 6}$$

$\mathrm{Ad}_{(e^{\hat{\xi}_{ab}\theta_{ab}})} \in \mathbb{R}^{6 \times 6}$ adjoint transformation associated with $e^{\hat{\xi}_{ab}\theta_{ab}} \in SO(3)$:

$$\mathrm{Ad}_{(e^{\hat{\xi}_{ab}\theta_{ab}})} = \begin{bmatrix} e^{\hat{\xi}_{ab}\theta_{ab}} & 0 \\ 0 & e^{\hat{\xi}_{ab}\theta_{ab}} \end{bmatrix} \in \mathbb{R}^{6 \times 6}$$

Chapter 2

Problem Settings and Foundations

2.1 Introduction

In this chapter, we give problem formulation of visual feedback attitude/pose synchronization on $SE(3)$. We first introduce a notion of visual robotic networks to be controlled throughout this work. Visual robotic networks consist of multiple rigid bodies, visibility structures and visual measurements. Whereas most works in cooperative control deal with only multiple agents and interconnection topologies (e.g. robotic networks [7]), this work explicitly formulates vision-based measured output available for bodies to implement control laws. This setting is one of the main contributions of this dissertation. As a result, interconnection topologies between bodies are regarded as visibility structures, where information flows are defined by who sees whom. We next give the definitions of visual feedback attitude/pose synchronization for visual robotic networks as the goals of this work. These goals are the same as in our previous works [46, 47] except for imposing the restriction of measured output. Finally, as foundations, we introduce passivity properties which play a central role for the design of control laws, some stability concepts of dynamical systems for the subsequent analysis, and review of previous results associated with this work.

This chapter is organized as follows. In Section 2.2, we introduce a notion of visual robotic networks to be controlled. Then, we give the definitions of visual feedback attitude/pose synchronization in Section 2.3. In Section 2.4, we introduce some important properties of dynamical systems and review our previous results as preliminaries of this work. Section 2.5 concludes this chapter.

2.2 Visual Robotic Network

In this section, we introduce a notion of visual robotic networks on $SE(3)$ to be controlled throughout this dissertation. Visual robotic networks consist of multiple rigid bodies,
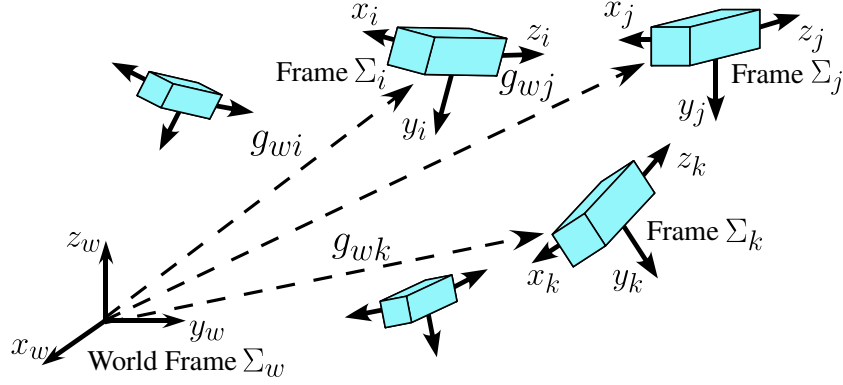
Figure 2.1: Rigid Body Motion

visual measurements and visibility structures defining information flows between bodies.

2.2.1 Rigid Body Motion

Throughout this work, we consider a network of n rigid bodies $\mathcal{V} := \{1, \cdots, n\}$ in 3D space (see Fig. 2.1). Let Σ_w be an inertial coordinate frame and Σ_i, $i \in \mathcal{V}$ body-fixed frames whose each origin is located at the center of mass of body i. Assume that all the coordinate frames are right-handed and Cartesian. Then, we denote by $p_{wi} \in \mathbb{R}^3$ the position of body i in Σ_w, and represent the rotation matrix of Σ_i relative to Σ_w by $e^{\hat{\xi}_{wi}\theta_{wi}} \in SO(3)$. Here, $\xi_{wi} \in \mathbb{R}^3$ ($\|\xi_{wi}\|_2 = 1$) and $\theta_{wi} \in (-\pi, \pi]$ specify the rotation axis and angle, respectively. The notation '$\wedge$' for $a \in \mathbb{R}^3$ describes the skew-symmetric operator such that $\hat{a}b = a \times b$, $b \in \mathbb{R}^3$ for the vector cross-product $\times$, i.e. $\hat{a}$ is an element of the 3×3 skew-symmetric matrix group $so(3)$. Also, the notation '$\vee$' is the inverse operator to '$\wedge$'. Hereafter, we use $\hat{\xi}\theta_{wi}$ to represent $\hat{\xi}_{wi}\theta_{wi}$ for simplicity. Then, the transformation $e^{\hat{\xi}\theta_{wi}}$ is orthogonal with unit determinant, i.e. an element of the *Special Orthogonal* group $SO(3)$. A configuration consists of the pair $(p_{wi}, e^{\hat{\xi}\theta_{wi}})$ and hence the configuration space of each body is the *Special Euclidean* group $SE(3)$, which is the product space of $\mathbb{R}^3$ with $SO(3)$. In this dissertation, we use the following homogeneous representation of $g_{wi} = (p_{wi}, e^{\hat{\xi}\theta_{wi}}) \in SE(3)$ to describe the pose (position and orientation) of body i in Σ_w.

$$g_{wi} = \begin{bmatrix} e^{\hat{\xi}\theta_{wi}} & p_{wi} \\ 0 & 1 \end{bmatrix} \in \mathbb{R}^{4 \times 4}, \ i \in \mathcal{V}.$$

We next introduce the velocity of each rigid body to represent the motion of Σ_i relative to Σ_w. We first define the body velocity of body i relative to Σ_w as

$$\hat{V}_{wi}^b := g_{wi}^{-1}\dot{g}_{wi} = \begin{bmatrix} \hat{\omega}_{wi}^b & v_{wi}^b \\ 0 & 0 \end{bmatrix} \in \mathbb{R}^{4 \times 4}, \tag{2.1}$$

11

or the vector form

$$V_{wi}^b = \begin{bmatrix} v_{wi}^b \\ \omega_{wi}^b \end{bmatrix} = \begin{bmatrix} e^{-\hat{\xi}\theta_{wi}}\dot{p}_{wi} \\ (e^{-\hat{\xi}\theta_{wi}}\dot{e}^{\hat{\xi}\theta_{wi}})^\vee \end{bmatrix} \in \mathbb{R}^6, \ i \in \mathcal{V}.$$

Here, $v_{wi}^b \in \mathbb{R}^3$ and $\omega_{wi}^b \in \mathbb{R}^3$ represent the linear and angular body velocities of body i relative to Σ_w, respectively. Also, the operator '∧' for $V \in \mathbb{R}^6$ generates an element of $se(3)$ as in (2.1), where $se(3)$ is the product space of $\mathbb{R}^3$ with $so(3)$. Then, each *rigid body motion* is represented by the following kinematic model which is directly given by (2.1).

$$\dot{g}_{wi} = g_{wi}\hat{V}_{wi}^b, \ i \in \mathcal{V}. \tag{2.2}$$

Let us next denote the pose of Σ_j relative to Σ_i by $g_{ij} = (p_{ij}, e^{\hat{\xi}\theta_{ij}}) \in SE(3)$, which is defined as

$$g_{ij} := g_{wi}^{-1}g_{wj} = \begin{bmatrix} e^{-\hat{\xi}\theta_{wi}}e^{\hat{\xi}\theta_{wj}} & e^{-\hat{\xi}\theta_{wi}}(p_{wj} - p_{wi}) \\ 0 & 1 \end{bmatrix} \in \mathbb{R}^{4\times4}.$$

We moreover define the body velocity of Σ_j relative to Σ_i as $V_{ij}^b := (g_{ij}^{-1}\dot{g}_{ij})^\vee$. Then, from the direct calculation, each *relative rigid body motion* is given as

$$\dot{g}_{ij} = -\hat{V}_{wi}^b g_{ij} + g_{ij}\hat{V}_{wj}^b$$

or the vector form

$$V_{ij}^b = -\mathrm{Ad}_{(g_{ij}^{-1})}V_{wi}^b + V_{wj}^b. \tag{2.3}$$

Here, $\mathrm{Ad}_{(g)} \in \mathbb{R}^{6\times6}$ is the adjoint transformation [32] associated with g which satisfies $\hat{V}' = g\hat{V}g^{-1}$ for $V' = \mathrm{Ad}_{(g)}V$. The block diagrams of the rigid body motion and the relative rigid body motion are illustrated in Figs. 2.2 and 2.3, respectively.

2.2.2 Visibility Structure

In visual robotic networks, we regard interconnection topologies between rigid bodies as *visibility structures*, where we say that body j is visible from body i if body i can extract visual information associated with body j from its vision. We describe visibility structures by similar notations to those in graph theory [70]. Namely, a set $\mathcal{E} \subset \mathcal{V} \times \mathcal{V}$ is defined so that $(j, i) \in \mathcal{E}$ means that body j is visible from body i. Then, similarly to neighbors in graph theory, we define the set of visible bodies from body i as

$$\mathcal{N}_i := \{j \in \mathcal{V} \mid (j, i) \in \mathcal{E}\}, \ i \in \mathcal{V}. \tag{2.4}$$

Let us now give the following assumptions on the visibility structure.
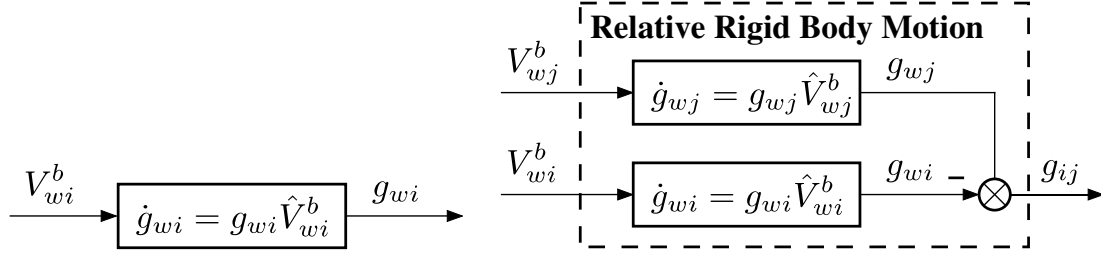
Figure 2.2: Block Diagram of Rigid Body Motion

Figure 2.3: Block Diagram of Relative Rigid Body Motion

Assumption 1.

- $\mathcal{N}_1 = \emptyset$.

- $|\mathcal{N}_i| = 1$ and $\mathcal{N}_i$ is fixed for all $i \in \mathcal{V} \setminus \{1\}$.

- $^\forall i \in \mathcal{V} \setminus \{1\}$, $^\exists v_1, \cdots, v_r \in \mathcal{V} \mid v_1 = 1,\ v_r = i$ and $(v_k, v_{k+1}) \in \mathcal{E}_V$ $^\forall k \in \{1, \cdots, r-1\}$.

Assumption 2.

- $\mathcal{N}_1 = \{n\}$.

- $\mathcal{N}_i = \{i - 1\}$ for all $i \in \mathcal{V} \setminus \{1\}$.

Here, $|\mathcal{N}_i|$ represents the number of components of $\mathcal{N}_i$. Then, Assumption 1 implies that visibility structures have leader-following structures since there exists one leader (rigid body 1) which has no visible body, the other bodies have a fixed visible body, and there exists a visibility path from each body to the leader. This visibility structure can be interpreted as a directed graph $G = (\mathcal{V}, \mathcal{E})$ by regarding $\mathcal{V}$ and $\mathcal{E}$ as the node set and the edge set, respectively (see Fig. 2.4). Then, Assumption 1 means that the visibility structure makes up a directed spanning tree [70] whose root is body 1. On the other hand, Assumption 2 means that the visibility structure has a ring topology (see Fig. 2.5).

2.2.3 Visual Measurements

We finally formulate *visual measurements* of each rigid body as measured output which is available for estimation and control. Suppose that each body j has s ($s \geq 4$) feature points, whose positions relative to Σ_j are denoted by $p_{jj_k} \in \mathbb{R}^3$, $k \in \{1, \cdots, s\}$. Then, the coordinate transformation g_{ij} yields those positions defined in Σ_i as follows.

$$\begin{bmatrix} p_{ij_k} \\ 1 \end{bmatrix} = g_{ij} \begin{bmatrix} p_{jj_k} \\ 1 \end{bmatrix},$$
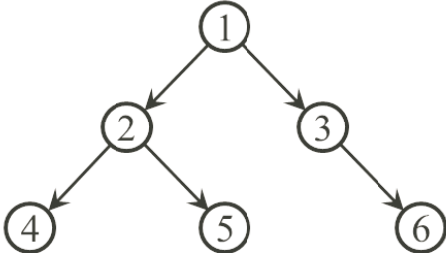
Figure 2.4: Visibility Structure Satisfying Assumption 1
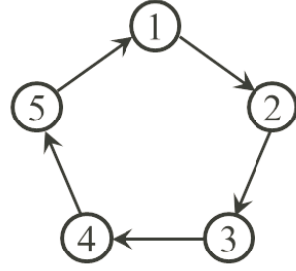
Figure 2.5: Visibility Structure Satisfying Assumption 2

Pinhole Camera   Panoramic Camera
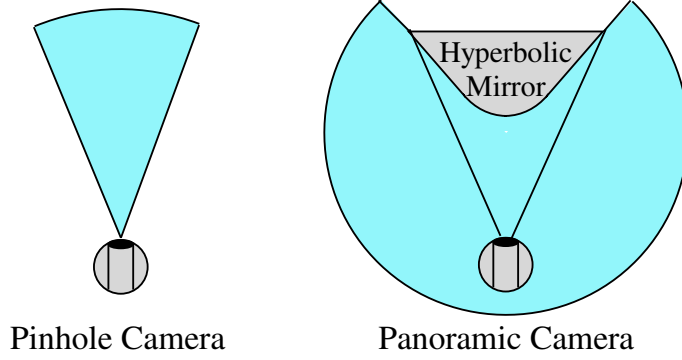
Figure 2.6: Camera Models

where $p_{ij_k} \in \mathbb{R}^3$ is the position of the k-th feature point defined in Σ_i.

We now define visual measurements of each rigid body. Throughout this work, we consider two kinds of camera models with *perspective projection* as vision models. One is a typical pinhole camera model, and the other is a panoramic camera model consisting of the pinhole camera model and a hyperbolic mirror to get a wider field of view (see Fig. 2.6). We first introduce visual measurements extracted by the pinhole camera model. We denote the k-th feature point p_{ij_k} projected onto the image plane of body i by $f_{ij_k} \in \mathbb{R}^2$, $k \in \{1, \cdots, s\}$. Then, perspective projection [32] gives

$$f_{ij_k} = \frac{\lambda_i}{z_{ij_k}} \begin{bmatrix} x_{ij_k} \\ y_{ij_k} \end{bmatrix}, \tag{2.5}$$

where we use the notation $p_{ij_k} = [x_{ij_k} \ y_{ij_k} \ z_{ij_k}]^\mathrm{T}$, and $\lambda_i > 0$, $i \in \mathcal{V}$ is a focal length of each vision (see Fig. 2.7).

We next formulate visual measurements extracted by the panoramic camera model. We denote the mirror coordinate frame of rigid body i by Σ_{m_i} where the origin is located

14
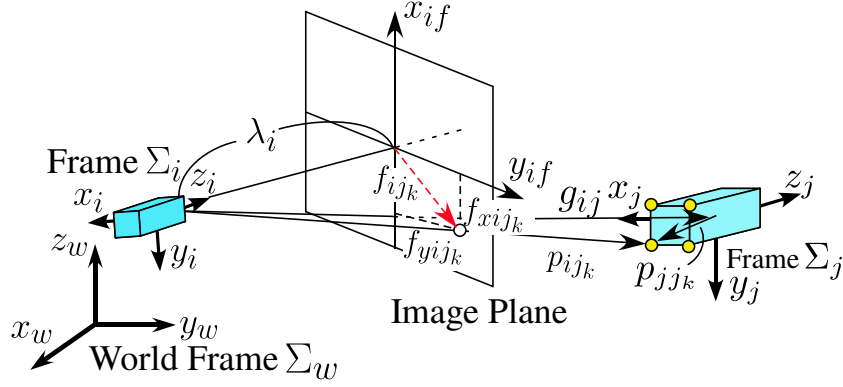
Figure 2.7: Perspective Projection Model

at the focus point (see Fig. 2.8), and the pose of Σ_{m_i} relative to Σ_w is described by $g_{wm_i} = (p_{wm_i}, e^{\hat{\xi}\theta_{wm_i}}) \in SE(3)$. We also denote the pose of body j and the position of the k-th feature point on body j relative to Σ_{m_i} by $g_{m_ij} = (p_{m_ij}, e^{\hat{\xi}\theta_{m_ij}}) \in SE(3)$ and $p_{m_ij_k} \in \mathbb{R}^3$, respectively. Then, similarly to (2.3), relative rigid body motion of body j relative to the mirror of body i is given by

$$\dot{g}_{m_ij} = -g_{im_i}^{-1}\hat{V}_{wi}^b g_{ij} + g_{m_ij}\hat{V}_{wj}^b,$$

or the vector form

$$V_{m_ij}^b := (g_{m_ij}^{-1}\dot{g}_{m_ij})^\vee = -\mathrm{Ad}_{(g_{m_ij}^{-1})}\mathrm{Ad}_{(g_{im_i}^{-1})}V_{wi}^b + V_{wj}^b, \tag{2.6}$$

where $g_{im_i} = (p_{im_i}, e^{\hat{\xi}\theta_{im_i}}) \in SE(3)$ is the pose of Σ_{m_i} relative to Σ_i. We next denote the point on the surface of the mirror of body i associated with the k-th feature point on body j by h_{ik} as shown in Fig. 2.8. Then, the k-th feature point on the image plane of body i, denoted by f_{ij_k}, is given by p_{ij_k} projected onto the image plane through h_{ik}. Now, let $a_i, b_i \in \mathbb{R}_+$ and $d_i := \sqrt{a_i^2 + b_i^2}$ be the hyperbolic mirror parameters of body i satisfying

$$\frac{(z_{m_ih_{ik}} + d_i)^2}{a_i^2} - \frac{x_{m_ih_{ik}}^2 + y_{m_ih_{ik}}^2}{b_i^2} = 1. \tag{2.7}$$

Here, $p_{m_ih_{ik}} := [x_{m_ih_{ik}} \ y_{m_ih_{ik}} \ z_{m_ih_{ik}}]^\mathrm{T} \in \mathbb{R}^3$ is the position of the point h_{ik} relative to Σ_{m_i}. We moreover denote the position of point h_{ik} relative to Σ_i by $p_{ih_{ik}} := [x_{ih_{ik}} \ y_{ih_iik} \ z_{ih_{ik}}]^\mathrm{T} \in \mathbb{R}^3$. Then, perspective projection (2.5) gives

$$f_{ij_k} = \frac{\lambda_i}{z_{ih_{ik}}}\begin{bmatrix} x_{ih_{ik}} \\ y_{ih_{ik}} \end{bmatrix}.$$

15
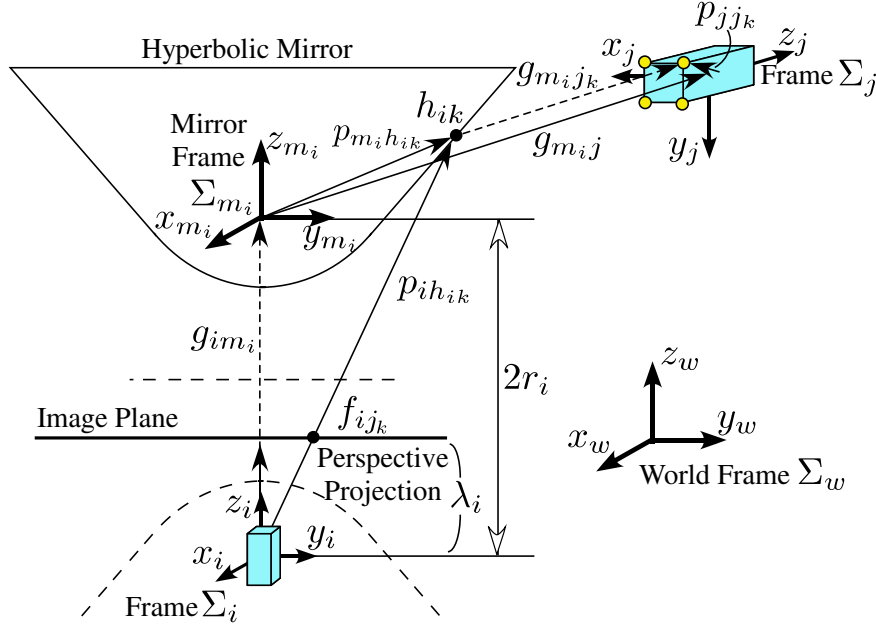
Figure 2.8: Panoramic Camera Model

We now set $p_{im_i} = [0\ 0\ 2d_i]^\mathrm{T}$ and $e^{\hat{\xi}\theta_{im_i}} = I_3$, and note that $p_{m_i h_{ik}} = cp_{m_i j_k}$ holds for $c \in (0, 1)$ (see Fig. 2.8). Then, substituting $cp_{m_i j_k}$ into (2.7) yields

$$c(p_{m_i j_k}) = \frac{b_i^2(d_i z_{m_i j_k} + a_i \|p_{m_i j_k}\|_2)}{a_i^2 x_{m_i j_k}^2 + a_i^2 y_{m_i j_k}^2 - b_i^2 z_{m_i j_k}^2}.$$

Finally, since $z_{ih_{ik}} = 2d_i + c(p_{m_i j_k})z_{m_i j_k}$ holds, f_{ij_k} is given by

$$f_{ij_k} = \frac{\lambda_i c(p_{m_i j_k})}{2d_i + c(p_{m_i j_k})z_{m_i j_k}} \begin{bmatrix} x_{m_i j_k} \\ y_{m_i j_k} \end{bmatrix}. \tag{2.8}$$

Suppose that each rigid body can extract the feature points of visible bodies from image data. Then, visual measurements of body i is defined as

$$f_i := \{f_{ij}\}_{j \in \mathcal{N}_i}, \ i \in \mathcal{V}, \tag{2.9}$$

where $f_{ij} := [f_{ij_1}^\mathrm{T} \ \cdots \ f_{ij_s}^\mathrm{T}]^\mathrm{T} \in \mathbb{R}^{2s}$. We finally assume that p_{jj_k}, $k \in \{1, \cdots, s\}$ are known *a priori*. Then, the visual measurements f_i depend only on the relative pose g_{ij} or $g_{m_i j}$, $j \in \mathcal{N}_i$. Fig. (2.9) illustrates the block diagram of the relative rigid body motion with the pinhole camera model.

Remark 1. If we select $a_i = 1$ and $b_i = \sqrt{-1}$, the feature point extracted by the panoramic camera model (2.8) is then equivalent to that of the pinhole camera model

16
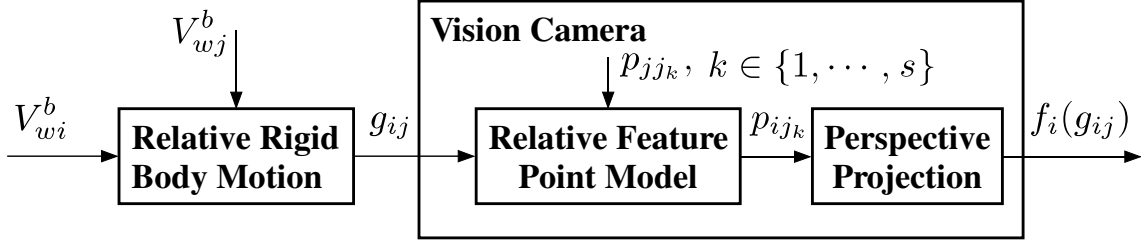
Figure 2.9: Block Diagram of Vision Model with Relative Rigid Body Motion

(2.5). Namely, a panoramic camera model includes a pinhole camera model as a special case.

Hereafter, the aggregate system consisting of n rigid bodies with rigid body motion (2.2), visibility structures (2.4) and visual measurements (2.9) is called *visual robotic network* Σ which is the controlled system throughout this work.

In most parts of this work, we consider V_{wi}^b as a control input. In contrast, some practical mechanical systems such as spacecraft or UAV systems use torque and force control. Even in such real systems, considering simplified dynamics can be useful at least to build a high-level planning controller generating desired trajectories under the assumption that these can be tracked by a lower level mechanical controller. In addition, it is also useful as a preliminary step towards an integrated controller.

2.3 Goals

In this section, we give the goals of this work. We first introduce the definition of visual feedback attitude synchronization for the visual robotic network Σ as the goal of the first half of this work. Then, visual feedback pose synchronization is defined for the goal of the second half of this work.

2.3.1 Definition of Visual Feedback Attitude Synchronization

As the goal of the first half of this work, we define attitude synchronization for the visual robotic network Σ, called *visual feedback attitude synchronization*, as follows.

Definition 1. *The visual robotic network Σ is said to achieve visual feedback attitude synchronization if control laws of rigid bodies consist only of visual measurements (2.9) and the following equations hold.*

$$\begin{cases} v_{wi}^b = v_{wj}^b \\ \lim_{t \to \infty} \phi(e^{\hat{\xi}\theta_{ij}}) = 0 \end{cases} \quad \forall i, j \in \mathcal{V}. \tag{2.10}$$

17
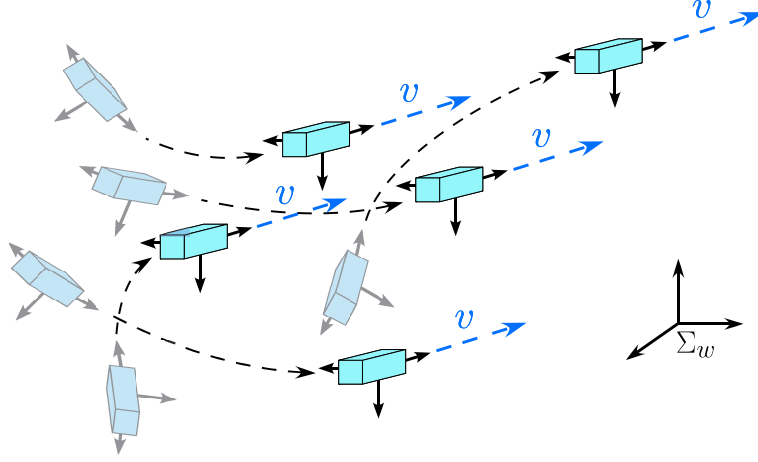
Figure 2.10: Visual Feedback Attitude Synchronization

Here, $\phi(e^{\hat{\xi}\theta}) \geq 0$ is energy of rotation defined as follows (see Appendix B.3 for the properties of $\phi(e^{\hat{\xi}\theta})$).

$$\phi(e^{\hat{\xi}\theta}) := \frac{1}{4}\|I_3 - e^{\hat{\xi}\theta}\|_F^2 = \frac{1}{2}\mathrm{tr}(I_3 - e^{\hat{\xi}\theta}) = 1 - \cos\theta.$$

Equations (2.10) mean that the orientations of all the rigid bodies asymptotically converge to a common value, and as the result, all the bodies move in the same direction (see Fig. 2.10).

2.3.2 Definition of Visual Feedback Pose Synchronization

We next give the definition of pose synchronization for the visual robotic network Σ, called *visual feedback pose synchronization*, as the goal of the second half of this work.

We first define virtual relative poses $\tilde{g}_{ij} \in SE(3)$ as

$$\tilde{g}_{ij} := \begin{bmatrix} e^{\hat{\xi}\theta_{ij}} & p_{ij} - d_{ij} \\ 0 & 1 \end{bmatrix}, \; i, j \in \mathcal{V},$$

where $d_{ij} \in \mathbb{R}^3$, $i, j \in \mathcal{V}$ are constant biases for rigid bodies to guarantee collision avoidance and visibility to neighbors when synchronization is achieved. We assume each body knows biases relative to its visible bodies (i.e. d_{ij}, $j \in \mathcal{N}_i$) *a priori*. Then, if Assumption 1 or 2 is satisfied, all the biases d_{ij}, $i, j \in \mathcal{V}$ are uniquely determined when all the orientations are synchronized (e.g. $d_{ji} = -d_{ij}$, $d_{ik} = d_{ij} + d_{jk}$). The second goal is now to design control laws so that the visual robotic network Σ achieves visual feedback pose synchronization defined as follows.
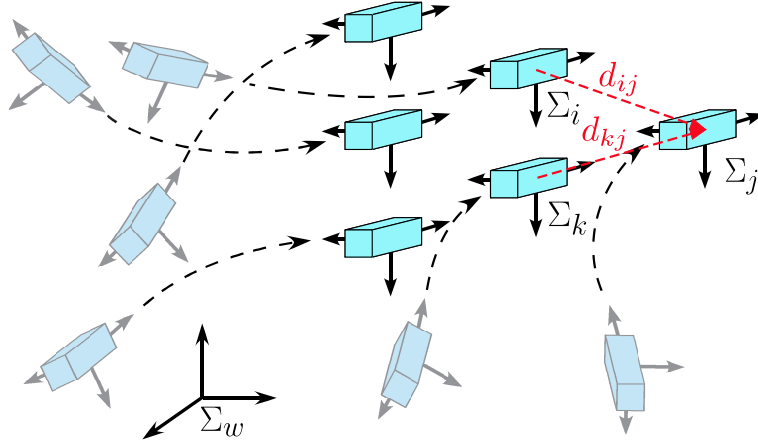
Figure 2.11: Visual Feedback Pose Synchronization

Definition 2. *The visual robotic network Σ is said to achieve visual feedback pose synchronization if control laws of rigid bodies consist only of visual measurements (2.9) and the following equation holds.*

$$\lim_{t \to \infty} \psi\left(\tilde{g}_{ij}\right) = 0 \ ^{\forall} i, j \in \mathcal{V}. \tag{2.11}$$

Here, $\psi(g) \geq 0$ is the total energy of translation and rotation defined as

$$\psi(g) := \|J(I_4 - g)\|_F^2 = \frac{1}{2}\|p\|_2^2 + \phi(e^{\hat{\xi}\theta}), \ J := \begin{bmatrix} \frac{1}{2}I_3 & 0 \\ 0 & \frac{1}{\sqrt{2}} \end{bmatrix} \in \mathbb{R}^{4 \times 4}.$$

Since the function $\psi(\tilde{g}_{ij})$ is defined by the weighted norm between I_4 and $\tilde{g}_{ij}$, (2.11) means that the relative positions of all the rigid bodies asymptotically converge to desired ones and all the orientations converge to a common value (see Fig. 2.11).

Remark 2. Equations (2.10) or (2.11) are the same as those of the definitions in [46] or [47, 48], respectively. Unlike [46, 47, 48] premising the measurement of actual relative poses g_{ij}, the objective of this work is to propose attitude/pose synchronization laws based only on visual measurements (2.9).

2.4 Foundations

In this section, we give foundations for this work. We first give the definition of passivity of dynamical systems, and we show that the rigid body motion (2.2) and the relative rigid body motion (2.3) have passivity which plays important roles to propose control laws for visual feedback attitude/pose synchronization. We next introduce some stability concepts of dynamical systems useful for the subsequent analysis. Finally, we review previous results associated with this work.

2.4.1 Passivity of Rigid Body Motion

We first introduce *passivity* of dynamical systems based on [49]. Let us consider a dynamical system represented by the state model

$$\begin{cases} \dot{x} = f(x, u) \\ y = h(x, u) \end{cases}, \qquad (2.12)$$

where $f : \mathbb{R}^n \times \mathbb{R}^p \to \mathbb{R}^n$ is locally Lipschitz, $h : \mathbb{R}^n \times \mathbb{R}^p \to \mathbb{R}^p$ is continuous, $f(0, 0) = 0$, and $h(0, 0) = 0$. Then, the definition of passivity is given as follows [49].

Definition 3. *The system (2.12) is said to be passive if there exists a continuously differentiable positive semidefinite function $W(x)$, called storage function, such that*

$$u^{\mathrm{T}} y \geq \dot{W} = \frac{\partial W}{\partial x} f(x, u) \ ^{\forall}(x, u) \in \mathbb{R}^n \times \mathbb{R}^p.$$

We next show that the rigid body motion (2.2) has passivity.

Lemma 1. *The time derivative of $\psi(g_{wi})$ along the trajectory of (2.2) satisfies*

$$\dot{\psi}(g_{wi}) = (V_{wi}^b)^{\mathrm{T}} e_i, \ \ e_i := \begin{bmatrix} e^{-\hat{\xi}\theta_{wi}} p_{wi} \\ \mathrm{sk}(e^{\hat{\xi}\theta_{wi}})^{\vee} \end{bmatrix} \in \mathbb{R}^6,$$

where $\mathrm{sk} : \mathbb{R}^{3 \times 3} \to so(3)$ is the skew-symmetric operator defined as $\mathrm{sk}(e^{\hat{\xi}\theta}) := (1/2)(e^{\hat{\xi}\theta} - e^{-\hat{\xi}\theta})$.

Proof. The time derivative of $\psi(g_{wi})$ along the trajectories of (2.2) yields

$$\begin{aligned} \dot{\psi}(g_{wi}) &= \frac{d}{dt}\left(\frac{1}{2}\|p_{wi}\|_2^2 + \phi(e^{\hat{\xi}\theta_{wi}})\right) \\ &= p_{wi}^{\mathrm{T}} \dot{p}_{wi} + (\mathrm{sk}(e^{\hat{\xi}\theta_{wi}})^{\vee})^{\mathrm{T}} \omega_{wi}^b \ \ (\because \text{Appendix B.3.2}) \\ &= p_{wi}^{\mathrm{T}} e^{\hat{\xi}\theta_{wi}} v_{wi}^b + (\mathrm{sk}(e^{\hat{\xi}\theta_{wi}})^{\vee})^{\mathrm{T}} \omega_{wi}^b \ \ (\because \text{Eq. (2.2)}) \\ &= \begin{bmatrix} (e^{-\hat{\xi}\theta_{wi}} p_{wi})^{\mathrm{T}} & (\mathrm{sk}(e^{\hat{\xi}\theta_{wi}})^{\vee})^{\mathrm{T}} \end{bmatrix} \begin{bmatrix} v_{wi}^b \\ \omega_{wi}^b \end{bmatrix} \\ &= (V_{wi}^b)^{\mathrm{T}} e_i. \end{aligned}$$

$\square$

Lemma 1 means that the rigid body motion (2.2) is passive from V_{wi}^b to e_i with the storage function $\psi(g_{wi})$. Attitude/Pose synchronization laws are build based on this passivity.

Remark 3. The term $\mathrm{sk}(e^{\hat{\xi}\theta_{wi}})^\vee$ is equivalent to $\xi_{wi} \sin\theta_{wi}$ (Appendix B.2.6), and hence $\mathrm{sk}(e^{\hat{\xi}\theta_{wi}})^\vee$ is interpreted as an operator extracting the direction and angle of rotation from $e^{\hat{\xi}\theta_{wi}}$. Note that $\mathrm{sk}(e^{\hat{\xi}\theta_{wi}})^\vee$ can be also viewed as the state vector with respect to the rotation as long as $\theta_{wi} \in [-\pi/2, \pi/2]$ since the rotation axis and angle uniquely determine the rotation matrix in the domain. The term $\dot{\phi}(e^{\hat{\xi}\theta_{wi}})$ is thus given by the inner product of the angular velocity and the state vector with respect to the rotation.

We also give passivity of the relative rigid body motion (2.3).

Lemma 2. *If $V_{wj}^b = 0$ holds, then the time derivative of $\psi(g_{ij})$ along the trajectory of (2.3) satisfies*

$$\dot{\psi}(g_{ij}) = (V_{wi}^b)^\mathrm{T}(-e_{ij}), \ e_{ij} := \begin{bmatrix} p_{ij} \\ \mathrm{sk}(e^{\hat{\xi}\theta_{ij}})^\vee \end{bmatrix} \in \mathbb{R}^6.$$

Proof. When $V_{wj}^b = 0$ holds, the time derivative of $\psi(g_{ij})$ along the trajectories of (2.3) gives

$$
\begin{aligned}
\dot{\psi}(g_{ij}) &= p_{ij}^\mathrm{T}\dot{p}_{ij} + (\mathrm{sk}(e^{\hat{\xi}\theta_{ij}})^\vee)^\mathrm{T}\omega_{ij}^b \\
&= p_{ij}^\mathrm{T}e^{\hat{\xi}\theta_{ij}}e^{-\hat{\xi}\theta_{ij}}\dot{p}_{ij} + (\mathrm{sk}(e^{\hat{\xi}\theta_{ij}})^\vee)^\mathrm{T}e^{\hat{\xi}\theta_{ij}}\omega_{ij}^b \quad (\because \text{Appendix B.2.7}) \\
&= \begin{bmatrix} p_{ij}^\mathrm{T} & (\mathrm{sk}(e^{\hat{\xi}\theta_{ij}})^\vee)^\mathrm{T} \end{bmatrix} \begin{bmatrix} e^{\hat{\xi}\theta_{ij}} & 0 \\ 0 & e^{\hat{\xi}\theta_{ij}} \end{bmatrix} \begin{bmatrix} v_{ij}^b \\ \omega_{ij}^b \end{bmatrix} \\
&= e_{ij}^\mathrm{T}\mathrm{Ad}_{(e^{\hat{\xi}\theta_{ij}})}V_{ij}^b \\
&= -e_{ij}^\mathrm{T}\mathrm{Ad}_{(e^{\hat{\xi}\theta_{ij}})}\mathrm{Ad}_{(g_{ij}^{-1})}V_{wi}^b \quad (\because \text{Eq. (2.3) with } V_{wj}^b = 0) \\
&= -e_{ij}^\mathrm{T}\mathrm{Ad}_{(-p_{ij})}V_{wi}^b \\
&= (V_{wi}^b)^\mathrm{T}(-e_{ij}) \quad (\because p_{ij}^\mathrm{T}\hat{p}_{ij}\omega_{wi}^b = -p_{ij}^\mathrm{T}\hat{\omega}_{wi}^b p_{ij} = 0, \quad \text{(Appendix B.1.2)})
\end{aligned}
$$

where we use the notation $V_{ij}^b = [(v_{ij}^b)^\mathrm{T} \ (\omega_{ij}^b)^\mathrm{T}]^\mathrm{T}$. $\qquad\square$

Lemma 2 means that the relative rigid body motion (2.3) is passive from V_{wi}^b to $-e_{ij}$ with the storage function $\psi(g_{ij})$ when $V_{wj}^b = 0$ holds. Estimation mechanism in control laws are build based on this passivity.

Remark 4. It should be noted that the position dynamics of the relative rigid body motion (2.3) has coupling terms associated with orientations as follows.

$$\dot{p}_{ij} = -v_{wi}^b + \hat{p}_{ij}\omega_{wi}^b + e^{\hat{\xi}\theta_{ij}}v_{wj}^b.$$

However, Lemma 2 says that we can decouple these terms by using the potential function $\psi(g_{ij})$. This property plays important roles in this work.

2.4.2   Stability of Dynamical Systems

We next give some *stability* concepts of dynamical systems based on [49, 50, 51] which are useful for the subsequent analysis.

Lyapunov Stability

We first consider the autonomous system

$$\dot{x} = f(x), \tag{2.13}$$

where $f : \mathcal{D} \to \mathbb{R}^n$ is a locally Lipschitz map from a domain $\mathcal{D} \subset \mathbb{R}^n$ into $\mathbb{R}^n$. We assume without loss of generality that $f(x)$ satisfies $f(0) = 0$, i.e. the origin $x = 0$ is an equilibrium point of the system (2.13). Then, [49] gives definitions of stability as follows.

Definition 4. *The equilibrium point $x = 0$ of (2.13) is stable if, for each $\epsilon \in \mathbb{R}_+$, there exists $\delta = \delta(\epsilon) \in \mathbb{R}_+$ such that*

$$\|x(0)\|_2 < \delta \Rightarrow \|x(t)\|_2 < \epsilon \; ^\forall t \geq 0.$$

In addition, $x = 0$ is said to be asymptotically stable if it is stable and δ can be chosen such that

$$\|x(0)\|_2 < \delta \Rightarrow \lim_{t \to \infty} x(t) = 0.$$

Moreover, the point is exponentially stable if there exist $c, k, \lambda \in \mathbb{R}_+$ such that

$$\|x(t)\|_2 < k\|x(t_0)\|_2 e^{-\lambda(t-t_0)} \; ^\forall t \geq t_0 \geq 0, \; ^\forall \|x(t_0)\|_2 < c.$$

Exponential stability plays an important role for stability analysis of perturbed systems mentioned later.

Input-to-state Stability

We next introduce the notion of *input-to-state stability* of dynamical systems. Let us consider the system

$$\dot{x} = f(t, x, u), \tag{2.14}$$

where $f : [0, \infty) \times \mathbb{R}^n \times \mathbb{R}^p \to \mathbb{R}^n$ is piecewise continuous in t and locally Lipschitz in x and u. Then, [49] defines input-to-state stability as follows.

Definition 5. *The system (2.14) is said to be input-to-state stable if there exist a class $\mathcal{KL}$ function α and a class $\mathcal{K}$ function β such that for any initial states $x(0)$ and any bounded input $u(t)$, the solution $x(t)$ exists for all $t \geq 0$ and satisfies*

$$\|x(t)\|_2 \leq \alpha(\|x(0)\|_2, t) + \beta \left(\sup_{0 \leq \tau \leq t} \|u(\tau)\|_2 \right). \tag{2.15}$$

Inequality (2.15) guarantees that for any bounded input $u(t)$, the state $x(t)$ would be bounded. Furthermore, as t increases, the state $x(t)$ would be ultimately bounded by a class $\mathcal{K}$ function of $\sup_{t \geq 0} \|u(t)\|_2$. If the system (2.14) is input-to-state stable and $u(t)$ converges to zero as $t \to \infty$, so does $x(t)$.

$\mathcal{L}_2$ Stability

We next give the notion of $\mathcal{L}_2$ *stability* as a variation of *input-to-output stability* concepts [49, 51]. In the context of this dissertation, it is sufficient to define $\mathcal{L}_2$ stability for the dynamical system

$$\begin{cases} \dot{x} = f(x, u) \\ y = h(x, u) \end{cases}, \tag{2.16}$$

where $f : \mathbb{R}^n \times \mathbb{R}^p \to \mathbb{R}^n$ and $h : \mathbb{R}^n \times \mathbb{R}^p \to \mathbb{R}^q$. However, to ensure correctness, we start with slightly formal descriptions using input-output maps.

Let us denote by Ξ the space of piecewise continuous, square-integrable functions $u : [0, \infty) \to \mathbb{R}^p$. Then, we define the space

$$\mathcal{L}_2 := \{u \in \Xi \mid \|u\|_{\mathcal{L}_2} < \infty\}, \ \|u\|_{\mathcal{L}_2} := \sqrt{\int_0^\infty \|u(t)\|_2^2 dt}.$$

In order to deal with unbounded growing signals like $u(t) = t$, we also introduce the extended $\mathcal{L}_2$ space, denoted by $\mathcal{L}_{2e}$, as follows.

$$\mathcal{L}_{2e} := \{u \in \Xi \mid u_\tau \in \mathcal{L}_2 \ ^\forall \tau \in [0, \infty)\}, \ u_\tau(t) := \begin{cases} u(t), & 0 \leq t \leq \tau \\ 0, & t > \tau \end{cases}.$$

Here, u_τ is called truncation of u. It is clear from the definitions that the extended space $\mathcal{L}_{2e}$ contains the unextended space $\mathcal{L}_2$ as a subset.

We next consider a causal[1] input-output mapping $H : \mathcal{L}_{2e} \to \mathcal{L}_{2e}$. Then, $\mathcal{L}_2$ stability is defined as follows [49, 51].

Definition 6. *A mapping $H : \mathcal{L}_{2e} \to \mathcal{L}_{2e}$ is $\mathcal{L}_2$-stable if there exist a class $\mathcal{K}$ function α, defined on $[0, \infty)$, and a nonnegative constant β such that*

$$\|(Hu)_\tau\|_{\mathcal{L}_2} \leq \alpha(\|u_\tau\|_{\mathcal{L}_2}) + \beta$$

for all $u \in \mathcal{L}_{2e}$ and $\tau \in [0, \infty)$. In addition, the mapping H is finite $\mathcal{L}_2$-gain stable if there exist nonnegative constants γ and β such that

$$\|(Hu)_\tau\|_{\mathcal{L}_2} \leq \gamma \|u_\tau\|_{\mathcal{L}_2} + \beta \tag{2.17}$$

---

[1]A map $H : \mathcal{L}_{2e} \to \mathcal{L}_{2e}$ is said to be causal if the output $(Hu)(\tau)$ at any time $\tau \in [0, \infty)$ is dependent only on the past and current profile of input $u(t)$, $t \leq \tau$, i.e. $(Hu)_\tau = (Hu_\tau)_\tau$ holds for all $u \in \mathcal{L}_{2e}$ and $\tau \in [0, \infty)$.

for all $u \in \mathcal{L}_{2e}$ and $\tau \in [0, \infty)$. Then, H is said to have finite $\mathcal{L}_2$-gain which is defined as

$$\gamma(H) := \inf\{\gamma \in [0, \infty) \mid {}^{\exists}\beta \text{ s.t. } (2.17) \text{ holds.}\}.$$

The constant β is called bias term. It is included in the definition to allow for systems where Hu does not vanish at $u = 0$. When the inequality (2.17) is satisfied, we are usually interested in the smallest possible γ for which there exists β satisfying (2.17). In visual feedback attitude/pose synchronization problems with Assumption 1, we utilize this notion as an indicator of a performance by regarding an individual velocity of a leader and total control errors of the visual robotic network Σ as the input and the output of error systems, respectively.

Stability of Perturbed Systems

We finally introduce a part of stability theory of perturbed systems based on [49]. Let us now consider the nonlinear system

$$\dot{x} = f(t, x) + g(t, x), \tag{2.18}$$

where $f : [0, \infty) \times \mathcal{D} \to \mathbb{R}^n$ and $g : [0, \infty) \times \mathcal{D} \to \mathbb{R}^n$ are piecewise continuous in time t and locally Lipschitz in x on $[0, \infty) \times \mathcal{D}$, and $\mathcal{D} \subset \mathbb{R}^n$ is a domain that contains the origin $x = 0$. We think of this system as a perturbation of the nominal system

$$\dot{x} = f(t, x). \tag{2.19}$$

Suppose the perturbation term $g(t, x)$ satisfies the following bound.

$$\|g(t, x)\|_2 \leq \delta(t) \; {}^{\forall}t \geq 0, \; {}^{\forall}x \in \mathcal{D}, \tag{2.20}$$

where $\delta : \mathbb{R} \to \mathbb{R}$ is nonnegative, continuous and bounded for all $t \geq 0$. Then, we get the following proposition from Lemmas 9.4 and 9.6 in [49].

Proposition 1. *Let $x = 0$ be an exponentially stable equilibrium point of the nominal system (2.19). Let $V(t, x)$ be a Lyapunov function the nominal system that satisfies*

$$c_1\|x\|_2^2 \leq V(t, x) \leq c_2\|x\|_2^2,$$

$$\frac{\partial V}{\partial t} + \frac{\partial V}{\partial x}f(t, x) \leq -c_3\|x\|_2^2,$$

$$\left\|\frac{\partial V}{\partial x}\right\|_2 \leq c_4\|x\|_2$$

for all $(t, x) \in [0, \infty) \times \mathcal{D}$ for some positive constants c_1, c_2, c_3 and c_4, where $\mathcal{D} := \{x \in \mathbb{R}^n \mid \|x\|_2 < r, \; r \in \mathbb{R}_+\}$. Suppose the perturbation term $g(t, x)$ satisfies (2.20) and $\lim_{t \to \infty} \delta(t) = 0$ holds. Then, provided $x(t_0)$ satisfies $\|x(t_0)\| < r\sqrt{c_1/c_2}$, the solution of the perturbed system (2.18) satisfies $\lim_{t \to \infty} x(t) = 0$.

In this dissertation, we often utilize this proposition for convergence analysis.

2.4.3 Review of Previous Works

We finally review the previous results presented in [46, 47, 48] and [44] as the basis of this work.

Attitude/Pose Synchronization

We first review one of the previous results presented in [46]. In order to achieve attitude synchronization (defined by (2.10) without the limitation of the measured output), [46] proposes the velocity input

$$\begin{cases} v_{wi}^b = v \\ \omega_{wi}^b = k_{Ri} \sum_{j \in \mathcal{N}_i} \text{sk}(e^{\hat{\xi}\theta_{ij}})^\vee \ , \ k_{Ri} \in \mathbb{R}_+, \ i \in \mathcal{V}, \end{cases} \tag{2.21}$$

where $v \in \mathbb{R}^3$ is a common body velocity among all the rigid bodies. Note that the present angular velocity input is formed by the output errors of passivity of the rigid body motion (2.2) (see Lemma 1). This passivity-based approach is originally proposed in [9, 58].

The authors in [46] show the following fact.

Fact 1. *Suppose that there exists $e^{\hat{\xi}\theta_a} \in SO(3)$ such that $e^{-\hat{\xi}\theta_a}e^{\hat{\xi}\theta_{wi}} \ \forall i \in \mathcal{V}$ are positive definite[2] at the initial time and the fixed interconnection topology is strongly connected [70]. Then, the velocity input (2.21) achieves attitude synchronization in the sense of (2.10).*

We next introduce the previous result presented in [47, 48]. The paper [47, 48] proposes the following velocity input to achieve pose synchronization (defined by (2.11) without the limitation of measured output).

$$V_{wi}^b = \begin{bmatrix} k_{pi}I_3 & 0 \\ 0 & k_{Ri}I_3 \end{bmatrix} \sum_{j \in \mathcal{N}_i} \begin{bmatrix} p_{ij} \\ \text{sk}(e^{\hat{\xi}\theta_{ij}})^\vee \end{bmatrix}, \ k_{pi}, k_{Ri} \in \mathbb{R}_+, \ i \in \mathcal{V}. \tag{2.22}$$

It should be again noted that the present velocity input is formed by the output errors of passivity of the rigid body motion (2.2) (see Lemma 1) which are dependent only on relative poses.

The authors in [47, 48] show the following fact for $d_{ij} = 0 \ \forall i, j \in \mathcal{V}$.

Fact 2. *Suppose that there exists $e^{\hat{\xi}\theta_a} \in SO(3)$ such that $e^{-\hat{\xi}\theta_a}e^{\hat{\xi}\theta_{wi}} \ \forall i \in \mathcal{V}$ are positive definite at the initial time and the fixed interconnection topology is strongly connected. Then, the velocity input (2.22) achieves pose synchronization in the sense of (2.11). In addition, if $e^{\hat{\xi}\theta_{ij}} \ \forall i, j \in \mathcal{V}$ are positive definite at the initial time, then the velocity input (2.22) achieves pose synchronization if and only if the fixed interconnection topology has a directed spanning tree [70].*

---

[2]Throughout this work, we refer to a real square matrix $M \in \mathbb{R}^{n \times n}$, not necessarily symmetric, as a positive definite matrix if and only if $x^\text{T}Mx > 0$ holds for all nonzero vectors $x \in \mathbb{R}^n$.

Visual Motion Observer

We finally review the pose estimation mechanism of a target object relative to vision, called *visual motion observer*, presented in [44]. Here, we deal with only the pinhole camera model for a vision model.

We consider the case that rigid body i sees body j. Notice then that, in order to implement the velocity input (2.21) or (2.22), body i has to estimate the relative pose g_{ij} by building a nonlinear observer since visual measurements (2.9) are only available for body i. Hereafter, we denote the estimate of g_{ij} by $\bar{g}_{ij} = (\bar{p}_{ij}, e^{\hat{\xi}\bar{\theta}_{ij}}) \in SE(3)$. Similarly to the Luenberger-type observer [71], we build a model of the actual relative rigid body motion (2.3) as

$$\bar{V}_{ij}^b := (\bar{g}_{ij}^{-1}\dot{\bar{g}}_{ij})^\vee = -\mathrm{Ad}_{(\bar{g}_{ij}^{-1})}V_{wi}^b + u_e. \tag{2.23}$$

Here, the term $u_e \in \mathbb{R}^6$ is external input to be determined so that the estimated value $\bar{g}_{ij}$ is driven to its actual value g_{ij}. Once the estimate $\bar{g}_{ij}$ is determined, the estimated measurements $\bar{f}_{ij}$ is also computed by (2.5).

In order to establish the estimation error system, we define the estimation error $g_{eij} = (p_{eij}, e^{\hat{\xi}\theta_{eij}}) \in SE(3)$ between the actual relative pose g_{ij} and its estimate $\bar{g}_{ij}$, and the estimation error vector $e_{eij} \in \mathbb{R}^6$ as

$$g_{eij} := \bar{g}_{ij}^{-1}g_{ij}, \ e_{eij} := \begin{bmatrix} p_{eij} \\ \mathrm{sk}(e^{\hat{\xi}\theta_{eij}})^\vee \end{bmatrix}.$$

Notice now that $e_{eij} = 0$ if and only if $g_{eij} = I_4$ for $\theta_{eij} \in (-\pi, \pi)$, i.e. $\bar{g}_{ij} = g_{ij}$ holds. It should be also noted that e_{eij} can be approximately reconstructed by visual measurements f_{ij} and the estimated relative pose $\bar{g}_{ij}$ (see Appendix A.1). By differentiating g_{eij} with respect to time with (2.3) and (2.23), the estimation error system is given by

$$\dot{g}_{eij} = -\hat{u}_e g_{eij} + g_{eij}\hat{V}_{wj}^b,$$

or the vector form

$$V_{eij}^b := (g_{eij}^{-1}\dot{g}_{eij})^\vee = -\mathrm{Ad}_{(g_{eij}^{-1})}u_e + V_{wj}^b. \tag{2.24}$$

Then, we have the following lemma.

Lemma 3. *If $V_{wj}^b = 0$ holds, then the time derivative of $\psi(g_{eij})$ along the trajectory of (2.24) satisfies*

$$\dot{\psi}(g_{eij}) = u_e^\mathrm{T}(-e_{eij}).$$

Figure 2.12: Block Diagram of Vision Motion Observer

Proof. When $V_{wj}^b = 0$ holds, the time derivative of $\psi(g_{eij})$ along the trajectories of (2.24) gives us

$$
\begin{aligned}
\dot{\psi}(g_{eij}) &= p_{eij}^{\mathrm{T}}\dot{p}_{eij} + (\mathrm{sk}(e^{\hat{\xi}\theta_{eij}})^{\vee})^{\mathrm{T}}\omega_{eij}^b \\
&= p_{eij}^{\mathrm{T}}e^{\hat{\xi}\theta_{eij}}e^{-\hat{\xi}\theta_{eij}}\dot{p}_{eij} + (\mathrm{sk}(e^{\hat{\xi}\theta_{eij}})^{\vee})^{\mathrm{T}}e^{\hat{\xi}\theta_{eij}}\omega_{eij}^b \quad (\because \text{Appendix B.2.7}) \\
&= \begin{bmatrix} p_{eij}^{\mathrm{T}} & (\mathrm{sk}(e^{\hat{\xi}\theta_{eij}})^{\vee})^{\mathrm{T}} \end{bmatrix} \begin{bmatrix} e^{\hat{\xi}\theta_{eij}} & 0 \\ 0 & e^{\hat{\xi}\theta_{eij}} \end{bmatrix} \begin{bmatrix} v_{eij}^b \\ \omega_{eij}^b \end{bmatrix} \\
&= e_{eij}^{\mathrm{T}}\mathrm{Ad}_{(e^{\hat{\xi}\theta_{eij}})}V_{eij}^b \quad (2.25) \\
&= -e_{eij}^{\mathrm{T}}\mathrm{Ad}_{(e^{\hat{\xi}\theta_{eij}})}\mathrm{Ad}_{(g_{eij}^{-1})}u_e \quad (\because \text{Eq. (2.24) with } V_{wj}^b = 0) \\
&= -e_{eij}^{\mathrm{T}}\mathrm{Ad}_{(-p_{eij})}u_e \\
&= u_e^{\mathrm{T}}(-e_{eij}), \quad (\because p_{eij}^{\mathrm{T}}\hat{p}_{eij}u_{eR} = -p_{eij}^{\mathrm{T}}\hat{u}_{eR}p_{eij} = 0 \text{ (Appendix B.1.2))}
\end{aligned}
$$

where we use the notations $V_{eij}^b = [(v_{eij}^b)^{\mathrm{T}} \ (\omega_{eij}^b)^{\mathrm{T}}]^{\mathrm{T}}$ and $u_e = [u_{ep}^{\mathrm{T}} \ u_{eR}^{\mathrm{T}}]^{\mathrm{T}}$. □

Lemma 3 means that the estimation error system (2.24) is passive from u_e to $-e_{eij}$ with the storage function $\psi(g_{eij})$ when $V_{wj}^b = 0$ holds.

Based on the passivity, the authors in [44] propose the observer input

$$
u_e = -k(-e_{eij}) = ke_{eij}, \ k \in \mathbb{R}_+, \quad (2.26)
$$

and give the following fact.

27

Fact 3. *If $V_{wj}^b = 0$ holds, then the equilibrium point $e_{eij} = 0$ for the closed-loop system (2.24) with (2.26) is asymptotically stable. In addition, given $\kappa \in \mathbb{R}_+$, if k satisfies*

$$k - \frac{1}{2\kappa^2} - \frac{1}{2} > 0,$$

then the closed-loop system with the input V_{wj}^b and the output e_{eij} has $\mathcal{L}_2$-gain smaller than or equal to κ.

The first claim means that the visual motion observer leads the estimate $\bar{g}_{ij}$ to the actual relative pose g_{ij} for a static body j. On the other hand, the second statement says that the observer works even for a moving body j, and the parameter κ is an indicator on estimation accuracy. The block diagram of the visual motion observer is illustrated in Fig. 2.12.

2.5 Chapter Summary

In this chapter, we have given the problem formulation of visual feedback attitude/pose synchronization on $SE(3)$. We have first introduced visual robotic networks to be controlled throughout this work. Here, in addition to multiple rigid bodies and interconnection topologies between bodies, we explicitly formulate the measured output of each body, which is one of the main contributions of this work. As a result, the interconnection topologies are regarded as visibility structures where information flows are defined by who sees whom. We have then given the definitions of visual feedback attitude/pose synchronization for visual robotic networks as the goals of this work. These goals are the same as in our previous works [46, 47, 48] except for imposing the restriction of measured output. We have next introduced passivity of the rigid body motion and the relative rigid body motion. This property would play a central role to propose visual feedback attitude/pose synchronization laws in the subsequent chapters. Then, some stability concepts of dynamical systems have been introduced for the subsequent analysis. Here, in addition to asymptotic stability analysis which implies synchronization in the sense of the definitions, we have introduced the notions of input-to-state stability and $\mathcal{L}_2$ stability for performance analysis of control laws for undesired disturbances. Finally, we have reviewed previous results associated with this work as foundations.

Chapter 3

Visual Feedback 3D Attitude Synchronization

3.1 Introduction

In this chapter, we investigate a leader-following visual feedback attitude synchronization problem for visual robotic networks Σ. The goal of this chapter is to propose a control law to achieve visual feedback attitude synchronization (2.10) for networks satisfying Assumption 1. We first propose a synchronization law based on the passivity-based attitude synchronization law and the visual motion observer introduced in Chapter 2. In the present estimation and control scheme, relative orientations necessary for the attitude synchronization law are estimated by a visual motion observer. We then prove synchronization, where passivity of the rigid body motion (2.2) and the relative rigid body motion (2.3) plays a central role. However, in the present control scheme, the leader does not rotate, and as a result, the network cannot change the direction of the movement. In order to overcome this issue, we next consider the case that the leader rotates independently. In this situation, we give tracking performance analysis of the network for the leader by employing the theory of input-to-state stability or $\mathcal{L}_2$ stability. Here, we regard the angular velocity of the leader as an external disturbance to the network. The effectiveness of the estimation and control mechanism is demonstrated through simulation in three dimensions and experiments on a planar testbed.

This chapter is organized as follows. In Section 3.2, we propose an estimation and control mechanism for the visual robotic network Σ to achieve visual feedback attitude synchronization. Then, we give the convergence analysis for a not rotating leader in Section 3.3. In Section 3.4, we analyze the tracking performance analysis of the network for a leader having arbitrary angular velocities. We finally give verifications of the present convergence and performance analysis through simulation and experiments in Section 3.5. Section 3.6 concludes this chapter.

3.2 Visual Feedback Attitude Synchronization Law

In this section, we propose a visual feedback attitude synchronization law for rigid bodies with the pinhole camera model (2.5). Unlike the previous work [46] premising the measurement of $e^{\hat{\xi}\theta_{ij}}$, the goal of this chapter is to propose a velocity law for visual feedback attitude synchronization (2.10) by using only visual measurements (2.9). Note thus that each body has to estimate relative poses g_{ij}, $j \in \mathcal{N}_i$ by a nonlinear observer since visual measurements (2.9) are two dimensional.

We use the same notation $\bar{g}_{ij} \in SE(3)$ for the estimate of g_{ij} and definitions $g_{eij} \in SE(3)$ and $e_{eij} \in \mathbb{R}^6$ for the estimation error between g_{ij} and $\bar{g}_{ij}$ as in Subsection 2.4.3. Notice again that $e_{eij} = 0$ if and only if $g_{eij} = I_4$ for $\theta_{eij} \in (-\pi, \pi)$, and then $\bar{g}_{ij} = g_{ij}$ holds. Therefore, both $\mathrm{sk}(e^{\hat{\bar{\xi}}\bar{\theta}_{ij}})^\vee = 0$ and $e_{eij} = 0$ mean $e^{\hat{\xi}\theta_{ij}} = I_3$, i.e. visual feedback attitude synchronization (2.10) is achieved if and only if $\mathrm{sk}(e^{\hat{\bar{\xi}}\bar{\theta}_{ij}})^\vee = 0$, $e_{eij} = 0$ with $v_{wi}^b = v$ for all $j \in \mathcal{N}_i$, $i \in \mathcal{V}$ ($v \in \mathbb{R}^3$ is a common linear velocity among all the rigid bodies).

In order to achieve visual feedback attitude synchronization (2.10), we propose the following control law.

$$\textit{Controller:} \begin{cases} v_{wi}^b = v, & \text{(3.1a)} \\ \omega_{wi}^b = k_{ci} \sum_{j \in \mathcal{N}_i} \mathrm{sk}(e^{\hat{\bar{\xi}}\bar{\theta}_{ij}})^\vee, & \text{(3.1b)} \end{cases}$$

$$\textit{Observer:} \begin{cases} \bar{V}_{ij}^b := (\bar{g}_{ij}^{-1}\dot{\bar{g}}_{ij})^\vee = -\mathrm{Ad}_{(\bar{g}_{ij}^{-1})}V_{wi}^b + u_{ij}, & \text{(3.1c)} \\ u_{ij} = k_{ei}\left(e_{eij} - \begin{bmatrix} 0 \\ \mathrm{sk}(e^{\hat{\bar{\xi}}\bar{\theta}_{ij}})^\vee \end{bmatrix}\right) + \begin{bmatrix} e^{\hat{\xi}\theta_{eij}}v \\ 0 \end{bmatrix}, & \text{(3.1d)} \end{cases}$$

where $j \in \mathcal{N}_i$, $i \in \mathcal{V}$ and $k_{ci}, k_{ei} \in \mathbb{R}_+$ $^\forall i \in \mathcal{V}$. The block diagram of the estimation and control mechanism (3.1) is shown in Fig. 3.1. The angular velocity input (3.1b) is the same as (2.21) except for using $e^{\hat{\bar{\xi}}\bar{\theta}_{ij}}$ instead of $e^{\hat{\xi}\theta_{ij}}$. In the nonlinear observer, (3.1c) simulates the relative rigid body motion (2.3) by utilizing the estimate $\bar{g}_{ij}$ as its state. Here, $u_{ij} \in \mathbb{R}^6$ is external input to be determined so that the estimated value $\bar{g}_{ij}$ is driven to its actual value g_{ij}, which is given by (3.1d). In (3.1d), e_{eij} (and hence $e^{\hat{\xi}\theta_{eij}}$) can be reconstructed by visual measurements f_{ij} (see Appendix A.1). This means that the present control law (3.1) can be calculated only by visual measurements (2.9) in the absence of communication or any measurements of own states. It is thus sufficient for visual feedback attitude synchronization to show that the present control law (3.1) achieves (2.10). For the panoramic camera model, if we deal with $\bar{g}_{m_ij}$, the appropriate relative rigid body motion model associated with (2.6) and $\mathrm{Ad}_{(g_{im_i}^{-1})}V_{wi}^b$ instead of $\bar{g}_{ij}$, (2.3) and V_{wi}^b, respectively, then the subsequent discussions hold. The details on the panoramic
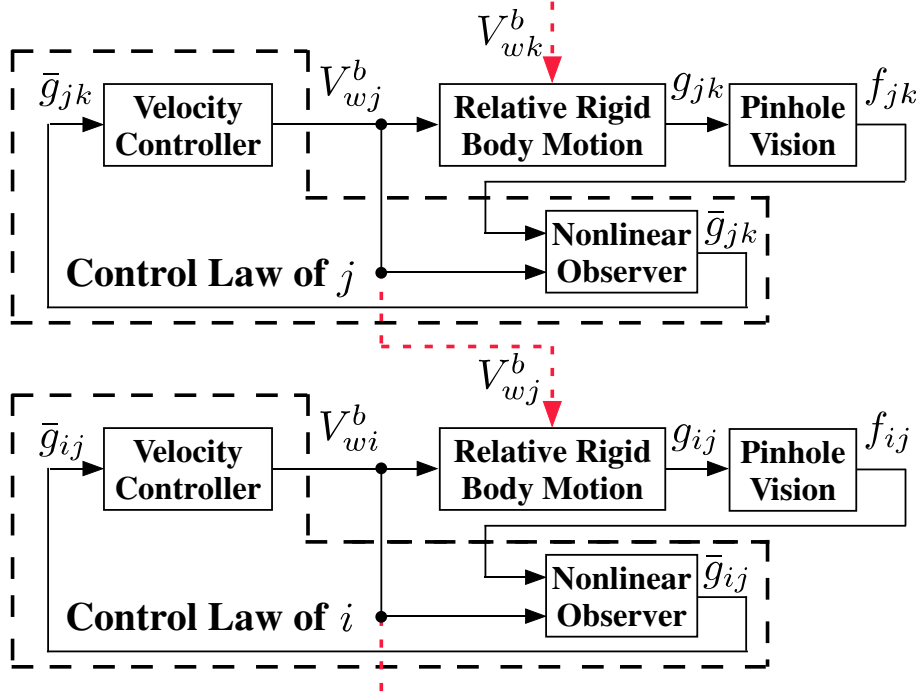
Figure 3.1: Block Diagram of Visual Feedback Attitude Synchronization Law

camera model are given in Chapter 4.

Remark 5. The structure of the angular velocity input (3.1b) is based on the passivity of the rigid body motion (2.2) similarly to (2.21). Moreover, the vision-based observer input (3.1d) is designed based on the fact that the estimation error system (2.24) is passive. Thus, the present estimation and control mechanism is called *passivity-based mechanism*.

3.3   Convergence Analysis

In this section, we give convergence analysis for the visual robotic network Σ with the present visual feedback attitude synchronization law (3.1). We assume that visibility structures in Σ satisfy Assumption 1. Then, it is shown that the control law (3.1) on Σ achieves visual feedback attitude synchronization in the sense of (2.10).

We first note that similarly to Subsection 2.4.3, differentiating g_{eij} with respect to time with (2.3) and (3.1c) gives the estimation error system (2.24) for each visible body pair (i,j), $(j,i) \in \mathcal{E}$, and the system (2.24) is passive from u_{ij} to $-e_{eij}$ with the storage function $\psi(g_{eij})$ when $V_{wj}^b = 0$ holds (see Lemma 3). We next regard $e^{\hat{\bar{\xi}}\bar{\theta}_{ij}}$ as the control error for each visible body pair (i,j), $(j,i) \in \mathcal{E}$ since both $e^{\hat{\bar{\xi}}\bar{\theta}_{ij}} = I_3$ and $e_{eij} = I_3$ mean

$e^{\hat{\xi}\theta_{ij}} = I_3$. Also, we think of the orientation part of (3.1c) as the control error system. We next introduce a total error system for each visible body pair by combining the control error system with the estimation error system (2.24) as follows.

$$\begin{bmatrix} \bar{\omega}_{ij}^b \\ V_{eij}^b \end{bmatrix} = \begin{bmatrix} -e^{-\hat{\bar{\xi}}\bar{\theta}_{ij}} & 0 & I_3 \\ 0 & -\mathrm{Ad}_{(g_{eij}^{-1})} \end{bmatrix} \begin{bmatrix} \omega_{wi}^b \\ u_{ij} \end{bmatrix} + \begin{bmatrix} 0 \\ V_{wj}^b \end{bmatrix}, \tag{3.2}$$

where we use the notation $\bar{V}_{ij}^b = [(\bar{v}_{ij}^b)^{\mathrm{T}} \ (\bar{\omega}_{ij}^b)^{\mathrm{T}}]^{\mathrm{T}}$. We now define a potential function $U_{aij} \geq 0$ as

$$U_{aij} := \phi(e^{\hat{\bar{\xi}}\bar{\theta}_{ij}}) + \psi(g_{eij}). \tag{3.3}$$

Then, we have the following lemma.

Lemma 4. *If $V_{wj}^b = 0$ holds, then the time derivative of U_{aij} along the trajectory of (3.2) satisfies*

$$\dot{U}_{aij} = [(\omega_{wi}^b)^{\mathrm{T}} \ u_{ij}^{\mathrm{T}}] \begin{bmatrix} -I_3 & 0 \\ 0 & -I_6 \\ I_3 \end{bmatrix} \begin{bmatrix} \mathrm{sk}(e^{\hat{\bar{\xi}}\bar{\theta}_{ij}})^{\vee} \\ e_{eij} \end{bmatrix}.$$

Proof. The time derivative of U_{aij} along the trajectory of (3.2) yields

$$\begin{aligned} \dot{U}_{aij} &= (\mathrm{sk}(e^{\hat{\bar{\xi}}\bar{\theta}_{ij}})^{\vee})^{\mathrm{T}}\bar{\omega}_{ij}^b + e_{eij}^{\mathrm{T}}\mathrm{Ad}_{(e^{\hat{\xi}\theta_{eij}})}V_{eij}^b \quad (\because \text{ Appendix B.3.2 and Eq. (2.25)}) \\ &= -(\mathrm{sk}(e^{\hat{\bar{\xi}}\bar{\theta}_{ij}})^{\vee})^{\mathrm{T}}(e^{-\hat{\bar{\xi}}\bar{\theta}_{ij}}\omega_{wi}^b - u_{Rij}) - e_{eij}^{\mathrm{T}}u_{ij} \quad (\because \text{ Eq. (3.2) with } V_{wj}^b = 0) \\ &= -(\mathrm{sk}(e^{\hat{\bar{\xi}}\bar{\theta}_{ij}})^{\vee})^{\mathrm{T}}\omega_{wi}^b + (\mathrm{sk}(e^{\hat{\bar{\xi}}\bar{\theta}_{ij}})^{\vee})^{\mathrm{T}}u_{Rij} - e_{eij}^{\mathrm{T}}u_{ij} \quad (\because \text{ Appendix B.2.7}) \\ &= [(\omega_{wi}^b)^{\mathrm{T}} \ u_{ij}^{\mathrm{T}}] \begin{bmatrix} -I_3 & 0 \\ 0 & -I_6 \\ I_3 \end{bmatrix} \begin{bmatrix} \mathrm{sk}(e^{\hat{\bar{\xi}}\bar{\theta}_{ij}})^{\vee} \\ e_{eij} \end{bmatrix}, \end{aligned}$$

where we use the notation $u_{ij} = [u_{pij}^{\mathrm{T}} \ u_{Rij}^{\mathrm{T}}]^{\mathrm{T}}$. $\square$

Lemma 4 means that the total error system (3.2) is passive, and hence it can be considered that the present control law (3.1) is based on this passivity.

Based on Lemma 4, we get the following theorem.

Theorem 1. *Consider the visual robotic network Σ with Assumption 1. Then, the control law (3.1) on Σ achieves visual feedback attitude synchronization.*
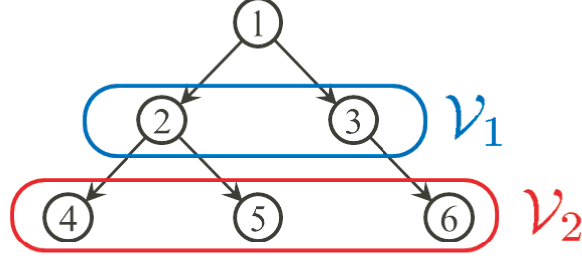
Figure 3.2: Definition of $\mathcal{V}_k$

Proof. We give the proof by dividing rigid bodies into some groups and using induction. Note first that under Assumption 1, each body except for the leader (body 1) has one fixed visible body and there exists a visibility path from each body to the leader (see Fig. 2.4). It should be also noted that the velocity input (3.1) makes the leader move with only v. We define rigid body sets $\mathcal{V}_k$, $k \in \mathbb{N}$ collecting bodies whose path length to the leader is equal to k (see Fig. 3.2).

We first consider each rigid body i in $\mathcal{V}_1$ whose visible body is body 1. Consider the potential function U_{ai1} (defined in (3.3) with $j = 1$) as a Lyapunov function candidate of the closed-loop system (3.2) and (3.1). Then, the time derivative of U_{ai1} along the trajectory of (3.2) yields

$$
\begin{aligned}
\dot{U}_{ai1} &= (\mathrm{sk}(e^{\hat{\bar{\xi}}\bar{\theta}_{i1}})^\vee)^{\mathrm{T}}\bar{\omega}_{i1}^b + e_{ei1}^{\mathrm{T}}\mathrm{Ad}_{(e^{\hat{\xi}\theta_{ei1}})}V_{ei1}^b \quad (\because \text{Appendix B.3.2 and Eq. (2.25)}) \\
&= -(\mathrm{sk}(e^{\hat{\bar{\xi}}\bar{\theta}_{i1}})^\vee)^{\mathrm{T}}(e^{-\hat{\bar{\xi}}\bar{\theta}_{i1}}\omega_{wi}^b - u_{Ri1}) - e_{ei1}^{\mathrm{T}}(u_{i1} - \mathrm{Ad}_{(e^{\hat{\xi}\theta_{ei1}})}V_{w1}^b) \quad (\because \text{Eq. (3.2)}) \\
&= -(\mathrm{sk}(e^{\hat{\bar{\xi}}\bar{\theta}_{i1}})^\vee)^{\mathrm{T}}((k_{ci} + k_{ei})\mathrm{sk}(e^{\hat{\bar{\xi}}\bar{\theta}_{i1}})^\vee - k_{ei}\mathrm{sk}(e^{\hat{\xi}\theta_{ei1}})^\vee) \\
&\qquad - k_{ei}e_{ei1}^{\mathrm{T}}e_{ei1} + k_{ei}(\mathrm{sk}(e^{\hat{\bar{\xi}}\bar{\theta}_{i1}})^\vee)^{\mathrm{T}}\mathrm{sk}(e^{\hat{\bar{\xi}}\bar{\theta}_{i1}})^\vee \quad (\because \text{Eq. (3.1)}) \\
&= -x_{i1}^{\mathrm{T}}Q_{ai}x_{i1}, \tag{3.4}
\end{aligned}
$$

where we use the following definitions.

$$
x_{i1} := \begin{bmatrix} \mathrm{sk}(e^{\hat{\bar{\xi}}\bar{\theta}_{i1}})^\vee \\ e_{ei1} \end{bmatrix} \in \mathbb{R}^9, \quad Q_{ai} := \begin{bmatrix} (k_{ci} + k_{ei})I_3 & 0 & -k_{ei}I_3 \\ & 0 & \\ -k_{ei}I_3 & & k_{ei}I_6 \end{bmatrix} \in \mathbb{R}^{9 \times 9}.
$$

Notice now that Q_{ai} is positive definite for any $k_{ci}, k_{ei} \in \mathbb{R}_+$, which can be shown by calculating the Schur complement [72]. This means that the equilibrium point $x_{i1} = 0$ is asymptotically stable. Then, we conclude from the definition of x_{i1} that all the bodies in $\mathcal{V}_1$ achieve visual feedback attitude synchronization in the sense of (2.10).

We next consider each rigid body i in $\mathcal{V}_2$ whose visible body exists in $\mathcal{V}_1$. Notice first that visible body j from body i has the transient angular velocity to achieve attitude

33

synchronization (i.e. $\omega_{wj}^b = k_{cj}\mathrm{sk}(e^{\hat{\bar{\xi}}\bar{\theta}_{j1}})^\vee$). We now substitute the present input (3.1) into the total error system (3.2) as follows.

$$
\begin{bmatrix} \bar{\omega}_{ij}^b \\ V_{eij}^b \end{bmatrix} = \begin{bmatrix} -e^{-\hat{\bar{\xi}}\bar{\theta}_{ij}} & 0 & I_3 \\ 0 & -\mathrm{Ad}_{(g_{eij}^{-1})} \end{bmatrix} \begin{bmatrix} k_{ci}\mathrm{sk}(e^{\hat{\bar{\xi}}\bar{\theta}_{ij}})^\vee \\ k_{ei}\left(e_{eij} - \begin{bmatrix} 0 \\ \mathrm{sk}(e^{\hat{\bar{\xi}}\bar{\theta}_{ij}})^\vee \end{bmatrix} \right) \end{bmatrix} + \begin{bmatrix} 0 \\ 0 \\ k_{cj}\mathrm{sk}(e^{\hat{\bar{\xi}}\bar{\theta}_{j1}})^\vee \end{bmatrix}. \quad (3.5)
$$

Here, it should be noted that the second term in (3.5) is equal to 0 when body j in $\mathcal{V}_1$ achieves visual feedback attitude synchronization. Notice also that $\bar{\omega}_{ij}^b$, V_{eij}^b and e_{eij} are functions of $e^{\hat{\bar{\xi}}\bar{\theta}_{ij}}$, $e^{\hat{\bar{\xi}}\bar{\theta}_{ij}}$ g_{eij} and $\dot{g}_{eij}$. Therefore, if we define the state $x_{ij} \in \mathbb{R}^9$ for (3.5) as

$$
x_{ij} := \begin{bmatrix} \mathrm{sk}(e^{\hat{\bar{\xi}}\bar{\theta}_{ij}})^\vee \\ e_{eij} \end{bmatrix}, \quad (3.6)
$$

we can apply Proposition 1 to the convergence analysis by regarding (3.5) as the perturbed system. Namely, it is sufficient to show that the equilibrium point $x_{ij} = 0$ for the system (3.5) without the second term is exponentially stable.

Consider the potential function U_{aij} defined in (3.3). Then, the time derivative of U_{aij} along the trajectory of (3.5) without the second term yields

$$
\dot{U}_{aij} = -x_{ij}^\mathrm{T} Q_{ai} x_{ij} \leq -\lambda_{min}(Q_{ai})\|x_{ij}\|_2^2 \leq 0, \quad (\because \text{Eq. (3.4)})
$$

where we use the following property for any symmetric and positive definite matrices $A \in \mathbb{R}^{n \times n}$ and vectors $a \in \mathbb{R}^n$ [72].

$$
\lambda_{min}(A)\|a\|_2^2 \leq a^\mathrm{T} A a \leq \lambda_{max}(A)\|a\|_2^2.
$$

Here, $\lambda_{min}(A)$ and $\lambda_{max}(A)$ denote the minimal eigenvalue and the maximum eigenvalue of A, respectively. Now, since U_{aij} monotonically decreases until $x_{ij} = 0$ is satisfied, there exists finite time $T > 0$ satisfying $U_{aij}(T) < 1$. Then, $\phi(e^{\hat{\bar{\xi}}\bar{\theta}_{ij}}) < 1$ and $\phi(e^{\hat{\xi}\theta_{eij}}) < 1$ hold from the definition of U_{aij}. We hence get the following inequalities for $t \geq T$ from the fact that $\phi(e^{\hat{\xi}\theta}) \leq \|\mathrm{sk}(e^{\hat{\xi}\theta})^\vee\|_2^2$ for $e^{\hat{\xi}\theta} > 0$ (see Appendix B.3.3).

$$
\dot{U}_{aij} \leq -\lambda_{min}(Q_{ai})\|x_{ij}\|_2^2 \leq -\lambda_{min}(Q_{ai})\left(\phi(e^{\hat{\bar{\xi}}\bar{\theta}_{ij}}) + \|p_{eij}\|_2^2 + \phi(e^{\hat{\xi}\theta_{eij}}) \right) \leq -\lambda_{min}(Q_{ai})U_{aij}.
$$

This means that the equilibrium point $x_{ij} = 0$ for the system (3.5) without the second term is exponentially stable after time T. We thus conclude from the definition of x_{ij} that all the rigid bodies in $\mathcal{V}_2$ achieves visual feedback attitude synchronization in the sense of (2.10).

We finally assume that each rigid body in $\mathcal{V}_l$ ($l \geq 3$) achieves visual feedback attitude synchronization among the groups in $\{\mathcal{V}_l, \mathcal{V}_{l-1}, \cdots, \mathcal{V}_1, \{1\}\}$ and consider each body in

34

$\mathcal{V}_{l+1}$. Then, from the definition of $\mathcal{V}_{l+1}$, each body i in $\mathcal{V}_{l+1}$ has its visible body j in $\mathcal{V}_l$. We hence obtain the following system.

$$
\begin{bmatrix} \bar{\omega}_{ij}^b \\ V_{eij}^b \end{bmatrix} = \begin{bmatrix} -e^{-\hat{\bar{\xi}}\bar{\theta}_{ij}} & 0 & I_3 \\ 0 & -\mathrm{Ad}_{(g_{eij}^{-1})} \end{bmatrix} \begin{bmatrix} k_{ci}\mathrm{sk}(e^{\hat{\bar{\xi}}\bar{\theta}_{ij}})^\vee \\ k_{ei}\left(e_{eij} - \begin{bmatrix} 0 \\ \mathrm{sk}(e^{\hat{\bar{\xi}}\bar{\theta}_{ij}})^\vee \end{bmatrix}\right) \end{bmatrix} + \begin{bmatrix} 0 \\ 0 \\ k_{cj}\mathrm{sk}(e^{\hat{\bar{\xi}}\bar{\theta}_{jk}})^\vee \end{bmatrix}, \quad (3.7)
$$

where $k \in \mathcal{N}_j$. Now, since visual feedback attitude synchronization is achieved among the groups in $\{\mathcal{V}_l, \mathcal{V}_{l-1}, \cdots, \mathcal{V}_1, \{1\}\}$, the second term of (3.7) in this case also eventually converges to 0. Namely, by the same analysis as for bodies in $\mathcal{V}_2$, we can show that each body in $\mathcal{V}_{l+1}$ also achieves visual feedback attitude synchronization among the groups in $\{\mathcal{V}_{l+1}, \cdots, \mathcal{V}_1, \{1\}\}$. This completes the proof. □

Remark 6. It should be noted that Theorem 1 proves synchronization for the system integrating the observers instead employing certainly equivalence principle. It is well known in robot control that proving stability for the integrated system in observer-based control strategies is much more difficult than the individual estimation and control problems even for a single passive system [73, 74, 75]. It should be also true or might be much harder for synchronization since it is required to estimate not their own but the other individuals' information only from relative measurements [76, 77].

In Theorem 1, we show only qualitative stability analysis which enables us to set any positive gains. However, it is often required us obtain good transient behavior until attitude synchronization. Then, we can apply Lyapunov stability by considering the total estimation and control system and introducing the total Lyapunov function for the visual robotic network Σ. This analysis yields gain conditions and they give gain setting guidelines. Refer to **Publications** [1] for the details.

Notice finally that the leader with the velocity input (3.1) does not rotate. Namely, all the rigid bodies would stop rotating in the final configuration though it is sometimes required for the visual robotic network Σ to move in the desired direction. Therefore, in the next section, we consider the case that the leader rotates independently, and we analyze the tracking performance of the other bodies based on the theory of input-to-state stability or $\mathcal{L}_2$ stability.

3.4 Performance Analysis

In this section, we give tracking performance analysis of the visual robotic network Σ for a leader having arbitrary angular velocities. In this analysis, we regard an angular velocity of the leader as an external disturbance to the network and evaluate the estimation and control errors by employing the theory of input-to-state stability or input-to-output stability. We first apply input-to-state stability analysis to the performance analysis,

where we respectively think of the velocity of the leader and the total estimation and control errors of all the other bodies as the external disturbance input to the network and the state of the total error system of the network. We also employ the theory of $\mathcal{L}_2$ stability as one of input-to-output stability for the performance analysis by regarding the total estimation and control errors as the output of the total error system.

3.4.1 Input-to-state Stability

We give input-to-state stability analysis for the visual feedback attitude synchronization law (3.1) as one of tracking performance analysis of the visual robotic network Σ for a rotating leader.

We first consider the case that rigid body i sees body j and apply the present control law (3.1). Here, we assume that body j moves with the common linear velocity v and arbitrary angular velocity ω_{wj}^b. Then, the closed-loop system (3.2) and (3.1) with $\omega_{wj}^b \neq 0$ is given by

$$\begin{bmatrix} \bar{\omega}_{ij}^b \\ V_{eij}^b \end{bmatrix} = \begin{bmatrix} -e^{-\hat{\bar{\xi}}\bar{\theta}_{ij}} & 0 & I_3 \\ 0 & -\mathrm{Ad}_{(g_{eij}^{-1})} \end{bmatrix} \begin{bmatrix} k_{ci}\mathrm{sk}(e^{\hat{\bar{\xi}}\bar{\theta}_{ij}})^\vee \\ k_{ei}\left(e_{eij} - \begin{bmatrix} 0 \\ \mathrm{sk}(e^{\hat{\bar{\xi}}\bar{\theta}_{ij}})^\vee \end{bmatrix} \right) \end{bmatrix} + \begin{bmatrix} 0 \\ \begin{bmatrix} 0 \\ \omega_{wj}^b \end{bmatrix} \end{bmatrix}. \tag{3.8}$$

We regard ω_{wj}^b and x_{ij} defined in (3.6) as the input and the state of the system (3.8), respectively. We then get the following lemma.

Lemma 5. *Consider the system (3.8). If $\bar{\theta}_{ij}(0) \in (-\pi/2, \pi/2)$ and $\theta_{eij}(0) \in (-\pi/2, \pi/2)$ hold and the gain conditions (3.9) are satisfied for any $\epsilon_i, \epsilon_i' \in \mathbb{R}_+$ ($\epsilon_i' > \epsilon_i$), then there exist a class-$\mathcal{KL}$ function α_2 and a class $\mathcal{K}$ function β_2 satisfying (3.10).*

$$\begin{cases} k_{ci} + k_{ei} > \epsilon_i \\ \frac{k_{ei}(k_{ci}-\epsilon_i)}{k_{ci}+k_{ei}-\epsilon_i} > \epsilon_i' \end{cases}, \tag{3.9}$$

$$\|x_{ij}(t)\|_2 \leq \alpha_2(\|x_{ij}(0)\|_2, t) + \beta_2\left(\sup_{0 \leq \tau \leq t} \|\omega_{wj}^b(\tau)\|_2 \right). \tag{3.10}$$

Proof. Consider the potential function U_{aij} defined in (3.3). Then, we get the following equality from (3.4) with $\omega_{wj}^b \neq 0$.

$$\begin{aligned} \dot{U}_{aij} &= -x_{ij}^\mathrm{T} Q_{ai} x_{ij} + (\mathrm{sk}(e^{\hat{\xi}\theta_{eij}})^\vee)^\mathrm{T} e^{\hat{\xi}\theta_{eij}} \omega_{wj}^b \\ &= -x_{ij}^\mathrm{T} Q_{ai} x_{ij} + (\mathrm{sk}(e^{\hat{\xi}\theta_{eij}})^\vee)^\mathrm{T} \omega_{wj}^b \quad (\because \text{Appendix B.2.7}). \end{aligned} \tag{3.11}$$

Let us now utilize completing square for any $\gamma_2 \in \mathbb{R}_+$ as follows.

$$(\mathrm{sk}(e^{\hat{\xi}\theta_{eij}})^\vee)^\mathrm{T} \omega_{wj}^b = -\frac{\gamma_2}{2}\left\| \omega_{wj}^b - \frac{1}{\gamma_2}\mathrm{sk}(e^{\hat{\xi}\theta_{eij}})^\vee \right\|_2^2 + \frac{\gamma_2}{2}\|\omega_{wj}^b\|_2^2 + \frac{1}{2\gamma_2}\|\mathrm{sk}(e^{\hat{\xi}\theta_{eij}})^\vee\|_2^2.$$

This yields

$$\dot{U}_{aij} \leq -x_{ij}^{\mathrm{T}} Q_{ai} x_{ij} + \frac{\gamma_2}{2}\|\omega_{wj}^b\|_2^2 + \frac{1}{2\gamma_2}\|\mathrm{sk}(e^{\hat{\xi}\theta_{eij}})^{\vee}\|_2^2.$$

Note here that by using the diagonal matrix $W_a \in \mathbb{R}^{9\times 9}$ whose (7,7), (8,8) and (9,9) elements are $1/(2\gamma_2)$ and the other elements are 0, the third term of the above inequality can be written by $x_{ij}^{\mathrm{T}} W_a x_{ij}$. This fact gives the following inequality for any $\epsilon_i \in \mathbb{R}_+$.

$$
\begin{aligned}
\dot{U}_{aij} &\leq -x_{ij}^{\mathrm{T}} Q_{ai} x_{ij} + \frac{\gamma_2}{2}\|\omega_{wj}^b\|_2^2 + x_{ij}^{\mathrm{T}} W_a x_{ij} + \epsilon_i\|x_{ij}\|_2^2 - \epsilon_i\|x_{ij}\|_2^2 \\
&= -x_{ij}^{\mathrm{T}} P_{ai} x_{ij} + \frac{\gamma_2}{2}\|\omega_{wj}^b\|_2^2 - \epsilon_i\|x_{ij}\|_2^2,
\end{aligned}
$$

where $P_{ai} \in \mathbb{R}^{9\times 9}$ is defined as

$$P_{ai} := Q_{ai} - W_a - \epsilon_i I_9.$$

Then calculating the Schur complement [72] of P_{ai} with $\epsilon_i' := 1/(2\gamma_2) + \epsilon_i$ gives the necessary and sufficient condition (3.9) for positive definiteness of P_{ai}. Therefore, if the conditions (3.9) are satisfied, we have

$$\dot{U}_{aij} \leq \frac{\gamma_2}{2}\|\omega_{wj}^b\|_2^2 - \epsilon_i\|x_{ij}\|_2^2.$$

Integrating the above inequality from 0 to T with respect to time yields

$$U_{aij}(T) - U_{aij}(0) \leq \frac{\gamma_2}{2}\int_0^T \|\omega_{wj}^b(t)\|_2^2 dt - \epsilon_i \int_0^T \|x_{ij}(t)\|_2^2 dt.$$

We thus obtain

$$\int_0^T \|x_{ij}(t)\|_2^2 dt \leq \frac{1}{\epsilon_i} U_{aij}(0) + \frac{\gamma_2}{2\epsilon_i}\int_0^T \|\omega_{wj}^b(t)\|_2^2 dt.$$

Finally, when $\bar{\theta}_{ij}(0) \in [-\pi/2, \pi/2]$ and $\theta_{eij}(0) \in [-\pi/2, \pi/2]$ hold, we get

$$
\begin{aligned}
U_{aij}(0) &= \phi(e^{\hat{\bar{\xi}}\bar{\theta}_{ij}}(0)) + \frac{1}{2}\|p_{eij}(0)\|_2^2 + \phi(e^{\hat{\xi}\theta_{eij}}(0)) \\
&\leq \|\mathrm{sk}(e^{\hat{\bar{\xi}}\bar{\theta}_{ij}}(0))^{\vee}\|_2^2 + \|p_{eij}(0)\|_2^2 + \|\mathrm{sk}(e^{\hat{\xi}\theta_{eij}}(0))^{\vee}\|_2^2 \quad (\because \text{Appendix B.3.3}) \\
&= \|x_{ij}(0)\|_2^2.
\end{aligned}
$$

This yields

$$\int_0^T \|x_{ij}(t)\|_2^2 dt \leq \frac{1}{\epsilon_i}\|x_{ij}(0)\|_2^2 + \frac{\gamma_2}{2\epsilon_i}\int_0^T \|\omega_{wj}^b(t)\|_2^2 dt.$$

Then, we conclude from [50] that the closed-loop system (3.8) is input-to-state stable and the definition of input-to-state stability gives (3.10). $\qquad\square$

37
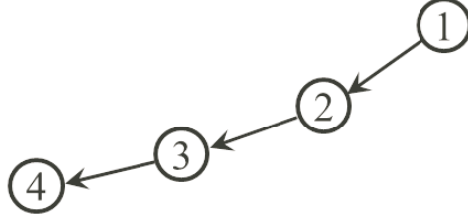
Figure 3.3: Chain-type Visibility Structure

Remark 7. Since ϵ_i and ϵ_i' are arbitrary positive scalars, the gain conditions (3.9) are satisfied for almost any positive gains k_{ci} and k_{ei}.

We next consider the case that m rigid bodies have the chain-type visibility structure, where body i sees body $i-1$ for $i \in \{2, \cdots, m\}$ (see Fig. 3.3). Then, we call the collection of the closed-loop system (3.2) and (3.1) for all the bodies *chain-type collective attitude error system* Σ_{ccola} whose state, denoted by $x_{ca} \in \mathbb{R}^{9(m-1)}$, is given by the stacked vector of $x_{i(i-1)}$, $i \in \{2, \cdots, m-1\}$. We now get the following lemma for Σ_{ccola}.

Lemma 6. *Consider the chain-type collective attitude error system* Σ_{ccola}. *If* $\bar{\theta}_{i(i-1)}(0) \in (-\pi/2, \pi/2)$, $\theta_{ei(i-1)}(0) \in (-\pi/2, \pi/2)$ *and the gain conditions (3.9) are satisfied for any* $\epsilon_i, \epsilon_i' \in \mathbb{R}_+$ ($\epsilon_i' > \epsilon_i$), $i \in \{2, \cdots, m\}$, *then there exist a class-$\mathcal{KL}$ function* α_c *and a class $\mathcal{K}$ function* β_c *satisfying*

$$\|x_{ca}(t)\|_2 \leq \alpha_c(\|x_{ca}(0)\|_2, t) + \beta_c \left(\sup_{0 \leq \tau \leq t} \|\omega_{w1}^b(\tau)\|_2 \right). \tag{3.12}$$

Proof. Notice that Lemma 5 means that the closed-loop system of rigid body i with the input $\omega_{w(i-1)}^b$ and the state $x_{i(i-1)}$ is input-to-state stable. It should be also noted that when we regard the angular velocity of body i as the input of the closed-loop system of body $i+1$, the input $\omega_{wi}^b = k_{ci}\text{sk}(e^{\hat{\xi}\bar{\theta}_{i(i-1)}})^\vee$ is a part of the state of that of body i (see Fig. 3.4). Therefore, we conclude from [50] that the cascade interconnection system of these systems is also input-to-state stable. By applying this property from the closed-loop system of body 2 to that of body m, we conclude that the chain-type collective attitude error system Σ_{ccola} is input-to-state stable. Finally, the definition of input-to-state stability gives (3.12). $\square$

We now show the main result of this subsection by using Lemma 6.

Theorem 2. *Consider the visual robotic network Σ with Assumption 1. Suppose that the leader has its own angular velocity (i.e. $\omega_{w1}^b \neq 0$). If $\bar{\theta}_{ij}(0) \in (-\pi/2, \pi/2)$, $\theta_{eij}(0) \in$*
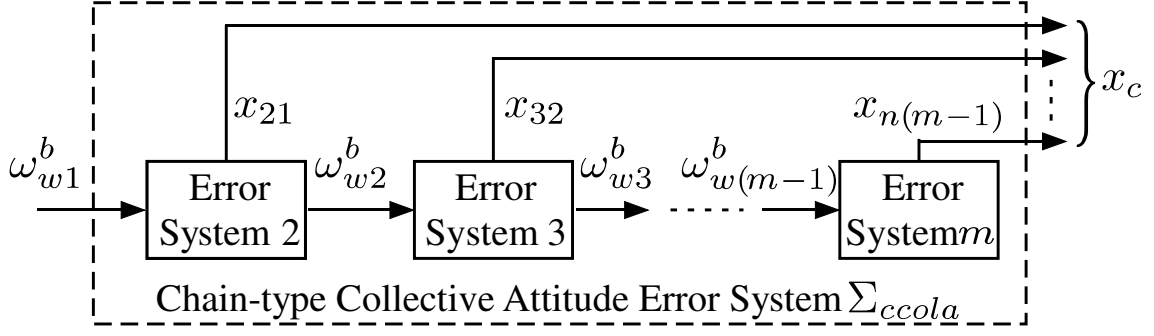
Figure 3.4: Chain-type Collective Attitude Error System Σ_{ccola}

$(-\pi/2, \pi/2)$ *and the gain conditions (3.9) are satisfied for any* $\epsilon_i, \epsilon_i' \in \mathbb{R}_+$ *($\epsilon_i' > \epsilon_i$), $j \in \mathcal{N}_i$, $i \in \mathcal{V}$, then there exist a class-$\mathcal{KL}$ function α_a and a class $\mathcal{K}$ function β_a satisfying*

$$\|x_a(t)\|_2 \leq \alpha_a(\|x_a(0)\|_2, t) + \beta_a \left(\sup_{0 \leq \tau \leq t} \|\omega_{w1}^b(\tau)\|_2 \right), \tag{3.13}$$

where $x_a \in \mathbb{R}^{9(n-1)}$ is the stacked vector of x_{ij}, $j \in \mathcal{N}_i$, $i \in \mathcal{V}$.

Proof. We first define the set of rigid bodies which are not visible bodies of any bodies as $\mathcal{V}_q := \{i \in \mathcal{V} \mid i \notin \mathcal{N}_j {}^\forall j \in \mathcal{V}\}$ (e.g. $\mathcal{V}_q = \{4, 5, 6\}$ in Fig. 3.2). We next denote each chain-type collective error system from the leader to body $i \in \mathcal{V}_q$ by Σ_{ccolai}. Then, we conclude from Lemma 6 that each Σ_{ccolai} is input-to-state-stable. Therefore, there exist class $\mathcal{KL}$ functions α_i and class $\mathcal{K}$ functions β_i satisfying

$$\|x_{ci}(t)\|_2 \leq \alpha_i(\|x_{ci}(0)\|_2, t) + \beta_i \left(\sup_{0 \leq \tau \leq t} \|\omega_{w1}^b(\tau)\|_2 \right), \ i \in \mathcal{V}_q, \tag{3.14}$$

where x_{ci} are the stacked vectors of x_{ij} for each Σ_{ccolai}. Note now that $\|\cdot\|_2$ and $\beta_i(\cdot, \cdot)$ respectively have the following properties for any vectors $a \in \mathbb{R}^n$, $b \in \mathbb{R}^m$.

$$\|a\|_2 \leq \left\| \begin{matrix} a \\ b \end{matrix} \right\|_2 \leq \|a\|_2 + \|b\|_2,$$

$$\beta_i(\|a\|_2, \cdot) + \beta_j(\|b\|_2, \cdot) \leq \beta_i \left(\left\| \begin{matrix} a \\ b \end{matrix} \right\|_2, \cdot \right) + \beta_j \left(\left\| \begin{matrix} a \\ b \end{matrix} \right\|_2, \cdot \right).$$

Then, summation of (3.14) for all $i \in \mathcal{V}_q$ gives

$$\|x_a(t)\|_2 \leq \sum_{i \in \mathcal{V}_q} \alpha_i(\|x_a(0)\|_2, t) + \sum_{i \in \mathcal{V}_q} \beta_i \left(\sup_{0 \leq \tau \leq t} \|\omega_{w1}^b(\tau)\|_2 \right).$$

39
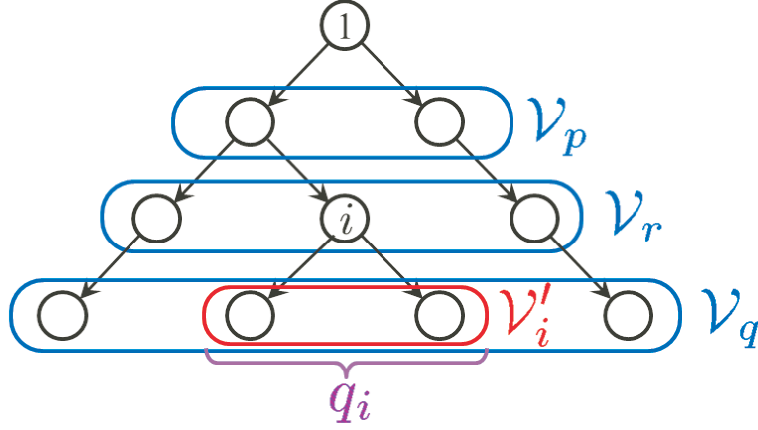
Figure 3.5: Definitions of Rigid Body Sets

Finally, defining α_a and β_a as

$$\alpha_a := \sum_{i \in \mathcal{V}_q} \alpha_i, \ \beta_a := \sum_{i \in \mathcal{V}_q} \beta_i \qquad (3.15)$$

yields (3.13). □

Equation (3.13) evaluates the estimation and control errors for the angular velocity of the leader. Therefore, this can be regarded as an indicator of the tracking performance of the group. However, since the derivation of explicit α_a and β_a is one of our future works, this analysis currently gives only qualitative evaluations for the performance. It is thus hard to decide estimation and control gains for a good tracking performance from this analysis. In the next subsection, we analyze the performance quantitatively by employing $\mathcal{L}_2$ stability in order to give a guideline for gain settings.

3.4.2 $\mathcal{L}_2$ Stability

We analyze the tracking performance of the visual robotic network Σ based on the theory of $\mathcal{L}_2$ stability, where we regard the angular velocity of the leader as an external disturbance to the network.

We first define rigid body sets for visibility structures satisfying Assumption 1 as follows (see Fig. 3.5).

$$\begin{cases} \mathcal{V}_p := \{i \in \mathcal{V} \mid 1 \in \mathcal{N}_i\} \\ \mathcal{V}_q := \{i \in \mathcal{V} \mid i \notin \mathcal{N}_j \ ^\forall j \in \mathcal{V}\} \\ \mathcal{V}_r := \mathcal{V} \setminus (\{1\} \cup \mathcal{V}_p \cup \mathcal{V}_q) \\ \mathcal{V}_i' := \{j \in \mathcal{V}_q \mid \ ^\exists v_1, \cdots, v_r \in \mathcal{V} \ s.t. \ v_1 = i, \ v_r = j \\ \qquad\qquad \text{and } (v_k, v_{k+1}) \in \mathcal{E} \ ^\forall k \in \{1, \cdots, r-1\}\} \end{cases} .$$
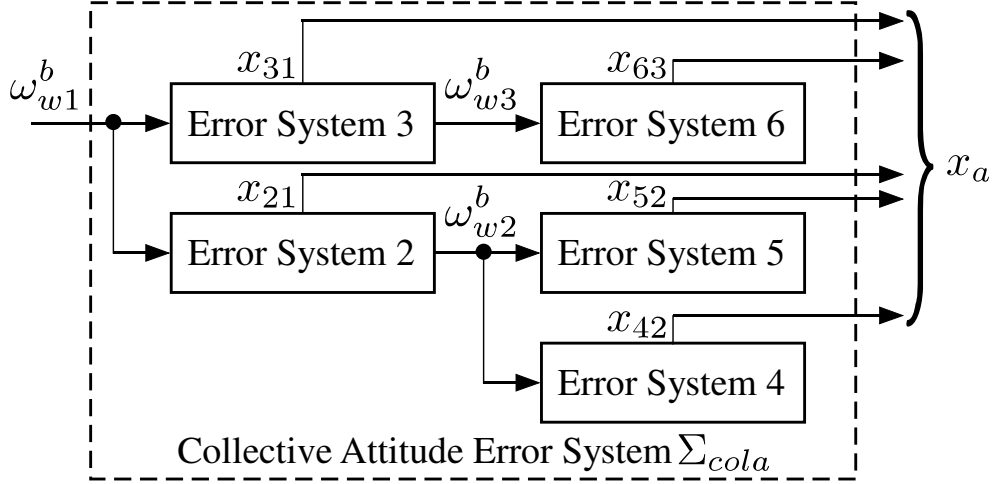
Figure 3.6: Collective Attitude Error System Σ_{cola}

We next reconsider the total error system (3.2). Then, the collection of the system (3.2) for all $j \in \mathcal{N}_i$, $i \in \mathcal{V}$ with the control law (3.1) is called *collective attitude error system* Σ_{cola}, whose state is x_a. The block diagram of the Σ_{cola} in the case of the visibility structure in Fig. 2.4 is illustrated in Fig. 3.6.

Then, we have the following theorem for the tracking performance of the visual robotic network Σ.

Theorem 3. *Consider the visual robotic network Σ with Assumption 1. Suppose that the leader has its own angular velocity (i.e. $\omega_{w1}^b \neq 0$). Then, for any $\epsilon_a, \kappa_{ai} \in \mathbb{R}_+$, $i \in \mathcal{V}_q$, the control law (3.1) on the visual robotic network Σ achieves*

$$\|x_a\|_{\mathcal{L}_2} \leq \kappa_a \|\omega_{w1}^b\|_{\mathcal{L}_2} + \delta_a, \ \kappa_a := \sqrt{\sum_{i \in \mathcal{V}_p} \frac{\kappa_{ai}}{2\epsilon_a}} \tag{3.16}$$

with a nonnegative scalar $\delta_a \geq 0$ if

$$\begin{cases} \begin{cases} k_{ei} > \epsilon_a + \frac{1}{2\kappa_{ai}} \\ \left(2k_{ei} - 2\epsilon_a - \frac{1}{\kappa_{ai}}\right)\left(\frac{1}{2}k_{ci} + k_{ei} - \epsilon_a\right) > 2k_{ei}^2 \end{cases}, \ i \in \mathcal{V}_p \\ \begin{cases} k_{cj} < 2(k_{ei} - \epsilon_a) \\ (2k_{ei} - k_{cj} - 2\epsilon_a)(k_{ci} + k_{ei} - \epsilon_a) > 2k_{ei}^2 \end{cases}, \ j \in \mathcal{N}_i, \ i \in \mathcal{V}_q \\ \begin{cases} k_{cj} < 2(k_{ei} - \epsilon_a) \\ (2k_{ei} - k_{cj} - 2\epsilon_a)\left(\frac{1}{2}k_{ci} + k_{ei} - \epsilon_a\right) > 2k_{ei}^2 \end{cases}, \ j \in \mathcal{N}_i, \ i \in \mathcal{V}_r \end{cases} \tag{3.17}$$

Proof. Define a potential function $U_a \geq 0$ based on passivity of the relative rigid body

41

motion (2.3) and the estimation error system (2.24) as

$$U_a := \sum_{i \in \mathcal{V}} \sum_{j \in \mathcal{N}_i} q_i U_{aij}.$$

Here, $q_i \in \mathbb{N}$ is $|\mathcal{V}_i'|$ for $i \in \mathcal{V} \setminus (\mathcal{V}_q \cup \{1\})$ and $q_i = 1$ for $i \in \mathcal{V}_q \cup \{1\}$ (see Fig. 3.5). Then, the time derivative of U_a along the trajectory of (3.2) yields

$$\dot{U}_a = \sum_{i \in \mathcal{V}} \sum_{j \in \mathcal{N}_i} q_i \left(-x_{ij}^{\mathrm{T}} Q_{ai} x_{ij} + (\mathrm{sk}(e^{\hat{\xi}\theta_{eij}})^{\vee})^{\mathrm{T}} \omega_{wj}^b \right) \quad (\because \text{Eq. (3.11))}.$$

Completing square for $(\mathrm{sk}(e^{\hat{\xi}\theta_{ei1}})^{\vee})^{\mathrm{T}} \omega_{w1}^b$, $i \in \mathcal{V}_p$ yields

$$
\begin{aligned}
(\mathrm{sk}(e^{\hat{\xi}\theta_{ei1}})^{\vee})^{\mathrm{T}} \omega_{w1}^b &= -\frac{\kappa_{ai}}{2} \left\| \omega_{w1}^b - \frac{1}{\kappa_{ai}} \mathrm{sk}(e^{\hat{\xi}\theta_{ei1}})^{\vee} \right\|_2^2 + \frac{\kappa_{ai}}{2} \|\omega_{w1}^b\|_2^2 + \frac{1}{2\kappa_{ai}} \|\mathrm{sk}(e^{\hat{\xi}\theta_{ei1}})^{\vee}\|_2^2 \\
&\leq \frac{\kappa_{ai}}{2} \|\omega_{w1}^b\|_2^2 + \frac{1}{2\kappa_{ai}} \|\mathrm{sk}(e^{\hat{\xi}\theta_{ei1}})^{\vee}\|_2^2
\end{aligned}
$$

for any $\kappa_{ai} \in \mathbb{R}_+$, $i \in \mathcal{V}_p$. On the other hand, we have for the other bodies in $\mathcal{V}_q \cup \mathcal{V}_r$

$$
\begin{aligned}
(\mathrm{sk}(e^{\hat{\xi}\theta_{eij}})^{\vee})^{\mathrm{T}} \omega_{wj}^b &= k_{cj} (\mathrm{sk}(e^{\hat{\xi}\theta_{eij}})^{\vee})^{\mathrm{T}} \mathrm{sk}(e^{\hat{\bar{\xi}}\bar{\theta}_{jk}})^{\vee} \quad (\because \text{Eq. (3.1))} \\
&= \frac{k_{cj}}{2} \Big(\|\mathrm{sk}(e^{\hat{\xi}\theta_{eij}})^{\vee}\|_2^2 + \|\mathrm{sk}(e^{\hat{\bar{\xi}}\bar{\theta}_{jk}})^{\vee}\|_2^2 \\
&\qquad\qquad - \|\mathrm{sk}(e^{\hat{\xi}\theta_{eij}})^{\vee} - \mathrm{sk}(e^{\hat{\bar{\xi}}\bar{\theta}_{jk}})^{\vee}\|_2^2 \Big), \quad (3.18)
\end{aligned}
$$

where $k \in \mathcal{N}_j$.

We next define nonpositive scalar functions $\Psi_{ai} \leq 0$, $i \in \mathcal{V}$ as

$$
\Psi_{ai} := \begin{cases}
-x_{i1}^{\mathrm{T}} \begin{bmatrix} \left(\frac{k_{ci}}{2} + k_{ei}\right) I_3 & 0 & -k_{ei} I_3 \\ 0 & & k_{ei} I_6 \\ -k_{ei} I_3 & & \end{bmatrix} x_{i1}, \ i \in \mathcal{V}_p \\[3em]
-x_{ij}^{\mathrm{T}} \begin{bmatrix} (k_{ci} + k_{ei}) I_3 & 0 & -k_{ei} I_3 \\ 0 & & \left(k_{ei} - \frac{k_{cj}}{2}\right) I_6 \\ -k_{ei} I_3 & & \end{bmatrix} x_{ij} - \frac{k_{cj}}{2} \|\mathrm{sk}(e^{\hat{\xi}\theta_{eij}})^{\vee} - \mathrm{sk}(e^{\hat{\bar{\xi}}\bar{\theta}_{jk}})^{\vee}\|_2^2, \\[1em]
\qquad\qquad\qquad\qquad\qquad\qquad\qquad\qquad k \in \mathcal{N}_j, \ j \in \mathcal{N}_i, \ i \in \mathcal{V}_q \\[2em]
-x_{ij}^{\mathrm{T}} \begin{bmatrix} \left(\frac{k_{ci}}{2} + k_{ei}\right) I_3 & 0 & -k_{ei} I_3 \\ 0 & & \left(k_{ei} - \frac{1}{2}k_{cj}\right) I_6 \\ -k_{ei} I_3 & & \end{bmatrix} x_{ij} - \frac{k_{cj}}{2} \|\mathrm{sk}(e^{\hat{\xi}\theta_{eij}})^{\vee} - \mathrm{sk}(e^{\hat{\bar{\xi}}\bar{\theta}_{jk}})^{\vee}\|_2^2, \\[1em]
\qquad\qquad\qquad\qquad\qquad\qquad\qquad\qquad k \in \mathcal{N}_j, \ j \in \mathcal{N}_i, \ i \in \mathcal{V}_r
\end{cases}
$$

and $\Psi_{a1} = 0$. Note here that the nonnegative terms in (3.18) are included in appropriate quadratic terms. Namely, Ψ_{ai}, $i \in \mathcal{V}_p \cup \mathcal{V}_r$ includes the first term of body i and the second

term of the body seeing body i. Then, we obtain

$$
\begin{aligned}
\dot{U}_a &\leq \sum_{i\in\mathcal{V}} q_i\Psi_{ai} + \sum_{i\in\mathcal{V}_p}\left(\frac{\kappa_{ai}}{2}\|\omega_{w1}^b\|_2^2 + \frac{1}{2\kappa_{ai}}\|\mathrm{sk}(e^{\hat{\xi}\theta_{ei1}})^\vee\|_2^2\right) \\
&= \sum_{i\in\mathcal{V}} q_i\Psi_{ai} + \sum_{i\in\mathcal{V}_p}\left(\frac{\kappa_{ai}}{2}\|\omega_{w1}^b\|_2^2 + \frac{1}{2\kappa_{ai}}\|\mathrm{sk}(e^{\hat{\xi}\theta_{ei1}})^\vee\|_2^2\right) + \sum_{i\in\mathcal{V}}\sum_{j\in\mathcal{N}_i} q_i(\epsilon_a\|x_{ij}\|_2^2 - \epsilon_a\|x_{ij}\|_2^2) \\
&\leq \sum_{i\in\mathcal{V}}\sum_{j\in\mathcal{N}_i} q_i(\Psi_{ai} + \epsilon_a\|x_{ij}\|_2^2) + \sum_{i\in\mathcal{V}_p}\frac{1}{2\kappa_{ai}}\|\mathrm{sk}(e^{\hat{\xi}\theta_{ei1}})^\vee\|_2^2 + \sum_{i\in\mathcal{V}_p}\frac{\kappa_{ai}}{2}\|\omega_{w1}^b\|_2^2 - \epsilon_a\|x_a\|_2^2 \quad (3.19)
\end{aligned}
$$

for any $\epsilon_a \in \mathbb{R}_+$. Here, we use the following property.

$$
\|x_a\|_2^2 \leq \sum_{i\in\mathcal{V}}\sum_{j\in\mathcal{N}_i} q_i\|x_{ij}\|_2^2.
$$

Finally, note that if the gain conditions (3.17) are satisfied, the summation of the first and second terms in (3.19) becomes nonpositive (this can be shown by calculating the Schur complement [72]). We thus get

$$
\dot{U}_a \leq \sum_{i\in\mathcal{V}_p}\frac{\kappa_{ai}}{2}\|\omega_{w1}^b\|_2^2 - \epsilon_a\|x_a\|_2^2.
$$

Integrating this inequality from 0 to T with respect to time yields

$$
U_a(T) - U_a(0) \leq \sum_{i\in\mathcal{V}_p}\frac{\kappa_{ai}}{2}\int_0^T\|\omega_{w1}^b(t)\|_2^2 dt - \epsilon_a\int_0^T\|x_a(t)\|_2^2 dt.
$$

Therefore, the following inequality holds true.

$$
\begin{aligned}
\|x_a\|_{\mathcal{L}_2} &\leq \sqrt{\sum_{i\in\mathcal{V}_p}\frac{\kappa_{ai}}{2\epsilon_a}\int_0^T\|\omega_{w1}^b(t)\|_2^2 dt + \frac{1}{\epsilon_a}U_a(0)} \\
&\leq \sqrt{\sum_{i\in\mathcal{V}_p}\frac{\kappa_{ai}}{2\epsilon_a}\|\omega_{w1}^b\|_{\mathcal{L}_2}} + \sqrt{\frac{1}{\epsilon_a}U_a(0)}.
\end{aligned}
$$

Here, we utilize the property for any nonnegative scalars $a, b \geq 0$ that $\sqrt{a+b} \leq \sqrt{a} + \sqrt{b}$. This completes the proof. □

Although κ_{ai} appears in only conditions of rigid body $i \in \mathcal{V}_p$, the arguments k_{ci}, $i \in \mathcal{V}_p$ also appear in the other constraints. This fact implicitly means that κ_a influences gains of all the bodies. Also, the conditions (3.17) for body $i \in \mathcal{V}_q \cup \mathcal{V}_r$ imply that rear bodies should move faster than forward bodies. This explains the intuition that motion of forward bodies has large influences on group motion while that of rear ones has small impact.

43
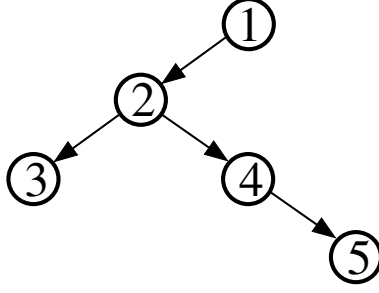
Figure 3.7: Visibility Structure in Simulation

Remark 8. Theorem 3 means that if we regard ω_{w1}^b as the disturbance input and x_a as the output of the collective attitude error system Σ_{cola}, then Σ_{cola} has $\mathcal{L}_2$-gain less than or equal to κ_a (see Fig. 3.6). This results can be regarded as extension of disturbance attenuation analysis of robot motion control as studied in [78, 79, 80]. Since κ_a evaluates the estimation and control errors for the individual angular velocity of the leader, it can be regarded as an indicator of the tracking performance of the group. Therefore, by setting control gains making κ_a small, we can achieve a high tracking performance. We can find these gains by using existing solvers for linear matrix inequalities.

3.5 Verifications

In this section, we demonstrate the effectiveness of the present control law (3.1) through simulation in three dimensions and experiments on a planar testbed. We first give simulation results to show the validity of the convergence analysis (Theorem 1) and the performance analysis (Theorem 3). We then show an experimental result for the effectiveness of the present control law.

3.5.1 Verifications through Simulation

We first demonstrate the validity of Theorems 1 and 3 through simulation in three dimensions. We consider the visual robotic network Σ with the visibility structure shown in Fig. 3.7 satisfying Assumption 1. We let initial conditions be

$$\begin{cases} p_{w1}(0) = [5 \ -5 \ 5]^{\mathrm{T}} \\ p_{w2}(0) = [0 \ 0 \ 0]^{\mathrm{T}} \\ p_{w3}(0) = [0 \ 0 \ -5]^{\mathrm{T}} \\ p_{w4}(0) = [-5 \ -5 \ -5]^{\mathrm{T}} \\ p_{w5}(0) = [-5 \ 0 \ -10]^{\mathrm{T}} \end{cases} [\mathrm{m}], \begin{cases} \xi\theta_{w1}(0) = [0 \ \frac{\pi}{4} \ 0]^{\mathrm{T}} \\ \xi\theta_{w2}(0) = [0 \ 0 \ 0]^{\mathrm{T}} \\ \xi\theta_{w3}(0) = [0 \ -\frac{\pi}{4} \ 0]^{\mathrm{T}} \\ \xi\theta_{w4}(0) = [0 \ \frac{\pi}{3} \ 0]^{\mathrm{T}} \\ \xi\theta_{w5}(0) = [0 \ 0 \ 0]^{\mathrm{T}} \end{cases} [\mathrm{rad}].$$
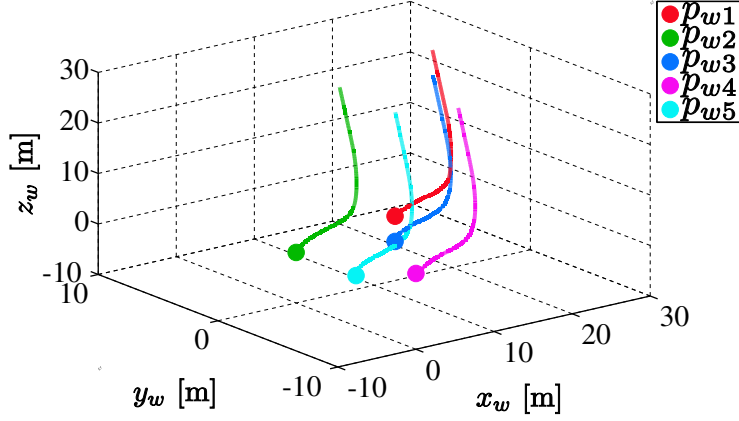
Figure 3.8: Position in Σ_w ($\kappa_a = 2$)
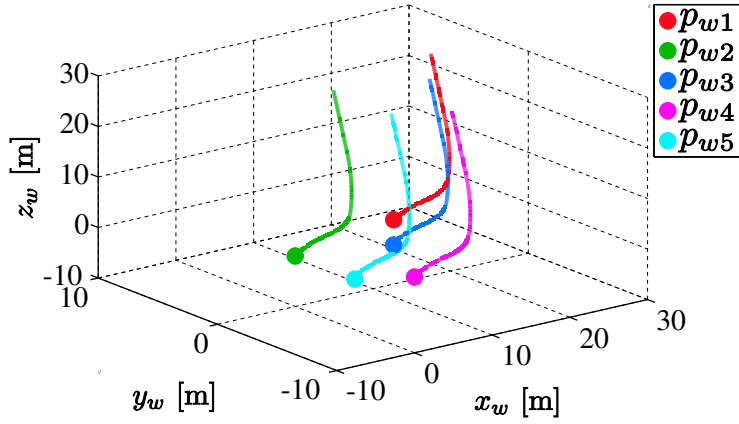
Figure 3.9: Position in Σ_w ($\kappa_a = 0.49$)

The common linear velocity is $v = [0 \quad 0 \quad 1]^{\mathrm{T}}$ [m/s]. Also, the angular velocity of the leader (rigid body 1) is set as

$$
\omega_{w1}^b(t) = \begin{cases} [0\ 0.1\ 0]^{\mathrm{T}}, & t \in [0,5) \\ [-0.1\ 0\ 0]^{\mathrm{T}}, & t \in [5,10) \\ [0\ -0.1\ 0]^{\mathrm{T}}, & t \in [10,20) \\ [0\ 0\ 0]^{\mathrm{T}}, & t \in [20,30) \end{cases} \quad [\mathrm{rad/s}].
$$

Then, it is expected that the network performs flocking-like behavior until 20s and visual feedback attitude synchronization is achieved after 20s. We finally apply the present

45
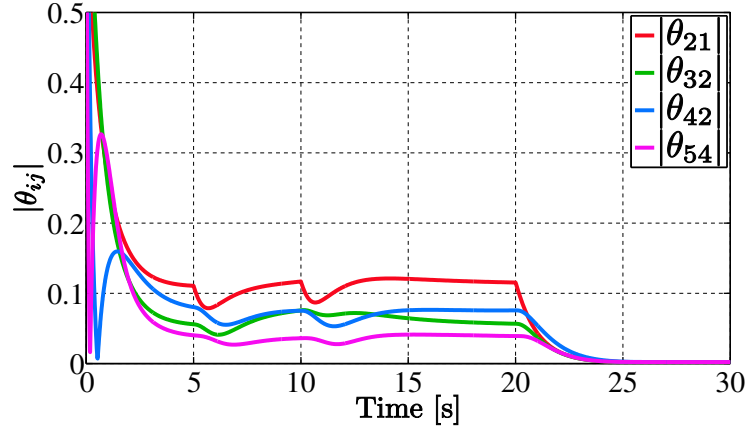
Figure 3.10: Rotation Angle Error ($\kappa_a = 2$)
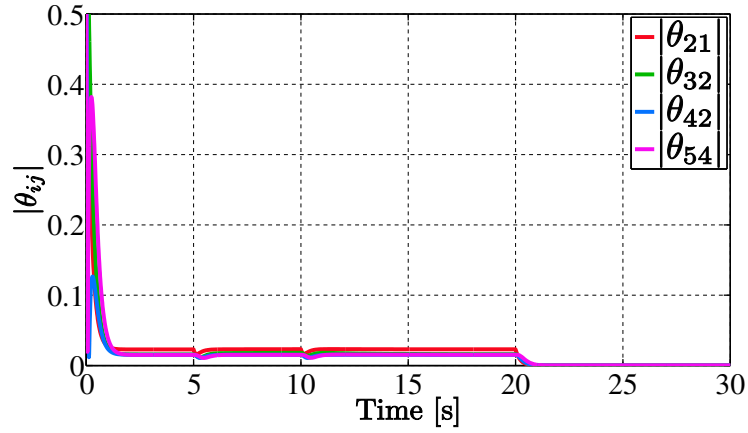
Figure 3.11: Rotation Angle Error ($\kappa_a = 0.49$)

control law (3.1) with the following gain settings.

$$\text{Gain A}: \begin{cases} k_{c2} = 2.73, \ k_{c3} = 4.45, \ k_{c4} = 5.69, \ k_{c5} = 8.38 \\ k_{e2} = 3.37, \ k_{e3} = 3.94, \ k_{e4} = 6.65, \ k_{e5} = 7.72 \end{cases},$$

$$\text{Gain B}: \begin{cases} k_{c2} = 11.28, \ k_{c3} = 19.93, \ k_{c4} = 18.99, \ k_{c5} = 19.99 \\ k_{e2} = 19.98, \ k_{e3} = 19.92, \ k_{e4} = 19.99, \ k_{e5} = 19.99 \end{cases}.$$

Both settings satisfy the gain conditions (3.17) and give the performance indicators $\kappa_a = 2.00$ for Gain A and $\kappa_a = 0.49$ for Gain B ($\epsilon_a = 0.5$).

The simulation results are shown in Figs. 3.8-3.13. Figs. 3.8 and 3.9 illustrate the trajectories of the rigid bodies in 3D space, where the circles represent the initial positions. The time responses of the absolute values of the relative rotation angles are shown in Figs.

46
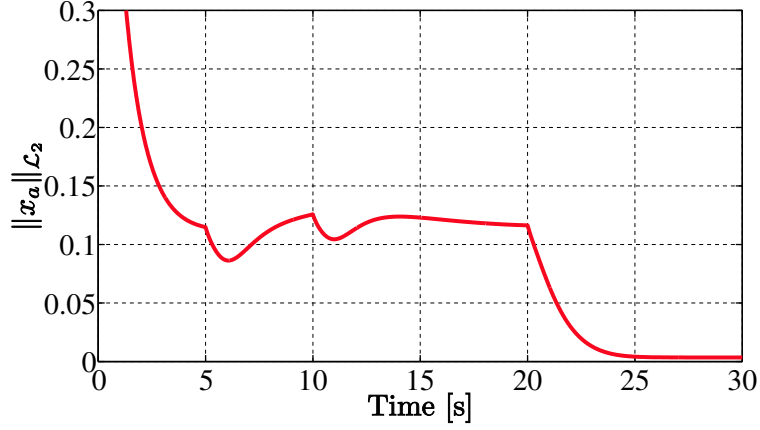
Figure 3.12: Control Performance ($\kappa_a = 2$)
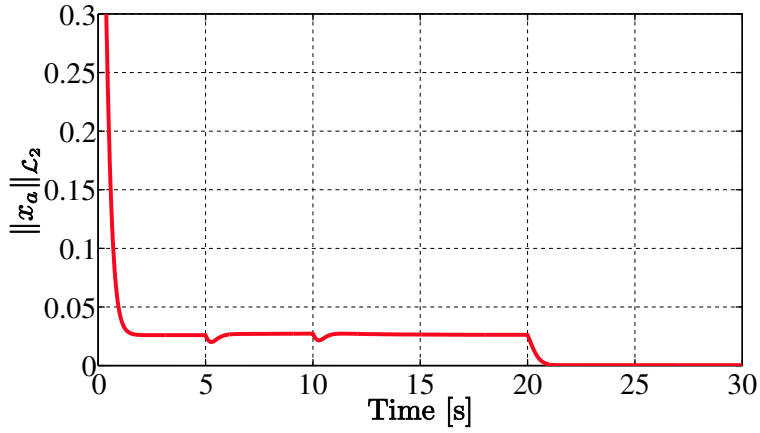
Figure 3.13: Control Performance ($\kappa_a = 0.49$)

3.10 and 3.11. We also depict the time responses of the norms of the total estimation and control error x_a in Figs. 3.12 and 3.13. We see from Figs. 3.8 and 3.9 that when the leader rotates, the other bodies track it successfully, and all the bodies eventually move in the same direction. Also, Figs. 3.10 and 3.11 show that all the orientations converge to a common value at around 25s, i.e. visual feedback attitude synchronization (2.10) is achieved by the present control law. We moreover see from Figs. 3.12 and 3.13 that the tracking performance is improved for the smaller κ_a. Therefore, κ_a is adequate for the performance indicator of the visual feedback attitude synchronization.
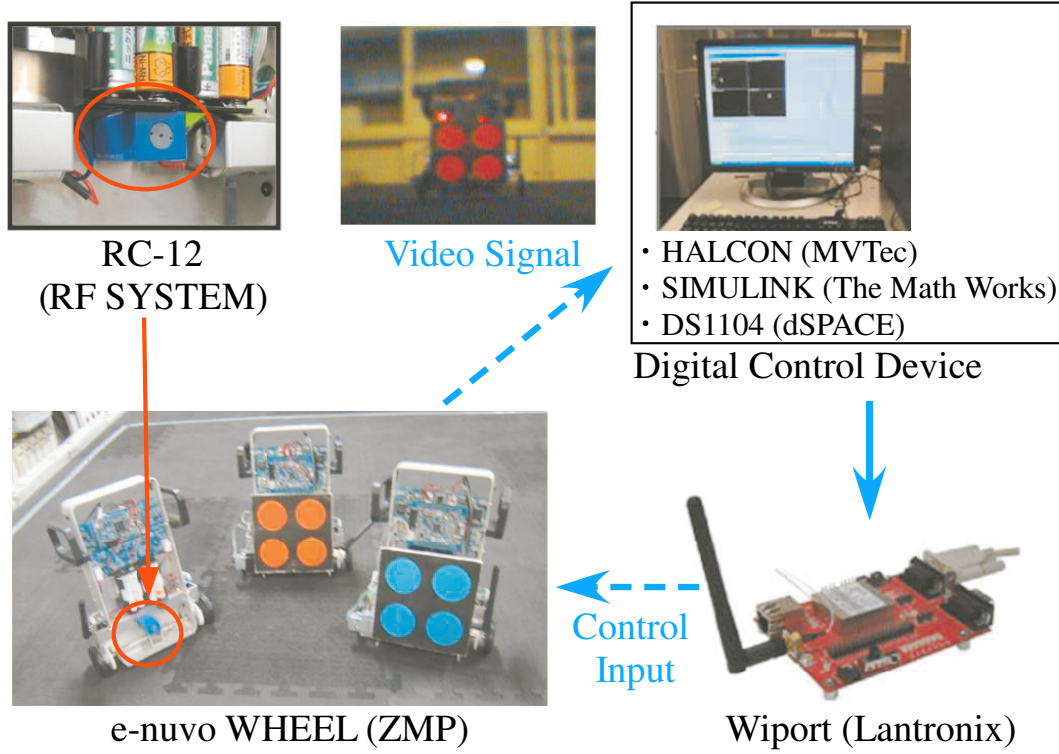
Figure 3.14: Experimental Environment

RC-12
(RF SYSTEM)

Video Signal

· HALCON (MVTec)
· SIMULINK (The Math Works)
· DS1104 (dSPACE)
Digital Control Device

e-nuvo WHEEL (ZMP)

Control
Input

Wiport (Lantronix)
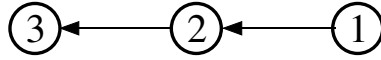
Figure 3.15: Visibility Structure in Experiment

3.5.2 Verifications through Experiments

We next present experimental results on a planar testbed to verify the effectiveness of the convergence analysis.

We use three wheeled mobile robots e-nuvo WHEEL (ZMP) as rigid bodies. We attach a plate with four colored circles to each robot in order to improve accuracy of extracting feature points. Each robot has a wireless on-board radio camera RC-12 (RF SYSTEM) to obtain visual measurements. We also use a camera MTV-7310 (komoto) attached above the experimental field to measure the actual poses of robots for verification. The frame rates of both cameras are 30fps. Transmitted video signals are loaded into PC via a frame grabber board PICOLO DILLIGENT (Euresys) and manipulated by image processing software HALCON (MVTec). The control and observer models are designed by Simulink (The Math Works) and calculated by DSP board DS1104 (dSPACE) in real time. Then, the control input is sent to robots via an embedded wireless communication
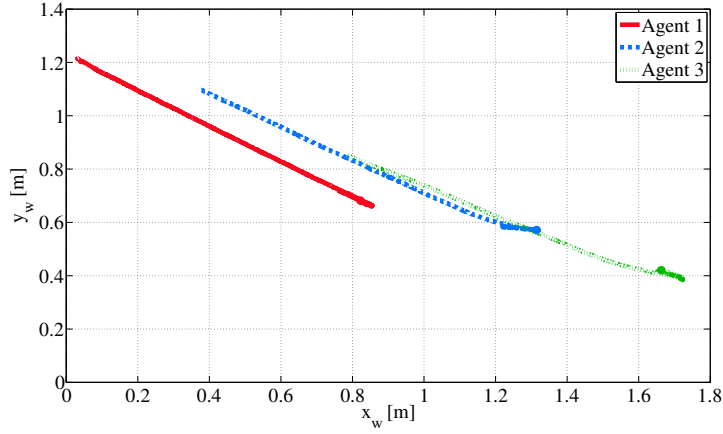
Figure 3.16: Position in Σ_w
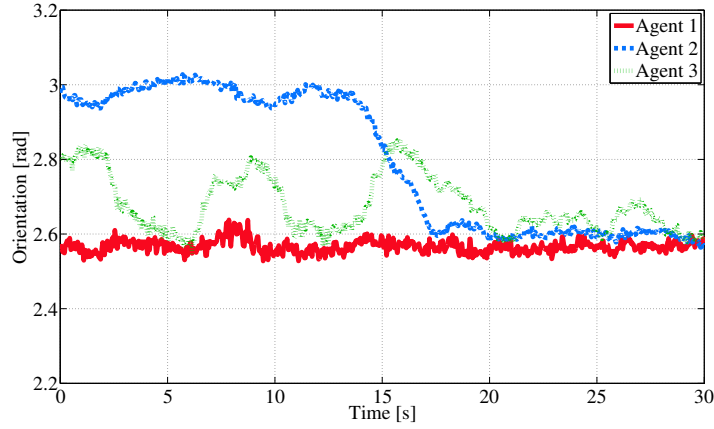
Figure 3.17: Rotation Angle in Σ_w

device Wiport (LANTRONIX). The sampling period of the controller is around 33ms. This experimental schematic is shown in Fig. 3.14. Although each robot can move only on 2D plane, the pose estimation algorithm is executed in three dimensions. Therefore, each robot implements the visual feedback velocity input projected onto the experimental field.

We use the visibility structure depicted in Fig. 3.15. Initial conditions are set as

$$\begin{cases} p_{w1}(0) = [0.823\ 0.682\ 0]^{\mathrm{T}} \\ p_{w2}(0) = [1.315\ 0.572\ 0]^{\mathrm{T}} \\ p_{w3}(0) = [1.663\ 0.421\ 0]^{\mathrm{T}} \end{cases} [\mathrm{m}], \quad \begin{cases} \xi\theta_{w1}(0) = [0\ 0\ 2.563]^{\mathrm{T}} \\ \xi\theta_{w2}(0) = [0\ 0\ 2.978]^{\mathrm{T}} \\ \xi\theta_{w3}(0) = [0\ 0\ 2.800]^{\mathrm{T}} \end{cases} [\mathrm{rad}].$$

We also set the common linear velocity as $v = [0\ 0.04\ 0]^{\mathrm{T}}$ [m/s] and do not apply any

49
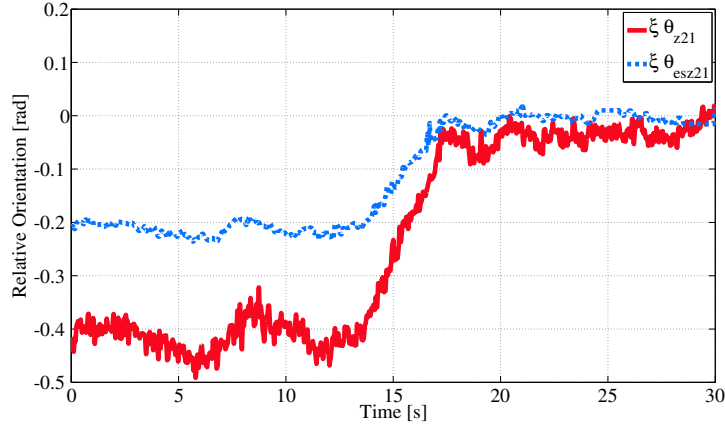
Figure 3.18: Actual (Measured) and Estimated Rotation Angle between 2 and 1
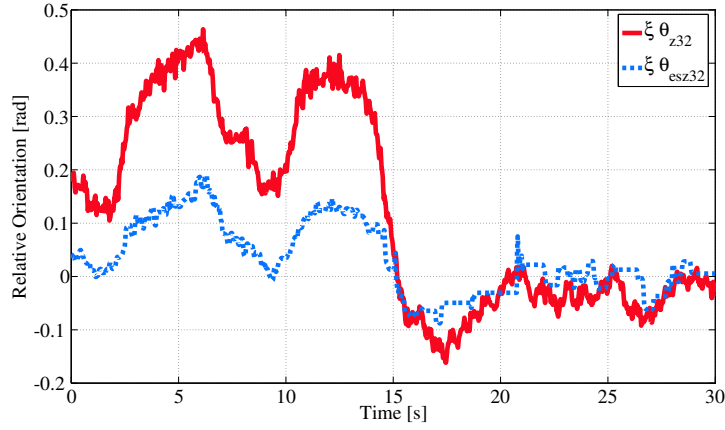
Figure 3.19: Actual (Measured) and Estimated Rotation Angle between 3 and 2

individual angular velocities to the leader. Therefore, we demonstrate only the validity of the convergence analysis (Theorem 1) in this experiment (the verification for the performance analysis is given in Chapter 4). We finally apply the control law (3.1) with the gains $k_{c2} = k_{c3} = 1$ and $k_{e2} = k_{e3} = 15$.

The experimental results are shown in Figs. 3.16-3.19. Fig. 3.16 illustrates the trajectories of the robots on the experimental field, Fig. 3.17 the time responses of the actual (measured) orientations and Figs. 3.18 and 3.19 the actual (measured) and the estimated relative orientations. We see from Figs. 3.16 and 3.17 that all the orientations converge to a common value (robot 1's value) at around 20s. This means that the proposed control law achieves visual feedback attitude synchronization in the sense of (2.10). Moreover, Fig. 3.19 shows that the error between actual (measured) and estimated orientations is small

enough to achieve stable attitudes. Thus, the visual feedback attitude synchronization law (3.1) works successfully.

3.6   Chapter Summary

In this chapter, we have investigated a visual feedback attitude synchronization problem for visual robotic networks Σ. We have first proposed a synchronization law to achieve visual feedback attitude synchronization in the sense of (2.10). Then, we have proved that the present estimation and control mechanism achieves synchronization under leader-following visibility structures in the absence of communication or any other measurements of the states. Here, passivity of the rigid body motion (2.2) and the relative rigid body motion (2.3) plays central roles for the design of the control law and the convergence analysis. We have also given both qualitative and quantitative tracking performance analysis of the network for a leader having individual angular velocities by employing the theory of input-to-state stability or $\mathcal{L}_2$ stability. Moreover, we have shown that the performance analysis based on $\mathcal{L}_2$ stability gives a guideline to decide estimation and control gains. The simulation results and the experimental results have finally demonstrated the validity of the main results in this chapter.

The main issues to be tackled are (i) to eliminate the assumption that all the rigid bodies have a common linear velocity v, (ii) to weaken the assumption of visibility structures, (iii) to introduce rigid body dynamics, and (iv) to employ a visibility maintenance algorithm. We address these issues in Chapter 5.

Chapter 4

Visual Feedback 3D Pose Synchronization

4.1 Introduction

In this chapter, we study a leader-following visual feedback pose synchronization problem for visual robotic networks Σ. The objective of this chapter is to present a control law to achieve visual feedback pose synchronization (2.11) for networks satisfying Assumption 1. We first propose a synchronization law based on the passivity-based pose synchronization law and the visual motion observer introduced in Chapter 2. In the present control scheme, relative poses necessary for pose synchronization laws are estimated by a visual motion observer. The present mechanism is hence completely constructed by visual measurements (2.9) extracted by vision. This means that each body is fully autonomous, which is one of the main contributions of this dissertation. We next prove pose synchronization, where passivity of the rigid body motion (2.2) and the relative rigid body motion (2.3) plays a crucial role. However, in the present control law, the leader does not move, and as a result, the network cannot move. In order to overcome this problem, we also consider the situation that the leader moves independently. In this case, we analyze the tracking performance of the network for the leader by employing the theory of input-to-state stability or $\mathcal{L}_2$ stability. Here, we regard the body velocity of the leader as an external disturbance to the network. The effectiveness of the control protocol is demonstrated through simulation in three dimensions and experiments on a planar testbed.

This chapter is organized as follows. In Section 4.2, we present an estimation and control law for the visual robotic network Σ to achieve visual feedback pose synchronization. We then analyze the convergence for a not moving leader in Section 4.3. In Section 4.4, we give the tracking performance analysis of the other rigid bodies in Σ for a leader having individual velocities. Finally, we perform simulation and experiments in order to confirm the effectiveness and validity of the present control scheme and the convergence and performance analysis in Section 4.5. Section 4.6 concludes this chapter.

4.2 Visual Feedback Pose Synchronization Law with a Panoramic Camera Model

In this section, we propose a visual feedback pose synchronization law. Unlike the previous work [47, 48] premising the measurement of g_{ij}, the goal of this chapter is to propose a velocity law for visual feedback pose synchronization (2.11) by using only visual measurements (2.9). Throughout this chapter, we deal with the panoramic camera model (2.8).

Note first that each rigid body has to estimate relative pose g_{m_ij}, denoted by $\bar{g}_{m_ij} \in SE(3)$ by a nonlinear observer similarly to Chapter 3. We define the desired relative pose $g_{dij} \in SE(3)$, the control error $g_{cij} = (p_{cij}, e^{\hat{\xi}\theta_{cij}}) \in SE(3)$ and the control error vector $e_{cij} \in \mathbb{R}^6$ as

$$g_{dij} := \begin{bmatrix} I_3 & d_{ij} \\ 0 & 1 \end{bmatrix}, \; g_{cij} := g_{dij}^{-1} g_{im_i} \bar{g}_{m_ij}, \; e_{cij} := \begin{bmatrix} p_{cij} \\ \mathrm{sk}(e^{\hat{\xi}\theta_{cij}})^\vee \end{bmatrix}.$$

It should be noted that $e_{cij} = 0$ if and only if $g_{cij} = I_4$ for $\theta_{cij} \in (-\pi, \pi)$ and hence $g_{im_i}\bar{g}_{m_ij} = g_{dij}$. We also define the estimation error $g_{eij} = (p_{eij}, e^{\hat{\xi}\theta_{eij}}) \in SE(3)$ between the actual relative pose g_{m_ij} and its estimate $\bar{g}_{m_ij}$ and the estimation error vector $e_{eij} \in \mathbb{R}^6$ as

$$g_{eij} := \bar{g}_{m_ij}^{-1} g_{m_ij}, \; e_{eij} := \begin{bmatrix} p_{eij} \\ \mathrm{sk}(e^{\hat{\xi}\theta_{eij}})^\vee \end{bmatrix},$$

where the definition of g_{eij} is different from that of Chapter 3. Then, both $e_{cij} = 0$ and $e_{eij} = 0$ mean $g_{ij} = g_{dij}$, i.e. visual feedback pose synchronization (2.11) is achieved if and only if $e_{cij} = 0$, $e_{eij} = 0$, $j \in \mathcal{N}_i$ $\forall i \in \mathcal{V}$.

In order to achieve visual feedback pose synchronization (2.11), we propose the following control law.

$$Controller: \; V_{wi}^b = k_{ci} \sum_{j \in \mathcal{N}_i} \mathrm{Ad}_{(g_{dij})} e_{cij}, \tag{4.1a}$$

$$Observer: \begin{cases} \bar{V}_{m_ij}^b := (\bar{g}_{m_ij}^{-1} \dot{\bar{g}}_{m_ij})^\vee = -\mathrm{Ad}_{(\bar{g}_{m_ij}^{-1})} \mathrm{Ad}_{(g_{im_i}^{-1})} V_{wi}^b + u_{ij}, & \tag{4.1b} \\ u_{ij} = k_{ei} \left(e_{eij} - \mathrm{Ad}_{(e^{-\hat{\xi}\theta_{cij}})} e_{cij} \right), & \tag{4.1c} \end{cases}$$

where $j \in \mathcal{N}_i$, $i \in \mathcal{V}$ and $k_{ci}, k_{ei} \in \mathbb{R}_+$ $\forall i \in \mathcal{V}$.

The block diagram of the estimation and control law (4.1) is shown in Fig. 4.1. The difference from the visual feedback attitude synchronization law (3.1) is to impose position feedback so as to achieve position coordination in addition to attitude feedback. As a result, the observer input is slightly different from (3.1d). In the nonlinear observer, (4.1b) simulates the relative rigid body motion (2.6) for the panoramic camera model by
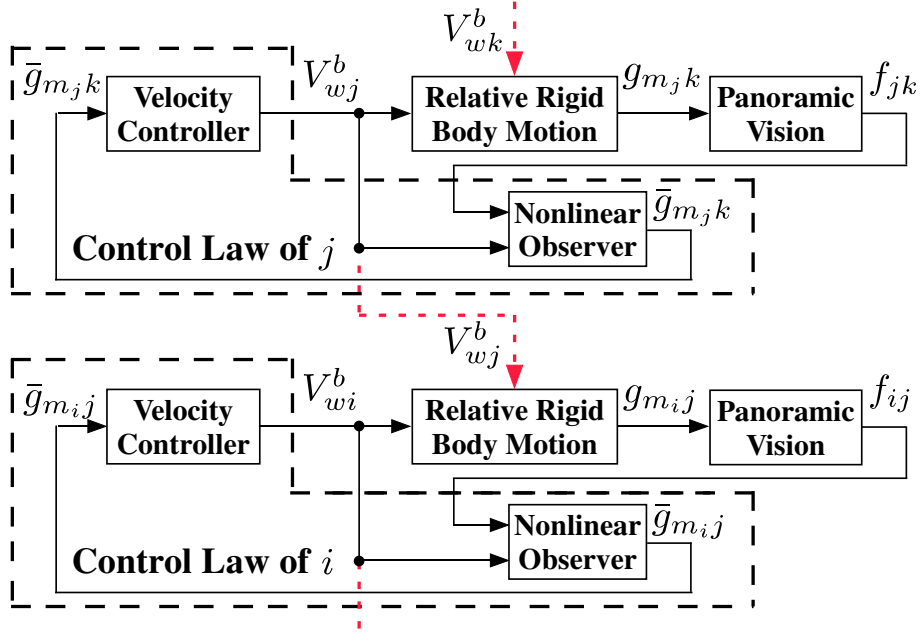
Figure 4.1: Block Diagram of Visual Feedback Pose Synchronization Law

utilizing the estimate $\bar{g}_{m_{ij}}$ as its state. Here, $u_{ij} \in \mathbb{R}^6$ is external input to be determined so that the estimated value $\bar{g}_{m_{ij}}$ is driven to its actual value $g_{m_{ij}}$, which is given by (4.1c). In (4.1c), e_{eij} can be reconstructed by visual measurements f_{ij} (see Appendix A.2). Also, the difference from the pose synchronization scheme (2.22) proposed in [47, 48] is to feedback the estimated relative pose $g_{im_i}\bar{g}_{m_{ij}}$ (with the biase d_{ij}) instead of the actual g_{ij}. Namely, the present estimation and control law (4.1) can be calculated only by visual measurements (2.9) in the absence of communication or any measurements of own states which makes rigid bodies fully autonomous.

4.3   Convergence Analysis

In this section, we give convergence analysis for the visual robotic network Σ with the present visual feedback pose synchronization law (4.1). We first assume that visibility structures in Σ satisfy Assumption 1. Then, it is shown that the control law (4.1) on Σ achieves visual feedback pose synchronization in the sense of (2.11). However, note that the control law (4.1) with Assumption 1 implies that the leader body does not move, and as a result, the network cannot move. Thus, we also give a control law containing a common desired body velocity among rigid bodies.

We first introduce control error systems for visible body pairs (i, j), $(j, i) \in \mathcal{E}$ by

differentiating control errors g_{cij} with respect to time as follows.

$$\begin{aligned}
\dot{g}_{cij} &= g_{dij}^{-1} g_{im_i} \dot{\bar{g}}_{mij} \quad (\because d_{ij} \text{ and } g_{im_i} \text{ is constant}) \\
&= g_{dij}^{-1} g_{im_i} (-g_{im_i}^{-1} \hat{V}_{wi}^b g_{im_i} \bar{g}_{mij} + \bar{g}_{mij} \hat{u}_{ij}) \quad (\because \text{Eq. (4.1b)}) \\
&= -g_{dij}^{-1} \hat{V}_{wi}^b g_{dij} g_{cij} + g_{cij} \hat{u}_{ij}.
\end{aligned}$$

In the vector form, the control error system is written by

$$V_{cij}^b := (g_{cij}^{-1} \dot{g}_{cij})^\vee = -\mathrm{Ad}_{(g_{cij}^{-1})} \mathrm{Ad}_{(g_{dij}^{-1})} V_{wi}^b + u_{ij}. \tag{4.2}$$

Then, combining the control error system (4.2) and the estimation error system (2.24) yields the following total error system.

$$\begin{bmatrix} V_{cij}^b \\ V_{eij}^b \end{bmatrix} = \begin{bmatrix} -\mathrm{Ad}_{(g_{cij}^{-1})} & I_6 \\ 0 & -\mathrm{Ad}_{(g_{eij}^{-1})} \end{bmatrix} \begin{bmatrix} \mathrm{Ad}_{(g_{dij}^{-1})} V_{wi}^b \\ u_{ij} \end{bmatrix} + \begin{bmatrix} 0 \\ V_{wj}^b \end{bmatrix}. \tag{4.3}$$

We now define a potential function $U_{ij} \geq 0$ as follows.

$$U_{ij} := \psi(g_{cij}) + \psi(g_{eij}). \tag{4.4}$$

Then, the following lemma holds for the total error system (4.3),

Lemma 7. *If $V_{wj}^b = 0$ holds, then the time derivative of U_{ij} along the trajectory of (4.3) satisfies*

$$\dot{U}_{ij} = u_{ceij}^{\mathrm{T}} \nu_{ij},$$

where

$$u_{ceij} := \begin{bmatrix} \mathrm{Ad}_{(g_{dij}^{-1})} V_{wi}^b \\ u_{ij} \end{bmatrix} \in \mathbb{R}^{12}, \ \nu_{ij} := \begin{bmatrix} -I_6 & 0 \\ \mathrm{Ad}_{(e^{-\hat{\xi}\theta_{cij}})} & -I_6 \end{bmatrix} e_{ij} \in \mathbb{R}^{12}, \ e_{ij} := \begin{bmatrix} e_{cij} \\ e_{eij} \end{bmatrix} \in \mathbb{R}^{12}.$$

Proof. When $V_{wj}^b = 0$ holds, the time derivative of U_{ij} along the trajectories of (4.3) yields

$$\begin{aligned}
\dot{U}_{ij} &= e_{cij}^{\mathrm{T}} \mathrm{Ad}_{(e^{\hat{\xi}\theta_{cij}})} V_{cij}^b + e_{eij}^{\mathrm{T}} \mathrm{Ad}_{(e^{\hat{\xi}\theta_{eij}})} V_{eij}^b \quad (\because \text{Appendix B.3.2 and Eq. (2.25)}) \\
&= e_{ij}^{\mathrm{T}} \begin{bmatrix} \mathrm{Ad}_{(e^{\hat{\xi}\theta_{cij}})} & 0 \\ 0 & \mathrm{Ad}_{(e^{\hat{\xi}\theta_{eij}})} \end{bmatrix} \begin{bmatrix} V_{cij}^b \\ V_{eij}^b \end{bmatrix} \\
&= e_{ij}^{\mathrm{T}} \begin{bmatrix} \mathrm{Ad}_{(e^{\hat{\xi}\theta_{cij}})} & 0 \\ 0 & \mathrm{Ad}_{(e^{\hat{\xi}\theta_{eij}})} \end{bmatrix} \begin{bmatrix} -\mathrm{Ad}_{(g_{cij}^{-1})} & I_6 \\ 0 & -\mathrm{Ad}_{(g_{eij}^{-1})} \end{bmatrix} u_{ceij} \quad (\because \text{Eq. (4.3) with } V_{wj}^b = 0) \\
&= e_{ij}^{\mathrm{T}} \begin{bmatrix} -\mathrm{Ad}_{(-p_{cij})} & \mathrm{Ad}_{(e^{\hat{\xi}\theta_{cij}})} \\ 0 & -\mathrm{Ad}_{(p_{eij})} \end{bmatrix} u_{ceij} \\
&= e_{ij}^{\mathrm{T}} \begin{bmatrix} -I_6 & \mathrm{Ad}_{(e^{\hat{\xi}\theta_{cij}})} \\ 0 & -I_6 \end{bmatrix} u_{ceij} \quad (\because p^{\mathrm{T}} \hat{p} u = -p^{\mathrm{T}} \hat{u} p = 0 \ \forall p, u \in \mathbb{R}^3 \ (\text{Appendix B.1.2})) \\
&= u_{ceij}^{\mathrm{T}} \nu_{ij}.
\end{aligned}$$

$\square$

Lemma 7 means that total error system (4.3) is passive from u_{ij} to ν_{ij} with the storage function U_{ij} when $V_{wj}^b = 0$ holds. Also, unlike the passivity of the relative rigid body motion (2.3), there exists the coupling term between position dynamics and orientation dynamics. It should be noted that the present input (4.1a) and (4.1c) are constructed by the output of the passivity.

We get the following theorem from Lemma 7.

Theorem 4. *Consider the visual robotic network Σ with Assumption 1. Then, the control law (4.1) on Σ achieves visual feedback pose synchronization.*

Proof. We use the same approach as in Theorem 1 to the proof. We first consider each rigid body i in $\mathcal{V}_1$ whose visible body is body 1 (see Fig. 3.2). Consider the potential function U_{i1} (defined in (4.4) with $j = 1$) based on passivity of the total error system (4.3). Then, the time derivative of U_{i1} along the trajectory of (4.3) yields

$$
\begin{aligned}
\dot{U}_{i1} &= \nu_{i1}^{\mathrm{T}} u_{cei1} \quad (\because \text{Lemma 7}) \\
&= -e_{i1}^{\mathrm{T}} \begin{bmatrix} -I_6 & \mathrm{Ad}_{(e^{\hat{\xi}\theta_{ci1}})} \\ 0 & -I_6 \end{bmatrix} \begin{bmatrix} k_{ci}I_6 & 0 \\ 0 & k_{ei}I_6 \end{bmatrix} \begin{bmatrix} -I_6 & 0 \\ \mathrm{Ad}_{(e^{-\hat{\xi}\theta_{ci1}})} & -I_6 \end{bmatrix} e_{i1} \quad (\because \text{Eq. (4.1)}) \\
&= -e_{i1}^{\mathrm{T}} Q_{i1} e_{i1}, \quad Q_{i1} := \begin{bmatrix} (k_{ci}+k_{ei})I_6 & -k_{ei}\mathrm{Ad}_{(e^{\hat{\xi}\theta_{ci1}})} \\ -k_{ei}\mathrm{Ad}_{(e^{-\hat{\xi}\theta_{ci1}})} & k_{ei}I_6 \end{bmatrix}.
\end{aligned}
$$

Notice here that Q_{i1} is positive definite for any $k_{ci}, k_{ei} \in \mathbb{R}_+$ and $e^{\hat{\xi}\theta_{cij}} \in SO(3)$, which can be shown by calculating the Schur complement [72]. Namely, the equilibrium point $e_{i1} = 0$ is asymptotically stable. Then, we conclude from the definition of e_{i1} that all the bodies in $\mathcal{V}_1$ achieves visual feedback pose synchronization in the sense of (2.11).

We next consider each rigid body i in $\mathcal{V}_2$ whose visible body exists in $\mathcal{V}_1$. Note first that visible body j from i has $V_{wj}^b = k_{cj}\mathrm{Ad}_{(g_{dj1})}e_{cj1}$. We now substitute the present input (4.1) into the total error system (4.3) as follows.

$$
\begin{bmatrix} V_{cij}^b \\ V_{eij}^b \end{bmatrix} = \begin{bmatrix} -\mathrm{Ad}_{(g_{cij}^{-1})} & I_6 \\ 0 & -\mathrm{Ad}_{(g_{eij}^{-1})} \end{bmatrix} \begin{bmatrix} k_{ci}e_{cij} \\ k_{ei}\left(e_{eij} - \mathrm{Ad}_{(e^{-\hat{\xi}\theta_{cij}})}e_{cij}\right) \end{bmatrix} + \begin{bmatrix} 0 \\ k_{cj}\mathrm{Ad}_{(g_{dj1})}e_{cj1} \end{bmatrix}. \quad (4.5)
$$

Here, it should be noted that the second term in (4.5) eventually goes to 0 since body j in $\mathcal{V}_1$ achieves visual feedback pose synchronization. Notice also that V_{cij}^b, V_{eij}^b, e_{cij} and e_{eij} are the functions of g_{cij}, $\dot{g}_{cij}$, g_{eij} and $\dot{g}_{eij}$. Therefore, if we regard e_{ij} as the state of (4.5), we can apply Proposition 1 to the convergence analysis by regarding (4.5) as the perturbed system. Namely, it is sufficient to show that the equilibrium point $e_{ij} = 0$ for the system (4.5) without the second term is exponentially stable. This can be proved by the same analysis as in the proof of Theorem 1 by introducing the potential function U_{ij}. Also, the convergence analysis for the other bodies in $\{\mathcal{V}_3, \mathcal{V}_4, \cdots\}$ is the same as in the proof of Theorem 1. $\square$

In Theorem 4, we show only qualitative stability analysis which enables us to set any positive gains. However, it is often required us obtain good transient behavior until attitude synchronization. Then, we can apply Lyapunov stability by considering the total estimation and control system and introducing the total Lyapunov function for the visual robotic network Σ. Refer to **Publications** [2] for the details.

Notice now that all the rigid bodies would stop in the final configuration though it is sometimes required for bodies to move in the desired direction while achieving pose synchronization. Therefore, we next add a common desired body velocity to all the bodies. Suppose that all the bodies have a common desired velocity $V_d \in \mathbb{R}^6$ and let us fix the form of each body velocity as

$$V_{wi}^b = \tilde{V}_{wi}^b + V_d$$

for some $\tilde{V}_{wi}^b \in \mathbb{R}^6$. Then, the control error system (4.2) can be simply represented by

$$V_{cij}^b = -\mathrm{Ad}_{(g_{cij}^{-1})}\mathrm{Ad}_{(g_{dij}^{-1})}(\tilde{V}_{wi}^b + V_d) + u_{ij}.$$

Also, the estimation error system (2.24) is derived as

$$V_{eij}^b = -\mathrm{Ad}_{(g_{eij}^{-1})}u_{ij} + \tilde{V}_{wj}^b + V_d.$$

Then, by proposing the following control law,

$$\textit{Controller}: \quad V_{wi}^b = k_{ci}\sum_{j\in\mathcal{N}_i}\mathrm{Ad}_{(g_{dij})}e_{cij} + \mathrm{Ad}_{(g_{dij})}V_d, \tag{4.6a}$$

$$\textit{Observer}: \begin{cases} \bar{V}_{m_ij}^b = -\mathrm{Ad}_{(\bar{g}_{m_ij}^{-1})}\mathrm{Ad}_{(g_{im_i}^{-1})}V_{wi}^b + u_{ij}, & (4.6b) \\[2mm] u_{ij} = k_{ei}\left(e_{eij} - \mathrm{Ad}_{(e^{-\hat{\xi}\theta_{cij}})}e_{cij}\right), & (4.6c) \end{cases}$$

we get the following equality from Lemma 7 with $V_{wj}^b \neq 0$.

$$\dot{U}_{ij} = -e_{ij}^{\mathrm{T}}Q_ie_{ij} + k_{cj}e_{eij}^{\mathrm{T}}\mathrm{Ad}_{(g_{djk})}e_{cjk} - e_{cij}^{\mathrm{T}}V_d + e_{eij}^{\mathrm{T}}\mathrm{Ad}_{(g_{djk})}V_d, \ k\in\mathcal{N}_j.$$

Here, $Q_i \in \mathbb{R}^{12\times12}$ is defined as

$$Q_i := \begin{bmatrix} (k_{ci}+k_{ei})I_6 & -k_{ei}\mathrm{Ad}_{(e^{-\hat{\xi}\theta_{cij}})} \\ -k_{ei}\mathrm{Ad}_{(e^{\hat{\xi}\theta_{cij}})} & k_{ei}I_6 \end{bmatrix}. \tag{4.7}$$

Note now that the new third and fourth terms vanish when $e_{ij} = 0$ which is exponentially stable for the corresponding nominal system. Therefore, we can apply Proposition 1 as in Theorem 1. Namely, even in the case with V_d, the following corollary holds.

Corollary 1. *Consider the visual robotic network Σ with Assumption 1. Then, the control law (4.6) on Σ achieves visual feedback pose synchronization.*

In the control law (4.6), each rigid body has to share a common desired velocity for the desired movement of the visual robotic network Σ. However, even without such common knowledge, it is often expected for followers to track the leader having arbitrary velocities within a bounded error and achieve flocking-like behavior. We thus analyze the tracking performance in the presence of arbitrary V_{w1}^b based on the theory of input-to-state stability or $\mathcal{L}_2$ stability in the next section.

4.4 Performance Analysis

In this section, we give tracking performance analysis of the visual robotic network Σ for a leader having individual velocities. In this analysis, we regard a body velocity of the leader as an external disturbance to the network and evaluate the estimation and control errors by employing the theory of input-to-state stability or $\mathcal{L}_2$ stability. We first apply input-to-state stability analysis to the performance analysis, where we respectively think of the velocity of the leader and the total estimation and control errors of all the other bodies as the external disturbance input and the state of the total error system of the network. We next employ the theory of $\mathcal{L}_2$ stability as one of input-to-output stability for the performance analysis by regarding the total estimation and control errors as the output of the total error system.

4.4.1 Input-to-state Stability

We give input-to-state stability analysis for the visual feedback pose synchronization law (4.1) as one of tracking performance analysis of the visual robotic network Σ for a leader moving independently.

We first consider the case that rigid body i sees body j and apply the present control law (4.1). Here, we assume that body j moves with arbitrary body velocity V_{wj}^b. Then, the closed-loop system (4.3) and (4.1) with $V_{wj}^b \neq 0$ is given by

$$
\begin{bmatrix} V_{cij}^b \\ V_{eij}^b \end{bmatrix} = \begin{bmatrix} -\mathrm{Ad}_{(g_{cij}^{-1})} & I_6 \\ 0 & -\mathrm{Ad}_{(g_{eij}^{-1})} \end{bmatrix} \begin{bmatrix} k_{ci}e_{cij} \\ k_{ei}\left(e_{eij} - \mathrm{Ad}_{(e^{-\hat{\xi}\theta_{cij}})}e_{cij}\right) \end{bmatrix} + \begin{bmatrix} 0 \\ V_{wj}^b \end{bmatrix}.
\tag{4.8}
$$

We regard V_{wj}^b and e_{ij} as the input and the state of the system (4.8), respectively. We then get the following lemma.

Lemma 8. *Consider the system (4.8). If $\bar{\theta}_{ij}(0) \in (-\pi/2, \pi/2)$ and $\theta_{eij}(0) \in (-\pi/2, \pi/2)$ hold and the gain conditions (4.9) are satisfied for any $\epsilon_i, \epsilon_i' \in \mathbb{R}_+$ ($\epsilon_i' > \epsilon_i$), then there*

exist a class-$\mathcal{KL}$ function α_2 and a class $\mathcal{K}$ function β_2 satisfying (4.10).

$$\begin{cases} k_{ci} + k_{ei} > \epsilon_i \\ \frac{k_{ei}(k_{ci} - \epsilon_i)}{k_{ci} + k_{ei} - \epsilon_i} > \epsilon_i' \end{cases}, \tag{4.9}$$

$$\|e_{ij}(t)\|_2 \le \alpha_2(\|e_{ij}(0)\|_2, t) + \beta_2\left(\sup_{0 \le \tau \le t} \|V_{wj}^b(\tau)\|_2\right). \tag{4.10}$$

Proof. We reconsider the potential function U_{ij} defined in (4.4). Then, we get the following equality from Lemma 7 with $V_{wj}^b \ne 0$.

$$\dot{U}_{ij} = -e_{ij}^{\mathrm{T}} Q_i e_{ij} + e_{eij}^{\mathrm{T}} \mathrm{Ad}_{(e^{\hat{\xi}\theta_{eij}})} V_{wj}^b, \tag{4.11}$$

where $Q_i \in \mathbb{R}^{12 \times 12}$ is defined as (4.7). Furthermore, completing square for $e_{eij}^{\mathrm{T}} \mathrm{Ad}_{(e^{\hat{\xi}\theta_{eij}})} V_{wj}^b$ with any $\gamma_2 \in \mathbb{R}_+$ yields

$$\begin{aligned} \dot{U}_{ij} &= -e_{ij}^{\mathrm{T}} Q_i e_{ij} + \frac{\gamma_2}{2} \|V_{wj}^b\|_2^2 + \frac{1}{2\gamma_2} \|e_{eij}\|_2^2 - \frac{\gamma_2}{2} \left\| \mathrm{Ad}_{(e^{\hat{\xi}\theta_{eij}})} V_{wj}^b - \frac{1}{\gamma_2} e_{eij} \right\|_2^2 \\ &\le -e_{ij}^{\mathrm{T}} Q_i e_{ij} + \frac{\gamma_2}{2} \|V_{wj}^b\|_2^2 + \frac{1}{2\gamma_2} \|e_{eij}\|_2^2. \end{aligned}$$

Note here that by using the diagonal matrix $W \in \mathbb{R}^{12 \times 12}$ whose $(7,7), \cdots, (12,12)$ elements are $1/(2\gamma_2)$ and the other elements are 0, the third term of the above inequality can be written by $e_{ij}^{\mathrm{T}} W e_{ij}$. This fact gives the following inequality for any $\epsilon_i \in \mathbb{R}_+$.

$$\begin{aligned} \dot{U}_{ij} &\le -e_{ij}^{\mathrm{T}} Q_i e_{ij} + \frac{\gamma_2}{2} \|V_{wj}^b\|_2^2 + e_{ij}^{\mathrm{T}} W e_{ij} + \epsilon_i \|e_{ij}\|_2^2 - \epsilon_i \|e_{ij}\|_2^2 \\ &= -e_{ij}^{\mathrm{T}} P_i e_{ij} + \frac{\gamma_2}{2} \|V_{wj}^b\|_2^2 - \epsilon_i \|e_{ij}\|_2^2, \end{aligned}$$

where $P_i \in \mathbb{R}^{12 \times 12}$ is defined as

$$P_i := Q_i - W - \epsilon_i I_{12}.$$

Then, calculating the Schur complement [72] of P_i with $\epsilon_i' := 1/(2\gamma_2) + \epsilon_i$ gives the necessary and sufficient condition (4.9) for positive definiteness of P_i. Therefore, if the conditions (4.9) are satisfied, we have

$$\dot{U}_{ij} \le \frac{\gamma_2}{2} \|V_{wj}^b\|_2^2 - \epsilon_i \|e_{ij}\|_2^2.$$

The remaining discussion is the same as in Lemma 5. $\qquad\square$

We next consider the case that m rigid bodies have the chain-type visibility structure, where body i sees body $i-1$ for $i \in \{2, \cdots, m\}$ (see Fig. 3.3). Then, we call the collection of the closed-loop system (4.3) and (4.1) for all the bodies *chain-type collective error system* Σ_{ccol} whose state, denoted by $x_{cp} \in \mathbb{R}^{12(m-1)}$, is given by the stacked vector of $e_{i(i-1)}$, $i \in \{2, \cdots, m-1\}$. We now get the following lemma for Σ_{ccol}.
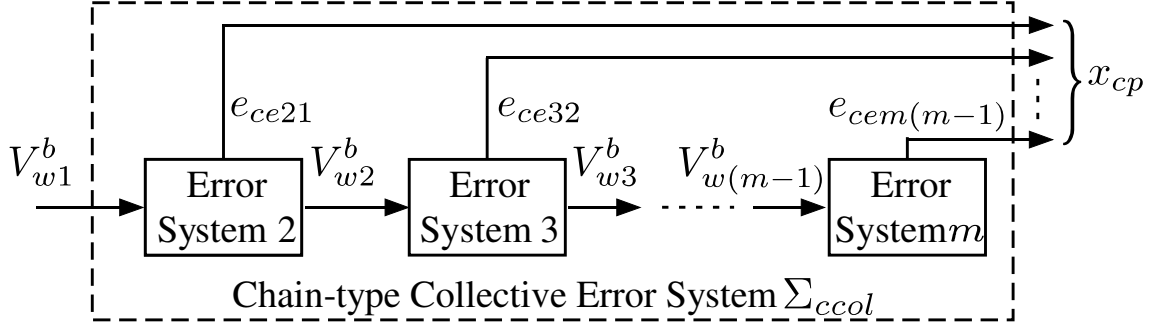
Figure 4.2: Chain-type Collective Error System Σ_{ccol}

Lemma 9. *Consider the chain-type collective error system Σ_{ccol}. If $\bar{\theta}_{i(i-1)}(0) \in (-\pi/2, \pi/2)$, $\theta_{ei(i-1)}(0) \in (-\pi/2, \pi/2)$ and the gain conditions (4.9) are satisfied for any $\epsilon_i, \epsilon'_i \in \mathbb{R}_+$ ($\epsilon'_i > \epsilon_i$), $i \in \{2, \cdots, m\}$, then there exist a class-$\mathcal{KL}$ function α_c and a class $\mathcal{K}$ function β_c satisfying*

$$\|x_{cp}(t)\|_2 \leq \alpha_c(\|x_{cp}(0)\|_2, t) + \beta_c \left(\sup_{0 \leq \tau \leq t} \|V^b_{w1}(\tau)\|_2 \right).$$

Proof. The approach of the proof is the same as in Lemma 6 (see Fig. 4.2). □

We finally show the main result of this subsection based on Lemma 9.

Theorem 5. *Consider the visual robotic network Σ with Assumption 1. Suppose that the leader has its own body velocity (i.e. $V^b_{w1} \neq 0$). If $\bar{\theta}_{ij}(0) \in (-\pi/2, \pi/2)$, $\theta_{eij}(0) \in (-\pi/2, \pi/2)$ and the gain conditions (4.9) are satisfied for any $\epsilon_i, \epsilon'_i \in \mathbb{R}_+$ ($\epsilon'_i > \epsilon_i$), $j \in \mathcal{N}_i$, $i \in \mathcal{V}$, then there exist a class-$\mathcal{KL}$ function α and a class $\mathcal{K}$ function β satisfying*

$$\|x_p(t)\|_2 \leq \alpha_a(\|x_p(0)\|_2, t) + \beta_a \left(\sup_{0 \leq \tau \leq t} \|V^b_{w1}(\tau)\|_2 \right), \tag{4.12}$$

where $x_p \in \mathbb{R}^{12(n-1)}$ is the stacked vector of e_{ij}, $j \in \mathcal{N}_i$, $i \in \mathcal{V}$.

Proof. We consider the body set $\mathcal{V}_q = \{i \in \mathcal{V} \mid i \notin \mathcal{N}_j \; ^\forall j \in \mathcal{V}\}$ defined in Chapter 3. We denote each chain-type collective error system from the leader to body $i \in \mathcal{V}_q$ by Σ_{ccoli}. Then, we conclude from Lemma 9 that each Σ_{ccoli} is input-to-state-stable. Therefore, there exist class $\mathcal{KL}$ functions α_i and class $\mathcal{K}$ functions β_i satisfying

$$\|x_{pi}(t)\|_2 \leq \alpha_i(\|x_{pi}(0)\|_2, t) + \beta_i \left(\sup_{0 \leq \tau \leq t} \|V^b_{w1}(\tau)\|_2 \right), \; i \in \mathcal{V}_q, \tag{4.13}$$

where x_{pi} are the stacked vectors of e_{ij} for each Σ_{ccoli}.

60
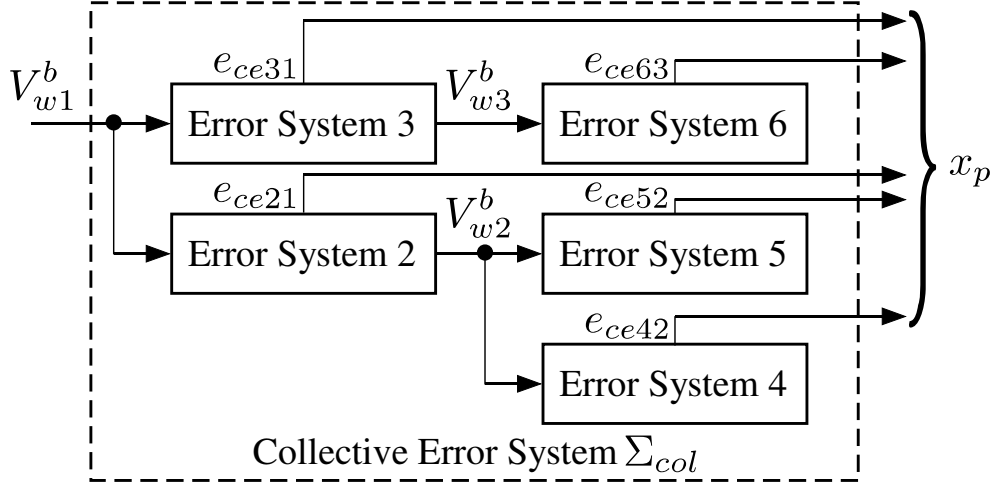
Figure 4.3: Collective Error System Σ_{col}

Then, summation of (4.13) for all $i \in \mathcal{V}_q$ gives

$$\|x_p(t)\|_2 \le \sum_{i \in \mathcal{V}_q} \alpha_i(\|x_{pi}(0)\|_2, t) + \sum_{i \in \mathcal{V}_q} \beta_i \left(\sup_{0 \le \tau \le t} \|V_{w1}^b(\tau)\|_2 \right).$$

Finally, defining α and β as

$$\alpha := \sum_{i \in \mathcal{V}_q} \alpha_i, \ \beta := \sum_{i \in \mathcal{V}_q} \beta_i \tag{4.14}$$

yields (4.12). $\qquad\square$

Similarly to the case of attitude synchronization, the gain conditions (3.9) are satisfied for almost any positive gains k_{ci} and k_{ei} since ϵ_i and ϵ_i' are arbitrary positive scalars.

Equation (4.12) evaluates the estimation and control errors for the velocity of the leader. Therefore, this can be regarded as an indicator of the tracking performance of the group. However, this analysis currently gives only qualitative evaluations for the performance, and hence it is hard to decide estimation and control gains for a good tracking performance from this analysis. In the next subsection, we analyze the performance quantitatively by employing $\mathcal{L}_2$ stability in order to give a guideline for gain settings.

4.4.2 $\mathcal{L}_2$ Stability

In this subsection, we analyze the tracking performance of the visual robotic network Σ for the leader moving independently (i.e. $V_{w1}^b \neq 0$) based on the theory of $\mathcal{L}_2$-gain performance analysis, where we regard V_{w1}^b as an external disturbance to the network.

We reconsider the total error system (4.3). Then, the collection of the system (4.3) for all $j \in \mathcal{N}_i$, $i \in \mathcal{V}$ with the control law (4.1) is called *collective error system* Σ_{col} whose state is x_p. The block diagram of the Σ_{col} in the case of the visibility structure in Fig. 2.4 is illustrated in Fig. 4.3.

Then, we have the following theorem for the tracking performance of the visual robotic network Σ.

Theorem 6. *Consider the visual robotic network Σ with Assumption 1 and suppose the leader has its own body velocity ($V_{w1}^b \neq 0$). Then, for any ϵ, $\kappa_i \in \mathbb{R}_+$, $i \in \mathcal{V}_q$, the control law (4.1) on the visual robotic network Σ achieves*

$$\|x_p\|_{\mathcal{L}_2} \leq \kappa \|V_{w1}^b\|_{\mathcal{L}_2} + \delta, \ \kappa := \sqrt{\sum_{i \in \mathcal{V}_p} \frac{\kappa_i}{2\epsilon}} \tag{4.15}$$

with a nonnegative scalar $\delta \geq 0$ if

$$\begin{cases} \begin{cases} k_{ei} - \frac{1}{2\kappa_i} - \epsilon > 0 \\ \left(k_{ci} + k_{ei} - \epsilon - \frac{2\kappa_i k_{ei}^2}{2\kappa_i(k_{ei}-\epsilon)-1} \right) I_6 - k_{ci}D_{i1} > 0 \end{cases}, \ i \in \mathcal{V}_p \\[4mm] \begin{cases} k_{cj} < 2(k_{ei} - \epsilon) \\ k_{cj} < \frac{2((k_{ci}-\epsilon)(k_{ei}-\epsilon)-k_{ei}\epsilon)}{k_{ci}+k_{ei}-\epsilon} \end{cases}, \ j \in \mathcal{N}_i, \ i \in \mathcal{V}_q \\[4mm] \begin{cases} k_{cj} < 2(k_{ei} - \epsilon) \\ \left(k_{ci} + k_{ei} - \epsilon - \frac{2k_{ei}^2}{2k_{ei}-k_{cj}-2\epsilon} \right) I_6 - k_{ci}D_{ij} > 0 \end{cases}, \ j \in \mathcal{N}_i, \ i \in \mathcal{V}_r \end{cases} \tag{4.16}$$

where $D_{ij} := (1/2)\mathrm{Ad}_{(g_{dij})}^{\mathrm{T}}\mathrm{Ad}_{(g_{dij})} \in \mathbb{R}^{6\times6}$.

Proof. Define a potential function $U_p \geq 0$ based on passivity of the relative rigid body motion (2.3) and the estimation error system (2.24) as

$$U_p := \sum_{i \in \mathcal{V}} \sum_{j \in \mathcal{N}_i} q_i U_{ij}.$$

Here, $q_i \in \mathbb{N}$ is defined as in Theorem 3. Then, the time derivative of U_p along the trajectory of (4.3) yields

$$\dot{U}_p = \sum_{i \in \mathcal{V}} \sum_{j \in \mathcal{N}_i} q_i \left(-e_{ij}^{\mathrm{T}} Q_i e_{ij} + e_{eij}^{\mathrm{T}} \mathrm{Ad}_{(e^{\hat{\xi}\theta_{eij}})} V_{wj}^b \right). \quad (\because \text{Eq. (4.11)})$$

Completing square for $e_{eij}^{\mathrm{T}} \mathrm{Ad}_{(e^{\hat{\xi}\theta_{eij}})} V_{wj}^b$, $i \in \mathcal{V}_p$ yields

$$\begin{aligned} e_{ei1}^{\mathrm{T}} \mathrm{Ad}_{(e^{\hat{\xi}\theta_{ei1}})} V_{w1}^b &= -\frac{\kappa_i}{2} \left\| \mathrm{Ad}_{(e^{\hat{\xi}\theta_{ei1}})} V_{w1}^b - \frac{1}{\kappa_i} e_{ei1} \right\|_2^2 + \frac{\kappa_i}{2} \|V_{w1}^b\|_2^2 + \frac{1}{2\kappa_i} \|e_{ei1}\|_2^2 \\ &\leq \frac{\kappa_i}{2} \|V_{w1}^b\|_2^2 + \frac{1}{2\kappa_i} \|e_{ei1}\|_2^2 \end{aligned}$$

62

for any $\kappa_i \in \mathbb{R}_+$, $i \in \mathcal{V}_p$. On the other hand, we have for the other bodies in $\{\mathcal{V}_q, \mathcal{V}_r\}$

$$
e_{eij}^{\mathrm{T}} \mathrm{Ad}_{(e^{\hat{\xi}\theta eij})} V_{wj}^b = k_{cj} e_{eij}^{\mathrm{T}} \mathrm{Ad}_{(e^{\hat{\xi}\theta eij})} \mathrm{Ad}_{(g_{djk})} e_{cjk} \quad (\because \text{Eq. (4.1)})
$$

$$
= \frac{k_{cj}}{2} \Big(\|e_{eij}\|_2^2 + \|\mathrm{Ad}_{(g_{djk})} e_{cjk}\|_2^2 - \|\mathrm{Ad}_{(e^{-\hat{\xi}\theta eij})} e_{eij} - \mathrm{Ad}_{(g_{djk})} e_{cjk})^\vee\|_2^2 \Big),
$$
(4.17)

where $k \in \mathcal{N}_j$. We now define $\Psi_i \leq 0$, $i \in \mathcal{V}$ as

$$
\Psi_i := \begin{cases}
-e_{i1}^{\mathrm{T}} \begin{bmatrix} (k_{ci} + k_{ei})I_6 - k_{ci}D_{i1} & -k_{ei}\mathrm{Ad}_{(e^{\hat{\xi}\theta ci1})} \\ -k_{ei}\mathrm{Ad}_{(e^{-\hat{\xi}\theta ci1})} & k_{ei}I_6 \end{bmatrix} e_{i1}, \; i \in \mathcal{V}_p \\[2em]
-e_{ij}^{\mathrm{T}} \begin{bmatrix} (k_{ci} + k_{ei})I_6 & -k_{ei}\mathrm{Ad}_{(e^{\hat{\xi}\theta cij})} \\ -k_{ei}\mathrm{Ad}_{(e^{-\hat{\xi}\theta cij})} & \left(k_{ei} - \frac{k_{cj}}{2}\right)I_6 \end{bmatrix} e_{ij} \\
\quad - \frac{k_{cj}}{2} \|\mathrm{Ad}_{(e^{-\hat{\xi}\theta eij})} e_{eij} - \mathrm{Ad}_{(g_{djk})} e_{cjk})^\vee\|_2^2, \; k \in \mathcal{N}_j, \; j \in \mathcal{N}_i, \; i \in \mathcal{V}_q \\[2em]
-e_{ij}^{\mathrm{T}} \begin{bmatrix} (k_{ci} + k_{ei})I_3 - k_{ci}D_{ij} & -k_{ei}\mathrm{Ad}_{(e^{\hat{\xi}\theta cij})} \\ -k_{ei}\mathrm{Ad}_{(e^{-\hat{\xi}\theta cij})} & \left(k_{ei} - \frac{k_{cj}}{2}\right)I_6 \end{bmatrix} e_{ij} \\
\quad - \frac{k_{cj}}{2} \|\mathrm{Ad}_{(e^{-\hat{\xi}\theta eij})} e_{eij} - \mathrm{Ad}_{(g_{djk})} e_{cjk})^\vee\|_2^2, \; k \in \mathcal{N}_j, \; j \in \mathcal{N}_i, \; i \in \mathcal{V}_r
\end{cases}
$$

and $\Psi_1 = 0$. Here, it should be noted that the nonnegative terms in (4.17) are included in appropriate quadratic terms.

Then, we obtain

$$
\dot{U}_p \leq \sum_{i\in\mathcal{V}} q_i \Psi_i + \sum_{i\in\mathcal{V}_p} \left(\frac{\kappa_i}{2} \|V_{w1}^b\|_2^2 + \frac{1}{2\kappa_i} \|e_{ei1}\|_2^2 \right) + \sum_{i\in\mathcal{V}} \sum_{j\in\mathcal{N}_i} q_i(\epsilon\|e_{ij}\|_2^2 - \epsilon\|e_{ij}\|_2^2)
$$

$$
\leq \sum_{i=2}^{n} \sum_{j\in\mathcal{N}_i} q_i(\Psi_i + \epsilon\|e_{ij}\|_2^2) + \sum_{i\in\mathcal{V}_p} \frac{1}{2\kappa_i} \|e_{ei1}\|_2^2 + \sum_{i\in\mathcal{V}_p} \frac{\kappa_i}{2} \|V_{w1}^b\|_2^2 - \epsilon\|x_p\|_2^2 \qquad (4.18)
$$

for any $\epsilon \in \mathbb{R}_+$, where we use the following property.

$$
\|x_p\|_2^2 \leq \sum_{i\in\mathcal{V}} \sum_{j\in\mathcal{N}_i} q_i \|e_{ij}\|_2^2.
$$

Finally, note that if the gain conditions (4.16) are satisfied, the summation of the first and second terms in (4.18) becomes nonpositive (this can be shown by calculating the Schur complement [72]). We thus get

$$
\dot{U}_p \leq \sum_{i\in\mathcal{V}_p} \frac{\kappa_i}{2} \|V_{w1}^b\|_2^2 - \epsilon\|x_p\|_2^2.
$$

63

Integrating this inequality from 0 to T with respect to time yields

$$U_p(T) - U_p(0) \leq \sum_{i \in \mathcal{V}_p} \frac{\kappa_i}{2} \int_0^T \|V_{w1}^b(t)\|_2^2 dt - \epsilon \int_0^T \|x_p(t)\|_2^2 dt.$$

Therefore, the following inequality holds true.

$$\|x_p\|_{\mathcal{L}_2} \leq \sqrt{\sum_{i \in \mathcal{V}_p} \frac{\kappa_i}{2\epsilon} \|V_{w1}^b\|_{\mathcal{L}_2}} + \sqrt{\frac{1}{\epsilon} U_p(0)}.$$

This completes the proof. $\qquad\qquad\square$

Similarly to Theorem 3, although κ_i appears in only the conditions of rigid body $i \in \mathcal{V}_p$, the arguments k_{ci}, $i \in \mathcal{V}_p$ also appear in the other constraints. This fact implicitly means that κ influences gains of all the bodies. Compared with the conditions (3.17) for visual feedback attitude synchronization, the conditions (4.16) include the information of desired biases d_{ij}. This is because the goal of visual feedback pose synchronization is to drive relative positions to the desired ones and thus control errors g_{cij} contain d_{ij}.

Remark 9. Theorem 6 means that if we regard V_{w1}^b as the disturbance input and x_p as the output of the collective error system Σ_{col}, then Σ_{col} has $\mathcal{L}_2$-gain less than or equal to κ. Since κ evaluates the estimation and control errors for the individual velocity of the leader, it can be regarded as an indicator of the tracking performance of the group. Therefore, by setting control gains making κ small, we can achieve a high tracking performance. We can find these gains by using existing solvers for linear matrix inequalities.

4.5 Verifications

In this section, we demonstrate the effectiveness of the present control law (4.1) through simulation in three dimensions and experiments on a planar testbed. We first give simulation results to show the validity of the convergence analysis (Theorem 4 and Corollary 1). We then show an experimental result for the effectiveness of the convergence and performance analysis (Theorems 4 and 6).

4.5.1 Verifications through Simulation

Consider five rigid bodies with the visibility structure depicted in Fig. 4.4 satisfying Assumption 1. We set biases as $d_{21} = [0\ 0\ 5]^T$, $d_{32} = [0\ -5\ 5]^T$ and $d_{42} = d_{53} = [0\ 5\ 5]^T$ [m] (see Fig. 4.5). Then, the control law (4.6) with $k_{c2} = 15$, $k_{c3} = 36$, $k_{c4} = 20$, $k_{c5} =$
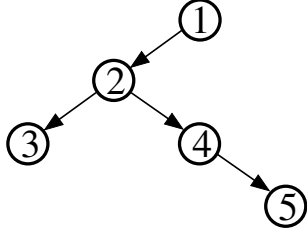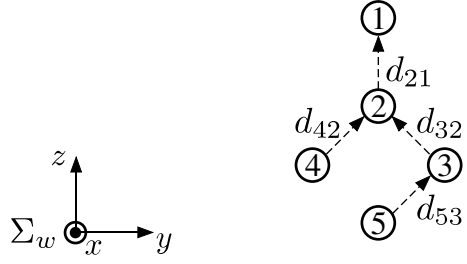
Figure 4.4: Visibility Structure in Simulation

Figure 4.5: Final Configuration in Simulation

50, $k_{ei} = 30$, $j \in \mathcal{N}_i$, $i \in \mathcal{V}$ and $V_d = [0.707\ 0\ 0.707\ 0\ 0\ 0]^\mathrm{T}$ [m/s, rad/s] is applied to each body under the following initial conditions.

$$\begin{cases} p_{w1}(0) = [10\ 0\ 10]^\mathrm{T} \\ p_{w2}(0) = [0\ -10\ 0]^\mathrm{T} \\ p_{w3}(0) = [0\ 0\ -10]^\mathrm{T} \\ p_{w4}(0) = [-10\ 0\ -10]^\mathrm{T} \\ p_{w5}(0) = [-10\ 0\ -20]^\mathrm{T} \end{cases} \text{[m]}, \quad \begin{cases} \xi\theta_{w1}(0) = [0\ \frac{\pi}{4}\ 0]^\mathrm{T} \\ \xi\theta_{w2}(0) = [0\ 0\ 0]^\mathrm{T} \\ \xi\theta_{w3}(0) = [0\ -\frac{\pi}{4}\ 0]^\mathrm{T} \\ \xi\theta_{w4}(0) = [\frac{\pi}{3}\ 0\ 0]^\mathrm{T} \\ \xi\theta_{w5}(0) = [\frac{\pi}{4}\ \frac{\pi}{4}\ 0]^\mathrm{T} \end{cases} \text{[rad]}.$$

Simulation results are shown in Figs. 4.6-4.8. Fig. 4.6 shows the trajectory of each rigid body in 3D space, where the circles represent the initial positions. Figs. 4.7 and 4.8 illustrate the errors between the desired relative positions and the actual ones, and the relative orientations, respectively. We see from Figs. 4.6 and 4.7 that every body eventually forms the desired configuration at around 1.5s. Fig. 4.8 shows that all the relative orientations asymptotically converge to 0 at around 2s, that is, the orientations of all the bodies asymptotically converge to that of body 1 . Thus, the present estimation and control scheme (4.6) achieves visual feedback pose synchronization (2.11).

4.5.2 Verifications through Experiments

We next present experimental results on a planar testbed to verify the effectiveness of the convergence and performance analysis.

We use three omnidirectional mobile robots (TOSADENSHI) with four wheels as rigid bodies. Each body is equipped with a pinhole camera FMVU-03MTC-CS (ViewPLUS) with a panoramic mirror HM-M15 (Accowle Vision). We attach a plate with four colored circles to each robot in order to improve accuracy of extracting feature points. We also utilize a camera FMVU-03MTC-CS attached above the experimental field to measure the actual poses of robots. The frame rate of the camera is 30fps. Transmitted video signals are loaded into PC and manipulated by image processing software Visual C++ (Microsoft). The control and observer models are designed by Simulink (The Math Works)
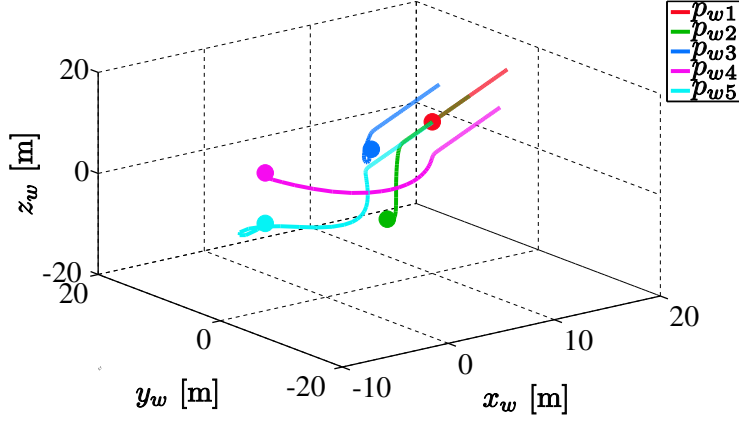
Figure 4.6: Position in Σ_w
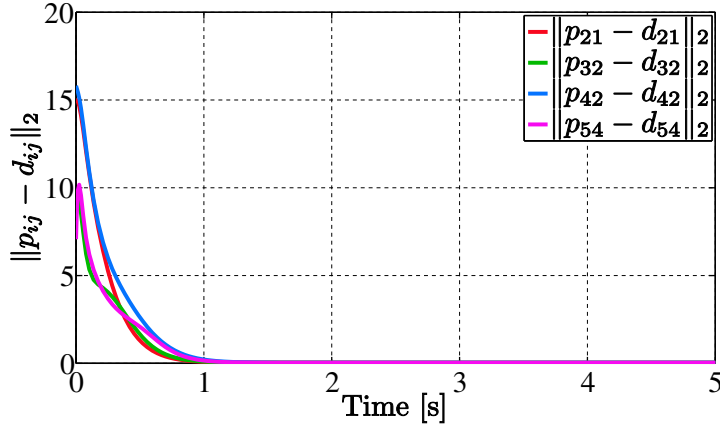
Figure 4.7: Position Error

and calculated by DSP board DS1104 (dSPACE) in real time. Then the control input in sent to robots via an embedded wireless communication device XBee (Digi International). The sampling period of the controller is around 20ms. This experimental schematic is shown in Fig. 4.9. Although each robot can move only on 2D plane, the pose estimation algorithm is executed in three dimensions. Therefore, each robot implements the visual feedback velocity input projected onto the experimental field.

We use the visibility structure depicted in Fig. 4.10. Let the position biases be
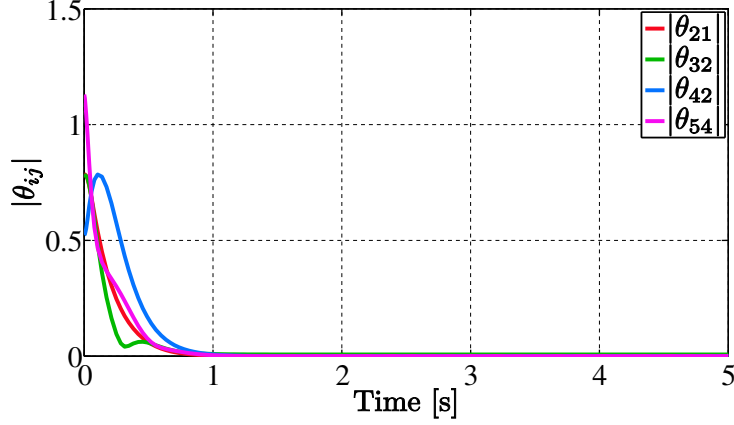
Figure 4.8: Rotation Angle Error

$d_{21} = d_{32} = [0\ 0.25\ 0]^{\mathrm{T}}$ [m] (see Fig. 4.11). The estimation and control gains are set as

$$\text{Gain A}: \begin{cases} k_{c2} = 5.0, \ k_{c3} = 5.7 \\ k_{e2} = 8.0, \ k_{e3} = 9.3 \end{cases},$$

$$\text{Gain B}: \begin{cases} k_{c2} = 0.37, \ k_{c3} = 0.5 \\ k_{e2} = 3.0, \ k_{e3} = 3.0 \end{cases},$$

where both settings satisfy the gain conditions (4.16) and we get the performance indicators $\kappa = 2.70$ for Gain A and $\kappa = 18.10$ for Gain B ($\epsilon = 0.5$). We also set the initial conditions as

$$\begin{cases} p_{w1}(0) = [0.96\ 0.27\ 0]^{\mathrm{T}} \\ p_{w2}(0) = [0.53\ 0.41\ 0]^{\mathrm{T}} \ \ [\mathrm{m}], \\ p_{w3}(0) = [0.13\ 0.51\ 0]^{\mathrm{T}} \end{cases} \begin{cases} \xi\theta_{w1}(0) = [0\ 0\ -0.06]^{\mathrm{T}} \\ \xi\theta_{w2}(0) = [0\ 0\ -0.72]^{\mathrm{T}} \ \ [\mathrm{rad}]. \\ \xi\theta_{w3}(0) = [0\ 0\ -1.54]^{\mathrm{T}} \end{cases}$$

Finally, we set the body velocity of the leader (rigid body 1) as

$$V_{w1}^{b}(t) = \begin{cases} [0.1\sin t\ 0.1\ 0\ 0\ 0\ 0]^{\mathrm{T}}, & t \in [0,5) \\ [0.1\sin t\ 0.1\ 0\ 0\ 0\ 0.15]^{\mathrm{T}}, & t \in [5,15) \\ [0.1\sin t\ 0.1\ 0\ 0\ 0\ 0]^{\mathrm{T}}, & t \in [15,30) \\ 0, & t \in [20,30) \end{cases} \quad [\mathrm{m/s,\ rad/s}].$$

The experimental results are shown in Figs. 4.12-4.15. Fig. 4.12 illustrates the trajectories of the robots on the experimental field for Gain A, Fig. 4.13 time responses of the relative positions and Fig. 4.14 the orientations in Σ_w. Also, Fig. 4.15 shows $\|x_p(t)\|_{\mathcal{L}_2}$ for Gain A and Gain B, respectively. We see from Figs. 4.12 and 4.13 that when the leader moves independently, the other robots track it successfully, and the
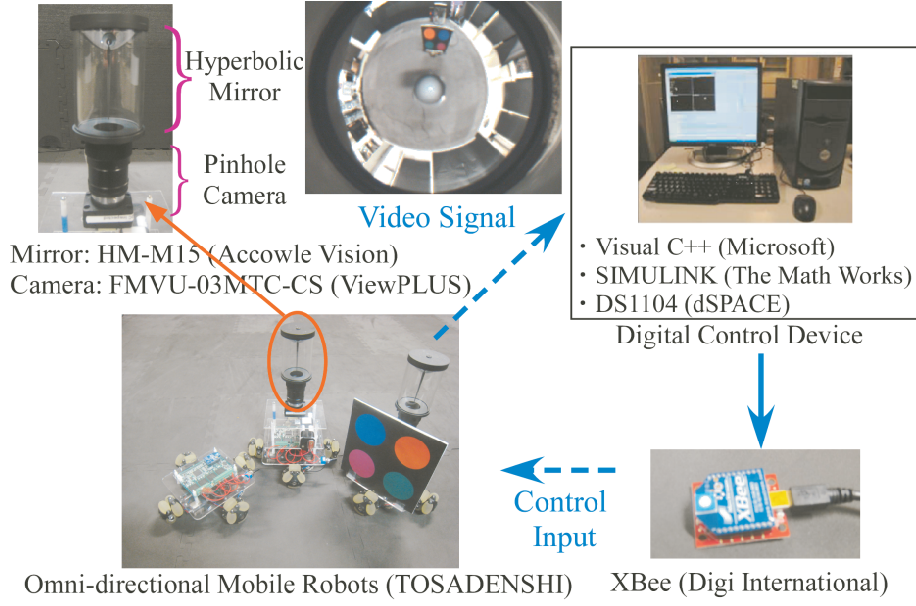
Figure 4.9: Experimental Environment
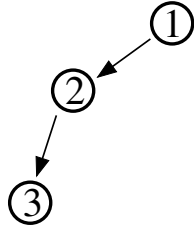
Figure 4.10: Visibility Structure in Experiment
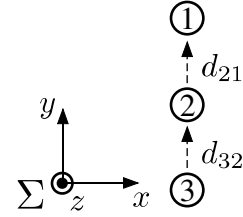
Figure 4.11: Final Configuration in Experiment

desired relative positions are almost achieved at around 35s when the leader is static. Moreover, Fig. 4.14 shows that all the orientations converge to almost a common value (robot 1's value) at that time. The results mean that the present control law (4.1) achieves visual feedback pose synchronization and thus the synchronization law works successfully.

Figs. 4.15 shows that the tracking performance is improved for the smaller κ. Therefore, κ is adequate for the performance indicator of the visual feedback pose synchronization.
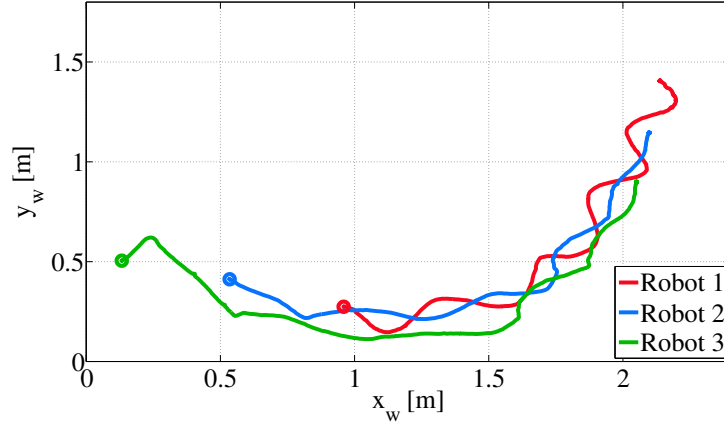
Figure 4.12: Position in Σ_w
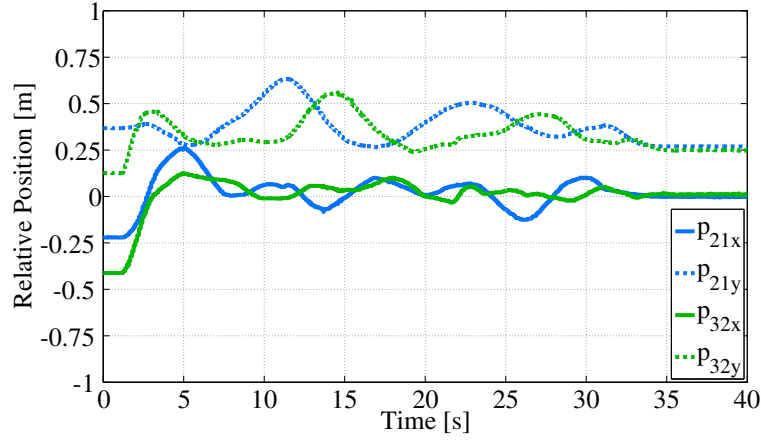
Figure 4.13: Relative Position in Σ_w

4.6 Chapter Summary

In this chapter, we have studied a visual feedback pose synchronization problem for visual robotic networks Σ. We have first presented a synchronization law to achieve visual feedback pose synchronization in the sense of (2.11). We have then proved that the present estimation and control scheme achieves synchronization under leader-following visibility structures in the absence of communication or any other measurements of the states. Here, passivity of the rigid body motion (2.2) and the relative rigid body motion (2.3) plays crucial roles for the design of the control law and the convergence analysis. We have next given both qualitative and quantitative tracking performance analysis of the network for a leader having individual body velocities by employing the theory of input-
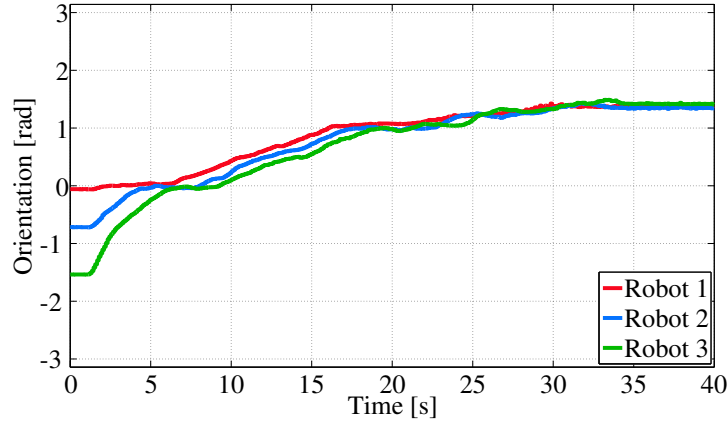
Figure 4.14: Rotation Angle in Σ_w
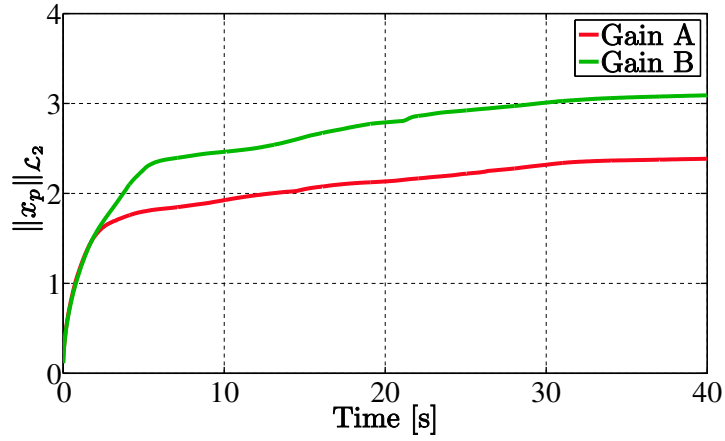
Figure 4.15: Tracking Performance

to-state stability or $\mathcal{L}_2$ stability. Moreover, we have shown that the performance analysis based on $\mathcal{L}_2$ stability gives a guideline to design estimation and control gains. Finally, the simulation results and the experimental results have demonstrated the validity of the main results in this chapter.

The main issues to be tackled are (i) to weaken the assumption of visibility structures, (ii) to take account of rigid body dynamics, and (iii) to employ a visibility maintenance algorithm and a collision avoidance mechanism. We address these issues in the next chapter.

70

Chapter 5

Further Developments on Visual Feedback Attitude/Pose Synchronization

5.1 Introduction

In this chapter, we give further developments on visual feedback attitude/pose synchronization investigated in Chapters 3 and 4. Although we deal with only the pinhole camera model (2.5) throughout this chapter, the model can be easily extended to the panoramic camera model (2.8) as shown in Chapter 4. We first propose a visual feedback attitude synchronization law integrating a linear velocity observer to overcome the issue that the present control protocol (3.1) presumes using a common linear velocity. Here, we newly present a velocity estimation mechanism incorporating passive velocity models of the leader. We next study visual feedback attitude synchronization in the absence of a leader. In this situation, we propose a different synchronization law from the present one for the visual robotic network Σ with ring-type visibility structures and prove synchronization in the different approach. Then, we also clarify the difficulties to handle wider classes of visibility structures for synchronization. We then integrate rigid body dynamics into visual robotic networks. Namely, we newly present a force and torque law to achieve visual feedback pose synchronization. Even here, passivity of the dynamics plays central roles for the design of the control scheme and the convergence analysis. We finally mention about collision avoidance and visibility maintenance necessary in practical.

This chapter is organized as follows. In Section 5.2, we newly propose an estimation and control mechanism for the visual robotic network Σ to achieve visual feedback attitude synchronization without common knowledge. We next tackle a visual feedback attitude synchronization problem without a leader in Section 5.3. In Section 5.4, we introduce rigid body dynamics and present a dynamic visual feedback pose synchronization law to achieve the same goal as in Chapter 4. In Sections 5.2-5.4, we prove that synchronization

is achieved by the present schemes. We finally address collision avoidance and visibility maintenance problems and propose their mechanisms in Section 5.5. Section 5.6 concludes this chapter.

5.2 Visual Feedback Attitude Synchronization with a Linear Velocity Observer

This section studies a visual feedback attitude synchronization problem taking account of linear velocity estimation. Although we have already proposed the attitude synchronization law (3.1) for visual robotic networks Σ in Chapter 3, we have supposed that all the rigid bodies in the network have a common linear velocities. Therefore, we newly present a control law with a linear velocity observer to make the bodies completely autonomous by integrating passive linear velocity models of the leader. Throughout this section, we consider leader-following type visibility structures satisfying Assumption 1.

5.2.1 Linear Velocity Model

Suppose that the linear velocity of the leader is given in the form of a finite Fourier series expansion as follows.

$$v_{w1}^b(t) = c + \sum_{i=1}^{l} \left(a_i \sin(w_i t) + b_i \cos(w_i t) \right), \tag{5.1}$$

where $a_i, b_i, c \in \mathbb{R}^3$ and the frequencies $w_i \in \mathbb{R}_+$, $i \in \{1, \cdots, l\}$ are supposed to be known *a priori*. Note here that a constant velocity model is the special case of (5.1) $(a_i = b_i = 0 \ ^\forall i)$.

Let us now show the passivity of (5.1). We define $z_{v0} \in \mathbb{R}^3, z_{vi} \in \mathbb{R}^3, i \in \{1, \cdots, l\}$, $z_v \in \mathbb{R}^{3l}$ and $x_v \in \mathbb{R}^{6l+3}$ as

$$z_{v0} := c, \ z_{vi} := a_i \sin(w_i t) + b_i \cos(w_i t), \ z_v := [z_{v1}^\mathrm{T} \ \cdots \ z_{vl}^\mathrm{T}]^\mathrm{T}, \ x_v := [z_{v0}^\mathrm{T} \ z_v^\mathrm{T} \ \dot{z}_v^\mathrm{T}]^\mathrm{T}.$$

Then, it is straightforward to see that the time evolution of v_{w1}^b is represented by the following linear time invariant system.

$$\dot{x}_v = A_v x_v, \ A_v := \begin{bmatrix} 0 & 0 & 0 \\ 0 & 0 & I_{3l} \\ 0 & -\mathrm{diag}(w_1^2, \cdots, w_l^2) \otimes I_3 & 0 \end{bmatrix} \in \mathbb{R}^{(6l+3) \times (6l+3)}, \tag{5.2a}$$

$$v_{w1}^b = C_v x_v, \ C_v := [\mathbf{1}_{l+1}^\mathrm{T} \otimes I_3 \ 0] \in \mathbb{R}^{3 \times (6l+3)}. \tag{5.2b}$$

We get the following lemma for the linear system (5.2b).

Lemma 10. *Define $B_v \in \mathbb{R}^{(6l+3) \times 3}$ as $B_v := C_v^{\mathrm{T}}$. Then, the linear system $(A_v, B_v, C_v, 0)$ with the state x_v is passive with respect to the storage function $S_v(x_v) := (1/2) x_v^{\mathrm{T}} P_v x_v \geq 0$ with*

$$P_v := \begin{bmatrix} I_{3(l+1)} & 0 \\ 0 & \mathrm{diag}(1/w_1^2, \cdots, 1/w_l^2) \otimes I_3 \end{bmatrix} \in \mathbb{R}^{(6l+3) \times (6l+3)}.$$

Proof. We denote the input of the system by $u_v \in \mathbb{R}^3$. Then, the time derivative of S_v along the trajectory of (5.2b) is given as follows.

$$\dot{S}_v = x_v^{\mathrm{T}} P_v (A_v x_v + B_v u_v) = x_v^{\mathrm{T}} \begin{bmatrix} 0 & 0 & 0 \\ 0 & 0 & I_{3l} \\ 0 & -I_{3l} & 0 \end{bmatrix} x_v + x^{\mathrm{T}} B_v u_v = (C_v x_v)^{\mathrm{T}} u_v.$$

This completes the proof. $\qquad\square$

Remark 10. A key example of (5.1) is a constant velocity (i.e. $v_{w1}^b = c_v$ [36, 37, 81] or a typical rectangular wave. The model is in practice useful not only for really constant velocities since any signal can be approximated by a piecewise step function and it can be also approximated by finite Fourier series expansions. Similarly, (5.1) is helpful even if v_{w1}^b is not really periodic, since a future profile of v_{w1}^b over a finite interval can be approximated as (5.1). Namely, it is possible to regard the estimation process over the infinite time interval as repeats of the estimation over a finite time interval. A variety of real periodic motion is also approximately described in the form of (5.1).

5.2.2 Visual Feedback Attitude Synchronization Law Integrating a Linear Velocity Observer

Based on Lemma 10, we propose the following control law.

$$Controller: \begin{cases} v_{wi}^b = \bar{v}_i, & (5.3\mathrm{a}) \\ \omega_{wi}^b = k_{ci} \displaystyle\sum_{j \in \mathcal{N}_i} \mathrm{sk}(e^{\hat{\bar{\xi}}\bar{\theta}_{ij}})^{\vee}, & (5.3\mathrm{b}) \end{cases}$$

$$Velocity\ Observer: \begin{cases} \dot{\bar{x}}_{vi} = A_v \bar{x}_{vi} + B_v u_{vi}, \ \bar{v}_i = C_v \bar{x}_{vi}, & (5.3\mathrm{c}) \\ u_{vi} = k_{vi} p_{eij}, & (5.3\mathrm{d}) \end{cases}$$

$$Pose\ Observer: \begin{cases} \bar{V}_{ij}^b := (\bar{g}_{ij}^{-1} \dot{\bar{g}}_{ij})^{\vee} = -\mathrm{Ad}_{(\bar{g}_{ij}^{-1})} V_{wi}^b + \begin{bmatrix} \bar{v}_i \\ 0 \end{bmatrix} + u_{ij}, & (5.3\mathrm{e}) \\ u_{ij} = k_{ei} \left(e_{eij} - \begin{bmatrix} 0 \\ \mathrm{sk}(e^{\hat{\bar{\xi}}\bar{\theta}_{ij}})^{\vee} \end{bmatrix} \right), & (5.3\mathrm{f}) \end{cases}$$

where $j \in \mathcal{N}_i$, $i \in \mathcal{V}$ and $k_{ci}, k_{vi}, k_{ei} \in \mathbb{R}_+$ $^{\forall}i \in \mathcal{V}$. Equations (5.3a) and (5.3b) represent velocity input where each rigid body feedbacks the estimated linear velocity denoted by $\bar{v}_i \in \mathbb{R}^3$ instead of a common v in (3.1a). In order to estimate the linear velocity of the leader, we newly build a linear velocity observer as in (5.3c) and (5.3d). Notice here that since each rigid body whose visible body is not the leader (body 1) cannot get the visual information associated with the leader, each body feedbacks the visual measurement of its visible body. Then, $\bar{x}_{vi} \in \mathbb{R}^{6l+3}$ is the estimate of x_v, and $u_{vi} \in \mathbb{R}^3$ is external input to be determined so that the estimated value $\bar{v}_i$ is driven to v_{wj}^b, $j \in \mathcal{N}_i$ (as a result, v_{w1}^b), which is given by (5.3d). Equations (5.3e) and (5.3f) represent the visual motion observer including the estimated linear velocity $\bar{v}_i$.

5.2.3   Convergence Analysis

We first define the estimation errors $v_{ei} \in \mathbb{R}^3$ and $x_{ei} \in \mathbb{R}^{6l+3}$ as follows.

$$v_{ei} := v_{wj}^b - \bar{v}_i, \; j \in \mathcal{N}_i, \; x_{ei} := \begin{cases} x_v - \bar{x}_{vi}, \; i \in \mathcal{V}_p \\ \bar{x}_{vj} - \bar{x}_{vi}, \; j \in \mathcal{N}_i, \; i \in \mathcal{V}_q \cup \mathcal{V}_r \end{cases}.$$

Then, when the linear velocity law (5.3a) is applied to every rigid body, we get the following estimation error system.

$$\dot{x}_v = A_v x_v, \; v_{w1}^b = C_v x_v, \; \dot{\bar{x}}_{vi} = A_v \bar{x}_{vi}, \; v_{wi}^b = C_v \bar{x}_{vi}, \; i \in \mathcal{V} \setminus \{1\}, \tag{5.4}$$

$$\dot{g}_{eij} = -\hat{u}_{ij} g_{eij} - \hat{\bar{V}}_i g_{eij} + g_{eij} V_{wj}^b, \tag{5.5}$$

$$\dot{x}_{ei} = A_v x_{ei} - B_v u_{vi}, \; v_{ei} = C_v x_{ei}, \tag{5.6}$$

where $\bar{V}_i := [\bar{v}_i^{\mathrm{T}} \; 0]^{\mathrm{T}} \in \mathbb{R}^6$. On the other hand, since the linear velocity estimation mechanism does not influence the orientation part of the relative rigid body motion model (see (5.3e)), we think of the orientation part of (5.3e) as the control error system similarly to Chapter 3.

We now get the following theorem for the present control law (5.3).

Theorem 7. *Consider the visual robotic network Σ with Assumption 1 and suppose that the leader moves with the velocity given by (5.1). Then, the control law (5.3) on Σ achieves visual feedback attitude synchronization.*

Proof. We give the proof by using induction. We first consider each rigid body i in $\mathcal{V}_1$ whose visible body is body 1 ($\mathcal{V}_k$ is defined in the proof of Theorem 1). Since the linear velocity estimation mechanism does not influence the orientation parts of the estimation error system and the control error system, the convergence analysis for the orientations is the same as in Theorem 1. It is thus sufficient for the proof to show that the linear velocity observer estimates v_{w1}^b correctly (i.e. $v_{ei} = 0$). We now consider the position part

of the estimation error system (5.5) and (5.6). Then, substituting the present control law (5.3) into the systems gives

$$\dot{x}_{ei} = A_v x_{ei} - k_{vi} B_v p_{ei1},$$

$$\dot{p}_{ei1} = -\hat{u}_{Ri1} p_{ei1} - u_{pi1} - \bar{v}_i + e^{\hat{\xi}\theta_{ei1}} v_{w1}^b$$

$$= -k_{ei} \left(\text{sk}(e^{\hat{\xi}\theta_{ei1}}) - \text{sk}(e^{\hat{\bar{\xi}}\bar{\theta}_{i1}}) \right) p_{ei1} - k_{ei} p_{ei1} + v_{ei} - v_{w1}^b + e^{\hat{\xi}\theta_{ei1}} v_{w1}^b.$$

Therefore, we obtain

$$\begin{bmatrix} \dot{x}_{ei} \\ \dot{p}_{ei1} \end{bmatrix} = \begin{bmatrix} A_v & -k_{vi} B_v \\ C_v & -k_{ei} I_3 \end{bmatrix} \begin{bmatrix} x_{ei} \\ p_{ei1} \end{bmatrix}$$
$$+ \begin{bmatrix} 0 \\ (e^{\hat{\xi}\theta_{ei1}} - I_3) v_{w1}^b + k_{ei} \left(\text{sk}(I_3 - e^{\hat{\bar{\xi}}\bar{\theta}_{i1}}) - \text{sk}(I_3 - e^{\hat{\xi}\theta_{ei1}}) \right) p_{ei1} \end{bmatrix}. \quad (5.7)$$

Note here that the second term in (5.7) is equal to 0 when the orientation of body i in $\mathcal{V}_1$ converges to that of the leader. Therefore, if we define the state $x_{i1}' \in \mathbb{R}^{6l+6}$ for (5.7) as $x_{i1}' := [x_{ei}^{\mathrm{T}}\ p_{ei1}^{\mathrm{T}}]^{\mathrm{T}}$, we can apply Proposition 1 to the convergence analysis by regarding (5.7) as the perturbed system. Namely, it is sufficient to show that the equilibrium point $x_{i1}' = 0$ for the system (5.7) without the second term is exponentially stable.

We view the system (5.7) as a linear time invariant system $\dot{x}_{i1}' = \Gamma x_{i1}'$ with the vanishing perturbation, where $\Gamma \in \mathbb{R}^{(6l+6)\times(6l+6)}$ is defined as

$$\Gamma := \begin{bmatrix} A_v & -k_{vi} B_v \\ C_v & -k_{ei} I_3 \end{bmatrix}.$$

Let $[y_0^{\mathrm{T}}\ \cdots\ y_{2l+1}^{\mathrm{T}}]^{\mathrm{T}} \in \mathbb{R}^{6l+6}$, $y_j \in \mathbb{R}^3$ be an eigenvector of Γ corresponding to an eigenvalue $\sigma \in \mathbb{C}$. Then, from the definition of Γ, we get the following equations.

$$(\sigma + k_{ei}) y_{2l+1} = \sum_{j=0}^{l} y_j, \quad k_{vi} y_{2l+1} = -\sigma y_0, \quad (5.8)$$

$$k_{vi} y_{2l+1} = y_{l+j} - \sigma y_j, \quad \sigma y_{l+j} = -w_j^2 y_j, \quad j \in \{1, \cdots, l\}. \quad (5.9)$$

From (5.9), we have

$$y_j = -\frac{k_{vi}\sigma}{\sigma^2 + w_j^2} y_{2l+1}. \quad (5.10)$$

Substituting the second equations of (5.8) and (5.10) into the first equation of (5.8) yields

$$\sigma + k_{ei} = -\frac{k_{vi}}{\sigma} - \sum_{j=1}^{l} \frac{k_{vi}\sigma}{\sigma^2 + w_j^2}.$$

We now denote $\sigma = \sigma_1 + \sqrt{-1}\sigma_2$, $\sigma_1, \sigma_2 \in \mathbb{R}$. Then, by comparing the coefficients of the real part, we have

$$\sigma_1 + k_{ei} = -k_{vi}\sigma_1 \left(\frac{1}{\sigma_1^2 + \sigma_2^2} + \sum_{j=1}^{l} \frac{\tilde{\sigma}_j}{\bar{\sigma}_j} \right),$$

where

$$\tilde{\sigma}_j := (\sigma_1^2 + \sigma_2^2 + w_j^2) \in \mathbb{R}, \ \bar{\sigma}_j = (\sigma_1^2 - \sigma_2^2 + w_j^2)^2 + 4\sigma_1^2\sigma_2^2 \in \mathbb{R}.$$

Since

$$k_{vi}\left(\frac{1}{\sigma_1^2 + \sigma_2^2} + \sum_{j=1}^{l} \frac{\tilde{\sigma}_j}{\bar{\sigma}_i} \right) \geq 0$$

holds, we see that σ_1 has to be negative. Therefore, the matrix Γ is Hurwitz and we conclude from the linearity of the system $\dot{x}_{i1}' = \Gamma x_{i1}'$ that the origin of the system is exponentially stable. This means that the linear velocity observer estimates v_{w1}^b correctly.

We next consider each rigid body i in $\mathcal{V}_2$ whose visible body is in $\mathcal{V}_1$. Notice again that the linear velocity estimation mechanism does not influence the orientation parts of the estimation error system and the control error system. Therefore, the convergence analysis for the orientations is the same as in Theorem 1. On the other hand, since body $j \in \mathcal{V}_1$ applies the linear velocity along the trajectory of the state space model $(A_v, B_v, C_v, 0)$ which is available for body i in $\mathcal{V}_2$ (see (5.3a) and (5.3c)), substituting the present control law (5.3) into the estimation error systems gives

$$\dot{x}_{ei} = A_v x_{ei} - k_{vi}B_v p_{eij} + k_{vj}B_v p_{ej1},$$
$$\dot{p}_{eij} = -k_{ei}\left(\mathrm{sk}(e^{\hat{\xi}\theta_{eij}}) - \mathrm{sk}(e^{\hat{\bar{\xi}}\bar{\theta}_{ij}}) \right) p_{eij} - k_{ei}p_{eij} + v_{ei} - v_{wj}^b + e^{\hat{\xi}\theta_{eij}}v_{wj}^b.$$

Therefore, we obtain

$$\begin{bmatrix} \dot{x}_{ei} \\ \dot{p}_{ei1} \end{bmatrix} = \begin{bmatrix} A_v & -k_{vi}B_v \\ C_v & -k_{ei}I_3 \end{bmatrix} \begin{bmatrix} x_{ei} \\ p_{ei1} \end{bmatrix}$$
$$+ \begin{bmatrix} k_{vj}B_v p_{ej1} \\ (e^{\hat{\xi}\theta_{ei1}} - I_3)v_{wj}^b + k_{ei}\left(\mathrm{sk}(I_3 - e^{\hat{\bar{\xi}}\bar{\theta}_{ij}}) - \mathrm{sk}(I_3 - e^{\hat{\xi}\theta_{eij}}) \right) p_{eij} \end{bmatrix}.$$

Notice now that similarly to the case of $\mathcal{V}_1$, the second term is equal to 0 when body $j \in \mathcal{V}_1$ achieves visual feedback attitude synchronization. The remaining convergence analysis is thus the same as in the case of $\mathcal{V}_1$. Namely, we can conclude that the orientations and the linear velocities of all the bodies in $\mathcal{V}_2$ converge to common values in $\{1\} \cup \mathcal{V}_1$. We can also apply the same analysis for the other bodies in $\mathcal{V}_k$, $k \in \{3, 4, \cdots\}$. $\qquad\square$
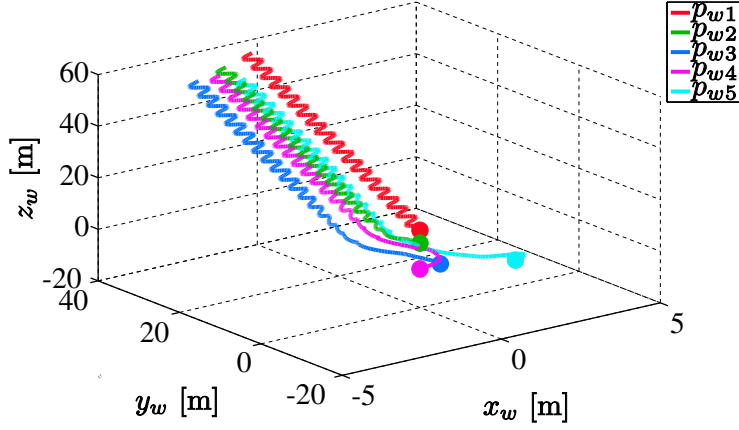
Figure 5.1: Position in Σ_w
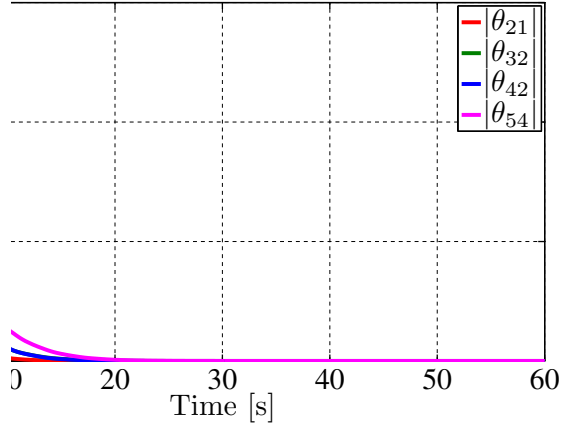
Figure 5.2: Orientation Error

In the present estimation and control mechanism (5.3), each rigid body feedbacks the estimated linear velocity and the velocity observer input is built by the estimation error associated with positions. Since the estimation error can be constructed by visual measurements (2.9) as shown in Appendix A, the present control law (5.3) is completely autonomous.

5.2.4 Verifications

We finally demonstrate the effectiveness of the present control law (5.3) through simulation in three dimensions. We consider the visual robotic network Σ with the visibility structure
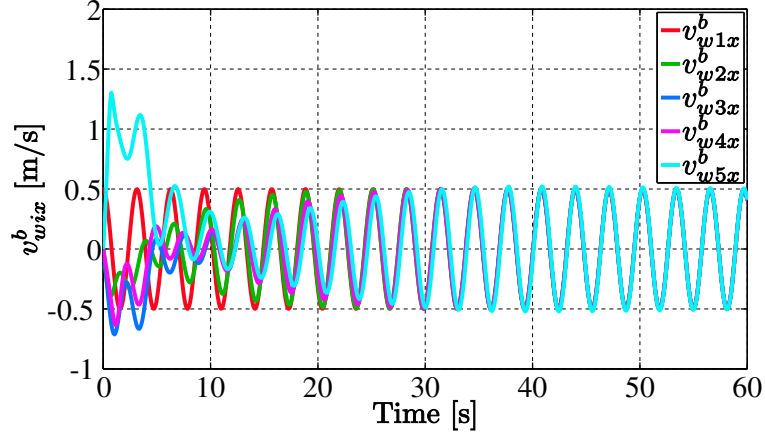
Figure 5.3: Linear Velocity (x-axis)
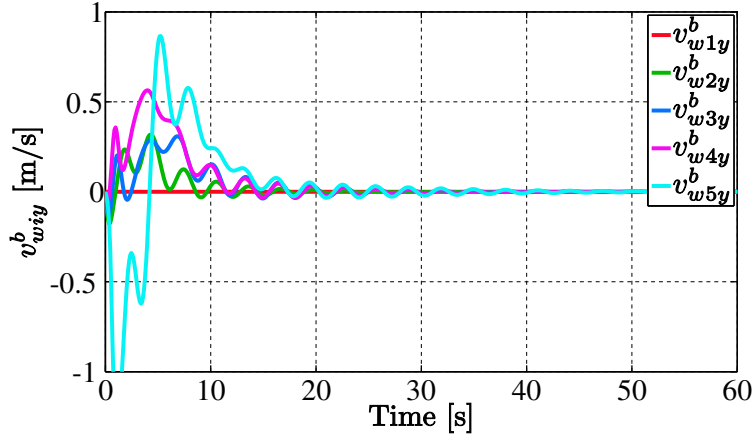
Figure 5.4: Linear Velocity (y-axis)

shown in Fig. 4.4 satisfying Assumption 1. Let initial conditions be

$$
\begin{cases}
p_{w1}(0) = [0\ 0\ 10]^{\mathrm{T}} \\
p_{w2}(0) = [0\ 0\ 5]^{\mathrm{T}} \\
p_{w3}(0) = [0\ -5\ 0]^{\mathrm{T}} \quad [\mathrm{m}], \\
p_{w4}(0) = [0\ 0\ -5]^{\mathrm{T}} \\
p_{w5}(0) = [3\ 0\ -10]^{\mathrm{T}}
\end{cases}
\begin{cases}
\xi\theta_{w1}(0) = [-\frac{\pi}{4}\ 0\ 0]^{\mathrm{T}} \\
\xi\theta_{w2}(0) = [0\ 0\ 0]^{\mathrm{T}} \\
\xi\theta_{w3}(0) = [-\frac{\pi}{4}\ 0\ 0]^{\mathrm{T}} \quad [\mathrm{rad}]. \\
\xi\theta_{w4}(0) = [0\ 0\ \frac{\pi}{3}]^{\mathrm{T}} \\
\xi\theta_{w5}(0) = [0\ -\frac{\pi}{3}\ 0]^{\mathrm{T}}
\end{cases}
$$

Also, the linear body velocity of the leader (rigid body 1) is set as $v(t) = [0.5\cos(2t)\ \ 0\ \ 1]^{\mathrm{T}}$ [m/s], and the angular velocity of the leader is 0. We finally apply the present control law (5.3) with $k_{vi} = 1$, $k_{ci} = 1$, $k_{ei} = 3\ ^{\forall}i \in \mathcal{V}$.

The simulation results are shown in Figs. 5.1-5.5. Fig. 5.1 illustrates the trajectories

78
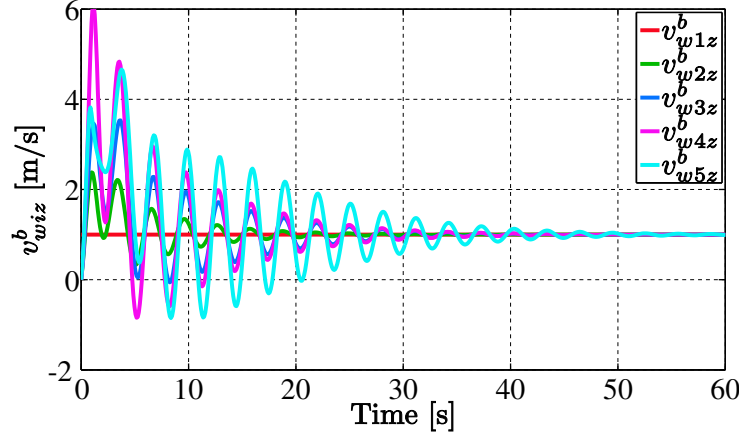
Figure 5.5: Linear Velocity (z-axis)

of the rigid bodies in 3D space, where the circles represent the initial positions. The time responses of the absolute values of the relative rotation angles are shown in Fig. 5.2. We also depict the time responses of the linear body velocity of each body in Figs. 5.3-5.5. We see from Figs. 5.1 and 5.2 that the present control law (5.3) achieves visual feedback attitude synchronization. Also, Figs. 5.3-5.5 show that the present linear velocity observer works successfully.

5.3 Visual Feedback Attitude Synchronization under Ring-type Visibility Structures

This section investigates a visual feedback attitude synchronization problem under ring-type visibility structures. We consider the visual robotic network Σ with visibility structures satisfying Assumption 2. The feature of the ring-type visibility structures is not to require the existence of a leader.

5.3.1 Visual Feedback Attitude Synchronization Law for Ring-type Visibility Structures

In order to achieve visual feedback attitude synchronization (2.10), we propose the following control law.

79

$$\text{Controller:} \begin{cases} v_{wi}^b = v, & \text{(5.11a)} \\ \omega_{wi}^b = k \sum_{j \in \mathcal{N}_i} \text{sk}(e^{\hat{\bar{\xi}}\bar{\theta}_{ij}})^\vee, & \text{(5.11b)} \end{cases}$$

$$\text{Observer:} \begin{cases} \bar{V}_{ij}^b := (\bar{g}_{ij}^{-1}\dot{\bar{g}}_{ij})^\vee = -\text{Ad}_{(\bar{g}_{ij}^{-1})}V_{wi}^b + u_{ij}, & \text{(5.11c)} \\ u_{ij} = ke_{eij} + \begin{bmatrix} e^{\hat{\xi}\theta_{eij}}v \\ 0 \end{bmatrix}, & \text{(5.11d)} \end{cases}$$

where $j \in \mathcal{N}_i$, $i \in \mathcal{V}$ and $k \in \mathbb{R}_+$ is a common gain among all the rigid bodies. It should be noted that the observer input (5.11d) is different from (3.1d).

5.3.2 Convergence Analysis

The present control input (5.11) gives the following theorem for visual robotic networks Σ with ring-type visibility structures.

Theorem 8. *Consider the visual robotic network Σ with Assumption 2. Then, the control law (5.11) on Σ achieves visual feedback attitude synchronization in the sense of (2.10) if $e^{\hat{\xi}\theta_{ij}}(t) > 0$, $e^{\hat{\bar{\xi}}\bar{\theta}_{ij}}(t) > 0$, $e^{\hat{\xi}\theta_{eij}}(t) > 0$, $j \in \mathcal{N}_i$, $i \in \mathcal{V}$ hold for all $t \geq 0$.*

Proof. Without loss of generality, we deal with the case that rigid body i sees body $i-1$ for $i \in \{2, \cdots, n\}$ and body 1 sees body n. Consider the potential function $U_a \geq 0$ defined in Chapter 3. Then, U_a can be rewritten as follows under the ring-type visibility structure.

$$U_a = \sum_{i=1}^{n} \left(\phi(e^{\hat{\bar{\xi}}\bar{\theta}_{i(i-1)}}) + \psi(g_{ei(i-1)}) \right),$$

where we regard the index '0' as 'n', i.e. $e^{\hat{\bar{\xi}}\bar{\theta}_{10}}$ and g_{e10} represent $e^{\hat{\bar{\xi}}\bar{\theta}_{1n}}$ and g_{e1n}, respectively. Similarly, we think of the index '-1' as '$n-1$' in the subsequent discussion.

Then, the time derivative of U_a yields

$$\dot{U}_a = -k \sum_{i=1}^{n} \Bigg(\|p_{ei(i-1)}\|_2^2 + \frac{1}{2}\|\text{sk}(e^{\hat{\bar{\xi}}\bar{\theta}_{i(i-1)}})^\vee - \text{sk}(e^{\hat{\xi}\theta_{ei(i-1)}})^\vee\|_2^2$$
$$+ \frac{1}{2}\|\text{sk}(e^{\hat{\bar{\xi}}\bar{\theta}_{(i-1)(i-2)}})^\vee - \text{sk}(e^{\hat{\xi}\theta_{ei(i-1)}})^\vee\|_2^2 \Bigg).$$

Therefore, $\dot{U}_a$ is nonpositive. We next consider the set $\mathcal{S} := \{x_a \in \mathbb{R}^{9(n-1)} \mid \dot{U}_a = 0\}$. Then, $\mathcal{S}$ can be written as

$$\mathcal{S} = \{x_a \in \mathbb{R}^{9(n-1)} \mid p_{ei(i-1)} = 0,$$
$$\text{sk}(e^{\hat{\bar{\xi}}\bar{\theta}_{i(i-1)}})^\vee = \text{sk}(e^{\hat{\xi}\theta_{ei(i-1)}})^\vee = \text{sk}(e^{\hat{\bar{\xi}}\bar{\theta}_{(i-1)(i-2)}})^\vee = \text{sk}(e^{\hat{\xi}\theta_{e(i-1)(i-2)}})^\vee \; \forall i \in \mathcal{V}\}.$$

80

Note here that since $\text{sk}(e^{\hat{\xi}\theta})^{\vee} = \xi \sin\theta$ holds, the following property is satisfied for $\theta \in (-\pi/2, \pi/2)$ and $\theta' \in (-\pi/2, \pi/2)$.

$$\text{sk}(e^{\hat{\xi}\theta}) = \text{sk}(e^{\hat{\xi}'\theta'}) \ \leftrightarrow \ e^{\hat{\xi}\theta} = e^{\hat{\xi}'\theta'}.$$

Therefore, if $e^{\hat{\xi}\theta_{i(i-1)}}(t) > 0$ and $e^{\hat{\bar{\xi}}\bar{\theta}_{i(i-1)}}(t) > 0$ hold for all $i \in \mathcal{V}$, we get

$$e^{\hat{\bar{\xi}}\bar{\theta}_{i(i-1)}} = e^{\hat{\xi}\theta_{ei(i-1)}} = e^{\hat{\bar{\xi}}\bar{\theta}_{(i-1)(i-2)}} = e^{\hat{\xi}\theta_{e(i-1)(i-2)}} \ ^{\forall}i \in \mathcal{V}.$$

Then, from $e^{\hat{\xi}\theta_{ei(i-1)}} = e^{-\hat{\bar{\xi}}\bar{\theta}_{i(i-1)}}e^{\hat{\xi}\theta_{i(i-1)}} = e^{-\hat{\bar{\xi}}\bar{\theta}_{(i-1)(i-2)}}e^{\hat{\xi}\theta_{(i-1)(i-2)}} = e^{\hat{\xi}\theta_{e(i-1)(i-2)}}$, we obtain $e^{\hat{\xi}\theta_{i(i-1)}} = e^{\hat{\xi}\theta_{(i-1)(i-2)}}$ for all $i \in \mathcal{V}$. Therefore, if $e^{\hat{\xi}\theta_{ij}} > 0$ is satisfied for all time, this means that $e^{\hat{\xi}\theta_{ij}} = I_3$ holds for all $i \in \mathcal{V}$. We finally conclude from LaSalle's Invariance Principle [49] that all the state trajectories converge to the set $\{x_a \in \mathbb{R}^{9(n-1)} \mid x_a = 0\}$ and this set is positively invariant (see (5.11)). This completes the proof. $\square$

Theorem 8 shows that visual feedback attitude synchronization is achieved even if a leader does not exist. However, to get this result, we utilize the additional assumptions associated with gains and orientation configurations. To weaken these assumptions and to tackle visual feedback pose synchronization problems under ring-type visibility structures are our future directions.

Remark 11. Throughout this dissertation, we consider the case that each rigid body sees only one body. The main reason of this limitation is that since each body has its own estimates of relative poses, we cannot directly utilize geometric properties such as

$$g_{ij} = g_{wi}^{-1}g_{wj}, \ g_{ji} = g_{ij}^{-1}, \ g_{ij}g_{jk} = g_{ik}$$

as used in [46, 47, 48]. Namely, $\bar{g}_{ji} = \bar{g}_{ij}^{-1}$ does not hold true.

5.4 Dynamic Visual Feedback Pose Synchronization

In this section, we integrate rigid body dynamics into visual robotic networks Σ. Namely, we consider the case that each body cannot directly apply velocity laws. We first introduce Newton-Euler equations to describe the dynamics. Then, we propose passivity-based force and torque input to achieve visual feedback pose synchronization in the sense of (2.11) and prove the synchronization.

5.4.1 Passivity of Newton-Euler Equations

In addition to the rigid body motion (2.2), we consider the following Newton-Euler equation [82] for the dynamics of rigid bodies.

$$\begin{bmatrix} m_i I_3 & 0 \\ 0 & J_i \end{bmatrix} \begin{bmatrix} \dot{v}_{wi}^b \\ \dot{\omega}_{wi}^b \end{bmatrix} + \begin{bmatrix} m_i \hat{\omega}_{wi}^b v_{wi}^b \\ \hat{\omega}_{wi}^b J_i \omega_{wi}^b \end{bmatrix} = \begin{bmatrix} f_i \\ \tau_i \end{bmatrix}, \ i \in \mathcal{V} \tag{5.12}$$

where, $m_i \in \mathbb{R}_+$ and $J_i \in \mathbb{R}^{3\times 3}$ are the mass and the inertia tensor of body i, respectively. Also, $f_i \in \mathbb{R}^3$ and $\tau_i \in \mathbb{R}^3$ are force and torque input of body i. In this problem, we take the approach that the force and torque input drives the actual velocity to the desired velocity consisting of the present velocity input (4.1a). In line with that, we use passivity of the rigid body dynamics (5.12).

We now define the positive definite matrix $M_i \in \mathbb{R}^{6\times 6}$ and the skew-symmetric matrix $C_i \in \mathbb{R}^{6\times 6}$ as

$$M_i := \begin{bmatrix} m_i I_3 & 0 \\ 0 & J_i \end{bmatrix}, \; C_i := \begin{bmatrix} m_i \hat{\omega}_{wi}^b & 0 \\ 0 & -\left(J_i \omega_{wi}^b\right)^\wedge \end{bmatrix}.$$

Then, the dynamics (5.12) is rewritten by

$$M_i \dot{V}_{wi}^b + C_i(\omega_{wi}^b)V_{wi}^b = F_i, \tag{5.13}$$

where $F_i = [f_i^T \; \tau_i^T]^T \in \mathbb{R}^6$ is force and torque input of body i. Then, the following lemma holds for the rigid body dynamics (5.13).

Lemma 11. *The time derivative of $U_{di} := (1/2)(V_{wi}^b)^T M_i V_{wi}^b \geq 0$ along the trajectory of (5.13) satisfies*

$$\dot{U}_{di} = F_i^T V_{wi}^b.$$

Proof. The time derivative of U_{di} along the trajectory of (5.13) yields

$$\begin{aligned} \dot{U}_{di} &= (V_{wi}^b)^T M_i \dot{V}_{wi}^b \\ &= -(V_{wi}^b)^T C_i(\omega_{wi}^b)\dot{V}_{wi}^b + (V_{wi}^b)^T F_i \\ &= F_i^T V_{wi}^b. \end{aligned}$$

$\square$

Lemma 11 means that the rigid body dynamics (5.13) is passive from F_i to V_{wi}^b. Namely, if we respectively consider F_i and V_{wi}^b as the input and the output of (5.13), there exists no coupling term between the position and the orientation dynamics.

5.4.2 Dynamic Visual Feedback Pose Synchronization Law

We first consider the force and torque input F_i to drive the actual velocity to the desired velocity, denoted by $V_{di} = [v_{di}^T, \omega_{di}^T]^T \in \mathbb{R}^6$, which is equal to the present velocity input (4.1a). We propose the following force and torque input based on [83].

$$F_i = M_i \dot{V}_{di} + C(\omega_{wi}^b)V_{di} + u_{ai}, \tag{5.14}$$

where $u_{ai} \in \mathbb{R}^6$ is new input to drive the actual velocity V_{wi}^b to the desired one V_{di}. Then, by defining the velocity error as $r_i = [r_{pi}^T \ r_{Ri}^T]^T := V_{wi}^b - V_{di} \in \mathbb{R}^6$, we get the following error dynamics.

$$M_i \dot{r}_i + C_i(\omega_{wi}^b) r_i = u_{ai}. \tag{5.15}$$

Then, the error dynamics (5.15) is passive from u_{ai} to r_i as in Lemma 11. Therefore, we can conclude that the equilibrium point $r_i = 0$ is asymptotically stable for the following input.

$$u_{ai} = -k_{ai} r_i, \tag{5.16}$$

where $k_{ai} \in \mathbb{R}_+$.

We now propose the following visual feedback attitude synchronization law.

$$\text{Controller:} \begin{cases} F_i = M_i \dot{V}_{di} + C(\omega_{wi}^b) V_{di} + \begin{bmatrix} 0 \\ e_{cij} \end{bmatrix} + u_{ai}, & (5.17a) \\[2ex] u_{ai} = -k_{ai} r_i, & (5.17b) \\[2ex] V_{di} = k_{ci} \sum_{j \in \mathcal{N}_i} \mathrm{Ad}_{(g_{dij})} e_{cij}, & (5.17c) \end{cases}$$

$$\text{Observer:} \begin{cases} \bar{V}_{ij}^b := (\bar{g}_{ij}^{-1} \dot{\bar{g}}_{ij})^\vee = -\mathrm{Ad}_{(\bar{g}_{ij}^{-1})} V_{wi}^b + u_{ij}, & (5.17d) \\[2ex] u_{ij} = k_{ei} \left(e_{eij} - \mathrm{Ad}_{(e^{-\hat{\xi}_{\theta cij}})} e_{cij} \right), & (5.17e) \end{cases}$$

where $j \in \mathcal{N}_i$, $i \in \mathcal{V}$. It should be noted that in the present control law (5.17), each rigid body requires its own body velocity information in addition to visual measurements (2.9). Moreover, $\dot{V}_{di}$ depends on $\dot{p}_{eij}$ and hence v_{wj}^b which is not available only from the visual measurements. In this work, we avoid the problem numerically by just replacing $\dot{p}_{eij}$ by the difference approximation of p_{eij} following [44]. A solution to work out this issue rigorously is to assume more information like optical flow [32]. Notice also that due to the limit of measured output, we propose slightly different force and torque input u_{ai} from (5.16).

5.4.3 Convergence Analysis

Combining the dynamic error system with (5.17a) and the estimation and control error systems yields the following total error system.

$$\begin{bmatrix} \dot{r}_i \\ V_{cij}^b \\ V_{eij}^b \end{bmatrix} = \begin{bmatrix} -M_i^{-1} C_i r_i + M_i^{-1} e_{cij} \\ -\mathrm{Ad}_{(g_{cij}^{-1})} r_i \\ 0 \end{bmatrix} + \begin{bmatrix} M_i^{-1} & 0 & 0 \\ 0 & -\mathrm{Ad}_{(g_{cij}^{-1})} & I_6 \\ 0 & 0 & -\mathrm{Ad}_{(g_{eij}^{-1})} \end{bmatrix} \begin{bmatrix} u_{ai} \\ \mathrm{Ad}_{(g_{dij}^{-1})} V_{wi}^b \\ u_{ij} \end{bmatrix} + \begin{bmatrix} 0 \\ 0 \\ V_{wj}^b \end{bmatrix}. \tag{5.18}$$

We also define the total error vector $e_{di} \in \mathbb{R}^{18}$ as $e_{di} := [r_i^{\mathrm{T}} \ e_{cij}^{\mathrm{T}} \ e_{eij}^{\mathrm{T}}]^{\mathrm{T}}$. We now define a potential function $U_{dij} \geq 0$ as follows.

$$U_{dij} := \frac{1}{2} r_i^{\mathrm{T}} M_i r_i + \psi(g_{cij}) + \psi(g_{eij}). \tag{5.19}$$

Then, the following lemma holds for the total error system (5.18),

Lemma 12. *If $V_{wj}^b = 0$ holds, then the time derivative of U_{dij} along the trajectory of (5.18) satisfies*

$$\dot{U}_{dij} = u_{dij}^{\mathrm{T}} \nu_{dij},$$

where

$$u_{dij} := \begin{bmatrix} u_{ai} \\ \mathrm{Ad}_{(g_{dij}^{-1})} V_{wi}^b \\ u_{ij} \end{bmatrix} \in \mathbb{R}^{18}, \ \nu_{dij} := \begin{bmatrix} I_6 & 0 & 0 \\ 0 & -I_6 & 0 \\ 0 & \mathrm{Ad}_{(e^{-\hat{\xi}\theta_{cij}})} & -I_6 \end{bmatrix} e_{dij} \in \mathbb{R}^{18}.$$

Proof. Lemmas 7 and 11 give the proof. □

Lemma 12 means that total error system (5.18) is passive from u_{dij} to ν_{dij} with the storage function U_{dij} when $V_{wj}^b = 0$ holds. It should be noted that the present input (5.17) is constructed by the output of the passivity.

We get the following theorem from Lemma 12.

Theorem 9. *Consider the visual robotic network Σ with the dynamics (5.13) and Assumption 1. Then, the control law (5.17) on Σ achieves visual feedback pose synchronization.*

Proof. We can prove this theorem by using the same approach as in Theorem 4. The difference is only that we introduce U_{dij} instead of U_{ij} and the time derivative of U_{dij} yields $-k_{ai}\|r_i\|_2^2$ which is negative definite associated with r_i. □

We can also analyze the tracking performance for the leader moving independently by utilizing the same approach as in Chapter 4. However, note again that the present control law (5.17) requires own velocity information and the difference approximation of v_{wj}^b.

5.5 Collision Avoidance and Visibility Maintenance

In motion coordination problems, it is necessary to tackle collision avoidance problems. On the other hand, in vision-based cooperative control, visibility has to be maintained since a neighbor is captured by a vision sensor. Visibility maintenance also requires collision avoidance since it is undesirable for rigid bodies to get too close to each other. We thus propose collision avoidance and connectivity maintenance algorithms in this section.
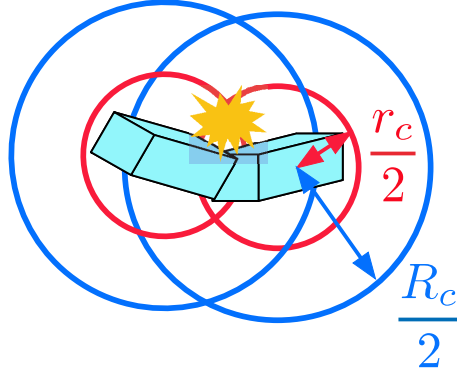
Figure 5.6: Collision

5.5.1 Definitions of Collision and Visibility

We first define collision as follows (see Fig. 5.6).

Definition 7. *Rigid bodies i and j are said to collide if and only if $||p_{ij}|| \leq r_c$, where $r_c \in \mathbb{R}_+$ is a collision distance.*

In order to avoid collisions with neighbors, we employ the following potential function $U_{caij} \geq 0$ as in [47] (see Fig. 5.7).

$$U_{caij} := \left(\min \left\{ 0, \frac{||p_{ij}||_2^2 - R_c^2}{||p_{ij}||_2^2 - r_c^2} \right\} \right)^2, \; j \in \mathcal{N}_i, \tag{5.20}$$

where $R_c \in \mathbb{R}_+$ ($R_c > r_c$) is the distance from which the function works to avoid collision. Then, the partial derivative of U_{caij} by p_{wi} gives

$$e^{-\hat{\xi}\theta_{wi}} \left(\frac{\partial U_{caij}}{\partial p_{wi}} \right)^{\mathrm{T}} = \begin{cases} 0 & \text{if } R_c \leq ||p_{ij}||_2 \\ -4 \frac{(R_c^2 - r_c^2)(||p_{ij}||_2^2 - R_c^2)}{(||p_{ij}||_2^2 - r_c^2)^3} p_{ij} & \text{if } r_c < ||p_{ij}||_2 < R_c \\ \text{not defined} & \text{if} ||p_{ij}||_2 = r_c \\ 0 & \text{if } ||p_{ij}||_2 < r_c \end{cases}.$$

Notice here that $e^{-\hat{\xi}\theta_{wi}}(\partial U_{caij}/\partial p_{wi})$ requires only relative pose information.

We next define visibility for the pinhole camera model (2.5). We denote the bearing angles of i with respect to its visible body $j \in \mathcal{N}_i$ by $\chi_{ij}, \zeta_{ij} \in \mathbb{R}$, where χ_{ij} and ζ_{ij} are associated with the z-axis and x-axis of Σ_i, respectively. Then, the angles are given as follows (see Fig. 5.8).

$$\chi_{ij} := \arctan \left(\frac{\sqrt{x_{ij}^2 + y_{ij}^2}}{z_{ij}} \right), \; \zeta_{ij} := \arctan \left(\frac{x_{ij}}{y_{ij}} \right),$$

85
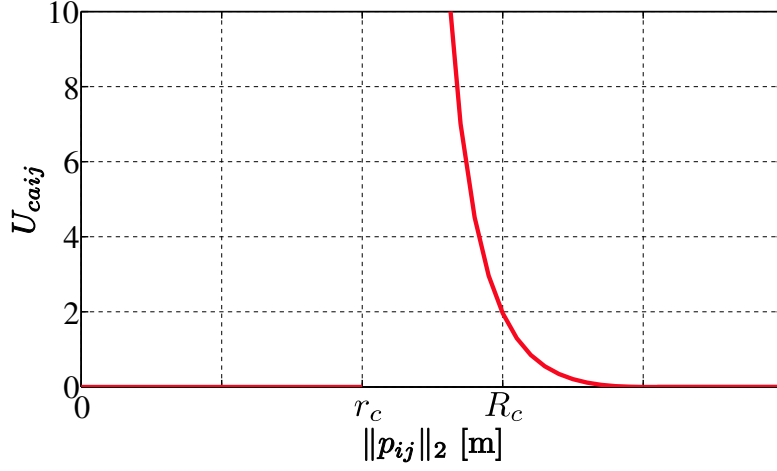
Figure 5.7: Artificial Potential Function for Collision Avoidance

where we use the notation $p_{ij} = [x_{ij} \ y_{ij} \ z_{ij}]^{\mathrm{T}}$. We now define visibility.

Definition 8. *Visibility of rigid body i for its visible body j is said to be maintained when $|\chi_{ij}| < \chi_M$ holds, where $\chi_M \in \mathbb{R}_+$ is the maximum view angle of the pinhole camera.*

Similarly to (5.20), we define the following potential function $U_{vmij} \geq 0$ to maintain visibility (see Fig. 5.9).

$$U_{vmij} := \frac{1}{2}(\chi_{vmij} + \chi_{vmji}), \ \chi_{vmij} := \left(\min \left\{ 0, \frac{\chi_{ij}^2 - \chi_m^2}{\chi_{ij}^2 - \chi_M^2} \right\} \right)^2 \geq 0, \qquad (5.21)$$

where $\chi_m \in \mathbb{R}_+$ ($\chi_M > \chi_m$) is the absolute angle from which the function works to maintain the visibility. Then, the partial derivative of U_{vmij} with respect to p_{wi} gives

$$e^{-\hat{\xi}\theta_{wi}} \left(\frac{\partial U_{vmij}}{\partial p_{wi}} \right)^{\mathrm{T}} =$$

$$\begin{cases} 0 & \text{if } \chi_M < \chi_{ij} \\ \text{not defined} & \text{if } \chi_{ij} = \chi_M \\ -\frac{4\chi_{ij}(\chi_{ij}^2 - \chi_m^2)(\chi_M^2 - \chi_m^2)}{\|p_{ij}\|_2^2 (\chi_M^2 - \chi_{ij}^2)^3} \left[z_{ij} \cos \zeta_{ij} \ z_{ij} \sin \zeta_{ij} \ -\sqrt{x_{ij}^2 + y_{ij}^2} \right]^{\mathrm{T}} & \text{if } \chi_m \leq \chi_{ij} < \chi_M \\ 0 & \text{if } \chi_{ij} < \chi_m \end{cases}.$$

On the other hand, the partial derivative of U_{vmij} with respect to $\Phi_{wi} = [\Phi_{wix} \ \Phi_{wiy} \ \Phi_{wiz}]^{\mathrm{T}} \in$

86
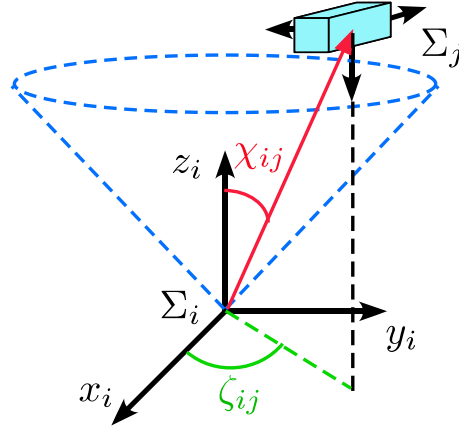
Figure 5.8: Visibility

$\mathbb{R}^3$ (the rotation of body i associated with Σ_w) yields

$$
e^{-\hat{\xi}\theta_{wi}} \left(\frac{\partial U_{vmij}}{\partial \Phi_{wi}} \right)^{\mathrm{T}} =
\begin{cases}
0 & \text{if } \chi_M < \chi_{ij} \\
\text{not defined} & \text{if } \chi_{ij} = \chi_M \\
-\frac{4\chi_{ij}(\chi_{ij}^2 - \chi_m^2)(\chi_M^2 - \chi_m^2)}{(\chi_M^2 - \chi_{ij}^2)^3} \begin{bmatrix} -\sin\zeta_{ij} & \cos\zeta_{ij} & 0 \end{bmatrix}^{\mathrm{T}} & \text{if } \chi_m \le \chi_{ij} < \chi_M \\
0 & \text{if } \chi_{ij} < \chi_m
\end{cases}.
$$

Similarly to U_{caij}, the time derivatives require only relative pose information.

5.5.2 Collision Avoidance and Visibility Maintenance Law

We now propose a collision avoidance and visibility maintenance algorithm. We first consider the previous work introduced in Subsection 2.4.3. Namely, we suppose that each rigid body has actual relative poses g_{ij}, $j \in \mathcal{N}_i$ and consider the pose synchronization law (2.22). Then, by employing functions (5.20) and (5.21), we modify the velocity input (2.22) as

$$
V_{wi}^b = \begin{bmatrix} k_{pi}I_3 & 0 \\ 0 & k_{Ri}I_3 \end{bmatrix} \sum_{j \in \mathcal{N}_i} \left(\begin{bmatrix} p_{ij} \\ \mathrm{sk}(e^{\hat{\xi}\theta_{ij}})^{\vee} \end{bmatrix} - \begin{bmatrix} e^{-\hat{\xi}\theta_{wi}} \left(\frac{\partial U_{caij}}{\partial p_{wi}} \right)^{\mathrm{T}} \\ 0 \end{bmatrix} \right.
$$
$$
\left. - \begin{bmatrix} e^{-\hat{\xi}\theta_{wi}} \left(\frac{\partial U_{vmij}}{\partial p_{wi}} \right)^{\mathrm{T}} \\ e^{-\hat{\xi}\theta_{wi}} \left(\frac{\partial U_{vmij}}{\partial \Phi_{wi}} \right)^{\mathrm{T}} \end{bmatrix} \right), \quad k_{pi}, k_{Ri} \in \mathbb{R}_+, \ i \in \mathcal{V}. \quad (5.22)
$$

Then, the following fact holds [84].
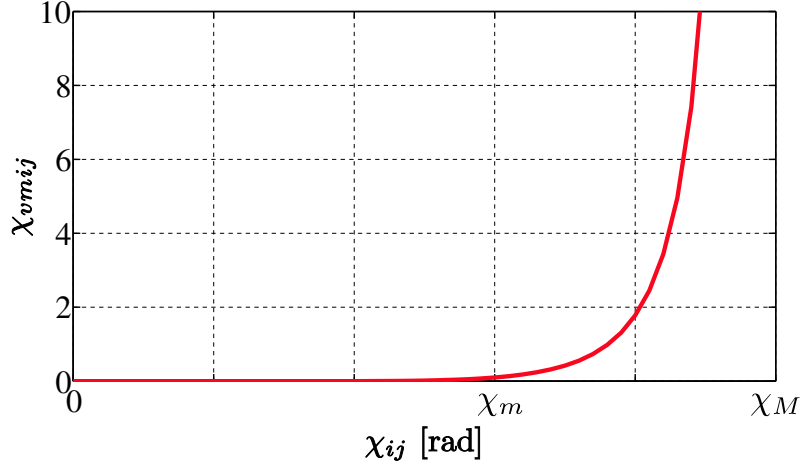
Figure 5.9: Artificial Potential Function for Visibility Maintenance

Fact 4. *Consider n rigid bodies represented by (2.2). Suppose that there exists $e^{\hat{\xi}\theta_a} \in SO(3)$ such that $e^{-\hat{\xi}\theta_a} e^{\hat{\xi}\theta_{wi}} \; \forall i \in \mathcal{V}$ are positive definite at the initial time, the undirected interconnection topology between bodies is fixed, connected, and the initial conditions satisfy $\|p_{ij}(0)\|_2^2 > r_c$ and $|\chi_{ij}(0)| < \chi_M$ for all $j \in \mathcal{N}_i$, $i \in \mathcal{V}$. Then, the control input (5.22) leads each body to avoid collisions with its neighbors and keep them within its field of view. In addition, all the poses converge to the poses satisfying*

$$
\begin{cases}
\sum_{j \in \mathcal{N}_i} \left(p_{ij} - \left(\frac{\partial U_{caij}}{\partial p_{wi}} \right)^{\mathrm{T}} - \left(\frac{\partial U_{vmij}}{\partial p_{wi}} \right)^{\mathrm{T}} \right) = 0 \\
\sum_{j \in \mathcal{N}_i} \left(\mathrm{sk}(e^{\hat{\xi}\theta_{ij}})^{\vee} - \left(\frac{\partial U_{vmij}}{\partial \Phi_{wi}} \right)^{\mathrm{T}} \right) = 0
\end{cases}
\forall i \in \mathcal{V}.
$$

Since the present input (5.22) is formed only by relative poses associated with neighbors, we get the following corollary.

Corollary 2. *The control law (5.22) is implementable with only visual measurements.*

We have shown the effectiveness through experiments in [84]. However, Corollary 2 shows only the possibility of the implementation of the collision avoidance and visibility maintenance algorithm and each rigid body implements the algorithm by using the estimates $\bar{g}_{ij}$ instead of the actual g_{ij} in our framework, which might cause collision or break visibility. The design of the control law to completely guarantee collision avoidance and visibility maintenance is one of our future works.

5.6   Chapter Summary

In this chapter, we have given further developments on visual feedback attitude/pose synchronization investigated in Chapters 3 and 4. We have first proposed a visual feedback attitude synchronization law integrating the passive linear velocity model of the leader to estimate the velocity, which enables for rigid bodies to be completely autonomous. We have then showed that the present scheme achieves visual feedback attitude synchronization. We have next studied visual feedback attitude synchronization for visual robotic networks without a leader. We have proposed a new attitude synchronization law for ring-type visibility structures and prove synchronization. In the convergence analysis, we have also clarified the difficulties to handle wider classes of visibility structures for synchronization. We have next integrated rigid body dynamics into visual robotic networks. Here, we have introduced Newton-Euler equations to describe the dynamics and proposed a force and torque input to achieve pose synchronization, where passivity of the dynamics plays central roles for the design of the control law and the convergence analysis. We have finally mentioned about collision avoidance and visibility maintenance necessary in practical.

Chapter 6

Conclusions

6.1 Dissertation Summary

In this dissertation, we have investigated visual feedback attitude/pose synchronization on $SE(3)$ for a group of rigid bodies equipped with vision sensors. The main feature of this work is that visual information extracted by a monocular camera is only available for each body to implement its control law. We have first introduced a notion of visual robotic networks consisting of multiple bodies with rigid body motion, visibility structures and visual measurements. Then, the visual robotic network becomes the robotic network regarding interconnection topologies between bodies as visibility structures and adding explicit formulation of measured output. This setting enables each body to be fully autonomous. We have next given the definitions of visual feedback attitude/pose synchronization as the goals of this work. The definitions require each body to utilize only visual measurements for the implementation of control laws in addition to those in our previous works.

We have next proposed visual feedback attitude/pose synchronization laws consisting of visual motion observers and synchronization laws. Here, passivity of rigid body motion plays a crucial role for the design of the present estimation and control mechanisms. We have then given the convergence and performance analysis for the visual robotic network with the present estimation and control schemes. In the analysis, we have focused mainly on leader-following visibility structures. It has first been shown via Lyapunov methods that the present laws achieve attitude/pose synchronization under leader-following type visibility structures, where passivity of rigid body motion also plays a central role. However, in the present control scheme, the leader does not rotate/move, and as a result, the network cannot rotate/move after attitude/pose synchronization. In order to overcome these issues, we have next considered the case that the leader rotates/moves independently. In this situation, we have analyzed the tracking performance of the network for the leader by employing the theory of input-to-state stability or $\mathcal{L}_2$ stability. Here, we have regarded the individual velocity of the leader as an external disturbance to the net-

work and evaluate the total estimation and control errors in the network. This analysis gives the guidelines to design the estimation and control gains of the present estimation and control mechanisms.

We have moreover given some further developments on visual feedback attitude/pose synchronization in regard to (i) linear velocity observers for attitude synchronization, (ii) ring-type visibility structures which does not require the existence of a leader, (iii) extension from velocity laws to force and torque ones by integrating Newton-Euler equations as rigid body dynamics, and (iv) visibility maintenance and collision avoidance. The effectiveness and validity of the present estimation and control schemes and the convergence and performance analysis have been demonstrated through simulation in three dimensions and experiments on a planar testbed.

6.2 Further Directions

The main further direction of this work is to extend the class of visibility structures for visual feedback attitude/pose synchronization. In fact, the current classes are very limited (the main reason of this problem is mentioned in Remark 11). Usage of more visual information such as optical flows or time-to-collision used in [59, 62] might be helpful to work out this issue.

Other future works are listed as follows.

- We propose visual feedback algorithms to guarantee collision avoidance and visibility maintenance. This dissertation has only shown that the collision avoidance law proposed in [47] and the present visibility maintenance law presuming the measurement of actual relative poses can be formed by estimated relative ones. A solution to this problem is to build collision avoidance and visibility maintenance laws by using visual measurements.

- We analyze the convergence analysis for switching visibility structures since visible rigid bodies of each body depend on its visibility. A solution to this issue is to utilize the concept of brief instability developed in [85] and introduce dwell time as used in [46, 47].

- Since we utilize a first-order Taylor expansion approximation to construct estimation errors from visual measurements in the present estimation mechanisms, we investigate the region of attraction.

Bibliography

[1] M. Dunbabin and L. Marques, eds., "Special Issue on Robots for Environmental Monitoring," *IEEE Robotics & Automation Magazine*, Vol. 19, No. 1, 2012.

[2] M. Dunbabin and L. Marques, "Robots for Environmental Monitoring: Significant Advancements and Applications," *IEEE Robotics & Automation Magazine*, Vol. 19, No. 1, pp. 24–39, 2012.

[3] N.E. Leonard, D.A. Paley, F. Lekien, R. Sepulchre, D.M. Fratatoni and R.E. Davis, "Collective Motion, Sensor Networks and Ocean Sampling," *Proceedings of the IEEE*, Vol. 95, No. 1, pp. 48–74, 2007.

[4] P. Ogren, E. Fiorelli and N.E. Leonard, "Cooperative Control of Mobile Sensor Networks: Adaptive Gradient Climbing in a Distributed Environment," *IEEE Transactions on Automatic Control*, Vol. 49, No. 8, pp. 1292–1302, 2004.

[5] M. Zhong and C.G. Cassandras, "Distributed Coverage Control and Data Collection with Mobile Sensor Networks," *IEEE Transactions on Automatic Control*, Vol. 56, No. 10, pp. 2445–2455, 2011.

[6] G.M. Hoffmann and C.J. Tomlin, "Mobile Sensor Network Control Using Mutual Information Methods and Particle Filters," *IEEE Transactions on Automatic Control*, Vol. 55, No. 1, pp. 32–47, 2010.

[7] F. Bullo, J. Cortes and S. Martinez, *Distributed Control of Robotic Networks*, Princeton Series in Applied Mathematics, 2009.

[8] H. Bai, M. Arcak and J.T. Wen, *Cooperative Control Design: A Systematic, Passivity-based Approach*, Springer, 2011.

[9] N. Chopra and M.W. Spong, "Passivity-based Control of Multi-agent Systems," in *Advances in Robot Control: From Everyday Physics to Human-Like Movements*, S. Kawamura and M. Svnin, eds., Springer, pp. 107–134, 2006.

[10] C.W. Reynolds, "Flocks, Herds and Schools: A Distributed Behavioral Model," *Computer Graphics*, Vol. 21, No. 4, pp. 25–34, 1987.

[11] T. Vicsek, A. Czirok, E. Ben-Jacob, I. Cohen and O. Shochet, "Novel Type of Phase Transition in a System of Self-driven Particles," *Physical Review Letters*, Vol. 75, No. 6, pp. 1226–129, 1995.

[12] A. Jadbabaie, J. Lin and A.S. Morse, "Coordination of Groups of Mobile Autonomous Agents Using Nearest Neighbor Rules," *IEEE Transactions on Automatic Control*, Vol. 48, No. 6, pp. 988–1001, 2003.

[13] S. Martinez, J. Cortes and F. Bullo, "Motion Coordination with Distributed Information," *IEEE Control Sytems Magazine*, Vol. 27, No. 4, pp. 75–88, 2007.

[14] D.A. Paley, N.E. Leonard, R. Sepulcre, D. Grunbaum and J.K. Parrish, "Oscillator Models and Collective Motion: Spatial Patterns in the Dynamics of Engineered and Biological Networks," *IEEE Control Systems Magazine*, Vol. 27, No. 4, pp. 89–105, 2007.

[15] R. Olfati-Saber, J.A. Fax and R.M. Murray, "Consensus and Cooperation in Networked Multi-agent Systems," *Proceedings of the IEEE*, Vol. 95, No. 1, pp. 215–233, 2007.

[16] W. Ren and R.W. Beard, *Distributed Consensus in Multi-vehicle Cooperative Control*, Springer, 2008.

[17] H. Tanner, A. Jadbabaie and G.J. Pappas, "Flocking in Fixed and Switching Networks," *IEEE Transactions on Automatic Control*, Vol. 52, No. 5, pp. 863–868, 2007.

[18] N. Moshtagh and A. Jadbabaie, "Distributed Geodesic Control Laws for Flocking of Nonholonomic Agents," *IEEE Transactions on Automatic Control*, Vol. 52, No. 4, pp. 681–686, 2007.

[19] R. Olfati-Saber, "Flocking for Multi-agent Dynamic Systems: Algorithms and Theory," *IEEE Transactions on Automatic Control*, Vol. 51, No. 3, pp. 401–420, 2006.

[20] D.J. Lee and M.W. Spong, "Stable Flocking of Multiple Inertial Agents on Balanced Graphs," *IEEE Transactions on Automatic Control*, Vol. 52, No. 8, pp. 1469–1475, 2007.

[21] A. Jadbabaie, N. Motee and M. Barahona, "On the Stability of the Kuramoto Model of Coupled Nonlinear Oscillators," *Proceedings of the 2004 American Control Conference*, pp. 4296–4301, 2004.

[22] N. Chopra and M.W. Spong, "On Synchronization of Kuramoto Oscillators," *Proceedings of the 44th IEEE Conference on Decision and Control and European Control Conference*, pp. 3916–3922, 2005.

[23] E.W. Justh and P.S. Krishnaprasad, "Natural Frames and Interacting Particles in Three Dimensions," *Proceedings of the 44th IEEE Conference on Decision and Control and European Control Conference*, pp. 2841–2846, 2005.

[24] S. Nair and N.E. Leonard, "Stable Synchronization of Rigid Body Networks," *Networks and Heterogeneous Media*, Vol. 2, No. 4, pp. 595–624, 2007.

[25] R. Sepulchre, D.A. Paley and N.E. Leonard, "Stabilization of Planer Collective Motion: All-to-all communication," *IEEE Transactions on Automatic Control*, Vol. 52, No. 5, pp. 811–824, 2007.

[26] R. Sepulchre, D.A. Paley and N.E. Leonard, "Stabilization of Collective Motion with Limited Communication," *IEEE Transactions on Automatic Control*, Vol. 53, No. 3, pp. 706–719, 2008.

[27] L. Scardovi, A. Sarlette and R. Sepulchre, "Synchronization and Balancing on the N-torus," *Systems & Control Letters*, Vol. 56, No. 5, pp. 335–341, 2007.

[28] L. Scardovi, N. Leonard, and R. Sepulchre, "Stabilization of Collective Motion in Three Dimensions," *Communications in Information and Systems, Brockett Legacy Issue*, Vol. 8, No. 3, pp. 473–500, 2008.

[29] J. Cortes, S. Martinez, T. Karatas and F. Bullo, "Coverage Control for Mobile Sensing Networks," *IEEE Transactions on Robotics and Automation*, Vol. 20, No. 2, pp. 243–255, 2004.

[30] W. Li and C.G. Cassandras, "Distributive Cooperative Coverage Control of Sensor Networks," *Proceedings of the 44th IEEE Conference on Decision and Control and European Control Conference*, pp. 2542–2547, 2005.

[31] P. Barooah and J. Hespanha, "Estimation on Graphs from Relative Measurements: Distributed Algorithms and Fundamental Limits," *IEEE Control Systems Magazine*, Vol. 27, No. 4, pp. 57–74, 2007.

[32] Y. Ma, S. Soatto, J. Kosecka and S.S. Sastry, *An Invitation to 3-D Vision,* Springer, Chapter 2, 2003.

[33] M. Bryson, A. Reid, F. Ramos and S. Sukkarieh, "Airborne Vision-based Mapping and Classification of Large Farmland Environments," *Journal of Field Robotics*, Vol. 27, No. 5, pp. 632–655, 2010.

[34] L. Merino, F. Caballero, J. Martinez-de Dios, J. Ferruz and A. Ollero, "A Cooperative Perception System for Multiple UAVs: Application to Automatic Detection of Forest Fires," *Journal of Field Robotics*, Vol. 23, No. 3, pp. 165–184, 2006.

[35] C.W. Reynolds, "An Evolved, Vision-based Behavioral Model of Coordinated Group Motion," in *From Animals to Animats 2: Proceedings of the 2nd International Conference on Simulation of Adaptive Behavior*, J.-A. Meyer, H.L. Roitblat and S.W. Wilson, eds., The MIT Press, pp. 384–392, 1993.

[36] F. Chaumette and S. Hutchinson, "Visual Servo Control, Part I: Basic Approaches," *IEEE Robotics and Automation Magazine*, Vol. 13, No. 4, pp. 82–90, 2006.

[37] F. Chaumette and S. Hutchinson, "Visual Servo Control, Part II: Advanced Approaches," *IEEE Robotics and Automation Magazine*, Vol. 14, No. 1, pp. 109–118, 2007.

[38] G.D. Hager and S. Hutchinson, eds., "Special Section on Vision-based Control of Robot Manipulators," *IEEE Transactions on Robotics and Automation*, Vol. 12, No. 5, pp. 649–650, 1996.

[39] B. Song, C. Ding, A.T. Kamal, J.A. Farrell and A.K. Roy-Chowdhury, "Distributed Camera Networks: Integrated Sensing and Analysis for Wide Area Scene Understanding," *IEEE Signal Processing Magazine*, Vol. 28, No. 3, pp. 20–31, 2011.

[40] V. Mohan, G. Sundaramoorthi and A. Tannenbaum, "Tubular Surface Segmentation for Extracting Anatomical Structures from Medical Imagery," *IEEE Transactions on Medical Imaging*, Vol. 29, No. 12, pp. 1945–1958, 2010.

[41] S. Han, A. Censi, A.D. Straw and R.M. Murray, "A Bio-plausible Design for Visual Pose Stabilization," *Proceedings of the 2010 IEEE/RSJ International Conference on Intelligent Robots and Systems*, pp. 5679–5686, 2010.

[42] A.K. Roy-Chowdhury and B. Song, *Camera Networks: The Acquisition and Analysis of Videos over Wide Areas*, Morgan and Claypool Publishers, 2011.

[43] T. Hatanaka, T. Ibuki, A. Gusrialdi and M. Fujita, "Coverage Control for Camera Sensor Networks: Its Implementation and Experimental Verification," *Proceedings of the 17th Mediterranean Conference on Control and Automation*, pp. 446–451, 2009.

[44] M. Fujita, H. Kawai and M.W. Spong, "Passivity-based Dynamic Visual Feedback Control for Three Dimensional Target Tracking: Stability and $\mathcal{L}_2$-gain Performance Analysis," *IEEE Transactions on Control Systems Technology*, Vol. 15, No. 1, pp. 40–52, 2007.

[45] H. Kawai, T. Murao and M. Fujita, "Passivity-based Visual Motion Observer with Panoramic Camera for Pose Control," *Journal of Intelligent and Robotic Systems*, Vol. 64, No. 3-4, pp. 561–583, 2011.

[46] Y. Igarashi, T. Hatanaka, M. Fujita and M.W. Spong, "Passivity-based Attitude Synchronization in $SE(3)$," *IEEE Transactions on Control Systems Technology*, Vol. 17, No. 5, pp. 1119–1134, 2009.

[47] T. Hatanaka, Y. Igarashi, M. Fujita and M.W. Spong, "Passivity-based Pose Synchronization in Three Dimensions," *IEEE Transactions on Automatic Control*, Vol. 57, No. 2, pp. 360–375, 2012.

[48] T. Ibuki, T. Hatanaka and M. Fujita, "Passivity-based Pose Synchronization Using Only Relative Pose Information under General Digraphs," *Proceedings of the 51st IEEE Conference on Decision and Control*, pp. 4709–4714, 2012.

[49] H.K. Khalil, *Nonlinear Systems, Third Edition*, Prentice Hall, 2002.

[50] E.D. Sontag, "Input to State Stability: Basic Concepts and Results," in *Nonlinear and Optimal Control Theory, Lecture Notes in Mathematics, Vol. 1932*, P. Nistri and G. Stefani, eds., Springer, pp. 163–220, 2008.

[51] A.J. van der Schaft, $\mathcal{L}_2$-*gain and Passivity Techniques in Nonlinear Control*, Springer, 1996.

[52] J. Thunberg, E. Montijano and X. Hu, "Distributed Attitude Synchronization Control," *Proceedings of the 50th IEEE Conference on Decision and Control and European Control Conference*, pp. 1962–1967, 2011.

[53] C. Li and Z. Qu, "Cooperative Attitude Synchronization for Rigid-body Spacecrafts via Varying Communication Topology," *International Journal of Robotics and Automation*, Vol. 26, No. 1, pp. 110–119, 2011.

[54] A. Sarlette, R. Sepulchre and N.E. Leonard, "Autonomous Rigid Body Attitude Synchronization," *Automatica*, Vol. 45, No. 2, pp. 572–577, 2009.

[55] W. Ren, "Distributed Cooperative Attitude Synchronization and Tracking for Multiple Rigid Bodies," *IEEE Transactions on Control Systems Technology*, Vol. 18, No. 2, pp. 383–392, 2010.

[56] S.-J. Chung and J.-J.E. Slotine, "Cooperative Robot Control and Concurrent Synchronization of Lagrangian Systems," *IEEE Transactions on Robotics*, Vol. 25, No. 3, pp. 686–700, 2009.

[57] Y.-C. Liu and N. Chopra, "Synchronization of Networked Robotic Systems on Strongly Connected Graphs," *Proceedings of the 49th IEEE Conference on Decision and Control*, pp. 3194–3199, 2010.

[58] N. Chopra, "Output Synchronization on Strongly Connected Graphs," *IEEE Transactions on Automatic Control*, Vol. 57, No. 11, pp. 2896–2901, 2012.

[59] N. Moshtagh, N. Michael, A. Jadbabaie and K. Daniilidis, "Vision-based, Distributed Control Laws for Motion Coordination of Nonholonomic Robots," *IEEE Transactions on Robotics*, Vol. 25, No. 4, pp. 851–860, 2009.

[60] E. Montijano, J. Thunberg, X. Hu and C. Sagues, "Multi-robot Distributed Visual Consensus Using Epipoles," *Proceedings of the 50th IEEE Conference on Decision and Control and European Control Conference*, pp. 2750–2755, 2011.

[61] Z. Kan, S. Subramanian, J. Shea and W.E. Dixon, "Vision Based Connectivity Maintenance of a Network with Switching Topology," *Proceedings of the 2010 IEEE Multiconference on Systems and Control*, pp. 1493–1498, 2010.

[62] A.K. Das, R. Fierro, V. Kumar, J.P. Ostrowski, J. Spletzer and C.J. Taylor, "A Vision-based Formation Control Framework," *IEEE Transactions on Robotics and Automation*, Vol. 18, No. 5, pp. 813–825, 2002.

[63] F. Morbidi, F. Bullo and D. Prattichizzo, "On Leader-follower Visibility Maintenance for Dubins-like Vehicles via Controlled Invariance," *Proceedings of the 47th IEEE Conference on Decision and Control*, pp. 1821–1826, 2008.

[64] F. Morbidi, G.L. Mariottini and D. Prattichizzo, "Observer Design via Immersion and Invariance for Vision-based Leader-follower Formation Control," *Automatica*, Vol. 46, No. 1, pp. 148–154, 2010.

[65] P. Vela, A. Betser, J. Malcolm and A. Tannenbaum, "Vision-based Range Regulation of a Leader-follower Formation," *IEEE Transactions on Control Systems Technology*, Vol. 17, No. 2, pp. 442–448, 2009.

[66] J.L. Giesbrecht, H.K. Goi, T.D. Barfoot and B.A. Francis, "A Vision-based Robotic Follower Vehicle," *Proceedings of the SPIE Defence, Security and Sensing*, Vol. 7332, pp. 14–17, 2009.

[67] R. Vidal, O. Shakernia and S.S. Sastry, "Following the Flock," *IEEE Robotics & Automation Magazine*, Vol. 11, No. 4, pp. 14–20, 2004.

[68] N. Cowan, O. Shakernia, R. Vidal and S.S. Sastry, "Vision-based Follow-the-leader," *Proceedings of the 2003 IEEE/RSJ International Conference on Intelligent Robots and Systems*, pp. 1796–1801, 2003.

[69] G.L. Mariottini, F. Morbidi, D. Prattichizzo, N. Vander Valk, N. Michael, G.J. Pappas and K. Daniilidis, "Vision-based Localization for Leader-follower Formation Control," *IEEE Transactions on Robotics*, Vol. 25, No. 6, pp. 1431–1438, 2009.

[70] C. Godsil and G. Royle, *Algebraic Graph Theory (Graduate Texts in Mathematics, 207)*, Springer, 2001.

[71] D.G. Luenberger, "An Introduction to Observers," *IEEE Transactions on Automatic Control*, Vol. AC-16, No. 6, pp. 596–602, 1971.

[72] R.A. Horn and C.R. Johnson, *Matrix Analysis*, Cambridge University Press, 1985.

[73] B. Brogliato, R. Lozano, B. Maschke and O. Egeland, *Dissipative Systems Analysis and Control: Theory and Applications, Second Edition*, Springer, 2006.

[74] S.P.M. Noijen, P.F. Lambrechts and H. Nijmeijer, "An Observer-controller Combination for a Unicycle Mobile Robot," *International Journal of Control*, Vol. 78, No. 2, pp. 81–87, 2005.

[75] H. Berghuis and H. Nijmeijer, "A Passivity Approach to Controller-observer Design for Robots," *IEEE Transactions on Robotics and Automation*, Vol. 9, No. 6, pp. 740–754, 1993.

[76] P. Yang, R.A. Freeman and K.M. Lynch, "A General Stability Condition for Multi-agent Coordination by Coupled Estimation and Control," *Proceedings of the 2007 American Control Conference*, pp. 723–728, 2007.

[77] A. R-Angeles and H. Nijmeijer, "Mutual Synchronization of Robots via Estimated State Feedback: A Cooperative Approach," *IEEE Transactions on Control Systems Technology*, Vol. 12, No. 4, pp. 542–554, 2004.

[78] S. Arimoto and T. Nakayama, "Another Language for Describing Motions of Mechatronics Systems: A Nonlinear Position-dependent Circuit Theory," *IEEE/ASME Transactions on Mechatronics*, Vol. 1, No. 2, pp. 168–180, 1996.

[79] J.M.A. Scherpen and R. Ortega, "On Nonlinear Control of Euler-lagrange Systems: Disturbance Attenuation Properties," *Systems & Control Letters*, Vol. 30, No. 1, pp. 490–56, 1997.

[80] S. Battilotti and L. Lanari, "Adaptive Disturbance Attenuation with Global Stability for Rigid and Elastic Joint Robots," *Automatica*, Vol. 33, No. 2, pp. 239–243, 1997.

[81] P.A. Vela and I.J. Ndiour, "Estimation Theory and Tracking of Deformable Objects," *Proceedings of the 2010 IEEE Multi-conference on Systems and Control*, pp. 1222–1233, 2010.

[82] R.M. Murray, Z. Li and S.S. Sastry, *A Mathematical Introduction to Robotic Manipulation*, CRC Press, 1994.

[83] B. Paden and R. Panja, "Globally Asymptotically Stable 'PD+' Controller for Robot Manipulators," *International Journal of Control*, Vol. 47, No. 6, pp. 1697–1712, 1988.

[84] M. Fujita, T. Hatanaka, N. Kobayashi, T. Ibuki and M.W. Spong, "Visual Motion Observer-based Pose Synchronization: A Passivity Approach," *Proceedings of the 48th IEEE Conference on Decision and Control and 28th Chinese Control Conference*, pp. 2402–2407, 2009.

[85] J. Hespanha, O.A. Yakimenko, I.I. Kaminer and A.M. Pascoal, "Linear Parametrically Varying Systems with Brief Instabilities: An Application to Vision/Inertial Navigation," *IEEE Transactions on Aerospace and Electronics Systems*, Vol. 40, No. 3, pp. 889–900, 2004.

Publications

Journal Papers

[1] T. Ibuki, T. Hatanaka and M. Fujita, "Visual Feedback Leader-following Attitude Synchronization," *Transactions of the Institute of Systems, Control and Information*, Vol. 24, No. 7, pp. 155–164, 2011 (in Japanese). [Chapter 3]

[2] T. Ibuki, T. Hatanaka and M. Fujita, "Visual Feedback Leader-following Pose Synchronization with a Panoramic Camera Model," *Transactions of the Institute of Systems, Control and Information*, Vol. 25, No. 6, pp. 135–144, 2012 (in Japanese). [Chapter 4]

[3] T. Ibuki, T. Hatanaka and M. Fujita, "Passivity-based Visual Feedback Pose Regulation Integrating a Target Motion Model in Three Dimensions," *SICE Journal of Control, Measurement, and System Integration*, Vol. 6, No. 5, to appear, 2013. [Chapter 5]

Refereed Conference Papers

[4] T. Hatanaka, T. Ibuki, A. Gusrialdi and M. Fujita, "Coverage Control for Camera Sensor Networks: Its Implementation and Experimental Verification," *Proceedings of the 17th Mediterranean Conference on Control and Automation*, pp. 446–451, 2009.

[5] M. Fujita, T. Hatanaka, N. Kobayashi, T. Ibuki and M.W. Spong, "Visual Motion Observer-based Pose Synchronization: A Passivity Approach," *Proceedings of the 48th IEEE Conference on Decision and Control and 28th Chinese Control Conference*, pp. 2402–2407, 2009. [Chapter 5]

[6] T. Ibuki, T. Hatanaka, M. Fujita and M.W. Spong, "Visual Feedback Attitude Synchronization in Leader-follower Type Visibility Structures," *Proceedings of the 49th IEEE Conference on Decision and Control*, pp. 2486–2491, 2010. [Chapter 3]

[7] T. Ibuki, T. Hatanaka, M. Fujita and M.W. Spong, "Visual Feedback Leader-following Pose Synchronization: Convergence Analysis," *Proceedings of the 2011 American Control Conference*, pp. 493–498, 2011. [Chapter 4]

[8] T. Ibuki, T. Hatanaka, M. Fujita and M.W. Spong, "Visual Feedback Pose Synchronization with a Generalized Camera Model," *Proceedings of the 50th IEEE Conference on Decision and Control and European Control Conference*, pp. 4999–5004, 2011. [Chapter 4]

[9] T. Ibuki, T. Hatanaka and M. Fujita, "Passivity-based Pose Synchronization Using Only Relative Pose Information under General Digraphs," *Proceedings of the 51st IEEE Conference on Decision and Control*, pp. 4709–4714, 2012.

[10] T. Ibuki, T. Hatanaka and M. Fujita, "Passivity-based Visual Pose Regulation for a Moving Target Object in Three Dimensions: Structure Design and Convergence Analysis," *Proceedings of the 51st IEEE Conference on Decision and Control*, pp. 5655-5660, 2012. [Chapter 5]

[11] T. Ibuki, Y. Namba, T. Hatanaka and M. Fujita, "Passivity-based Discrete Visual Motion Observer Taking Account of Camera Frame Rates," *Proceedings of the 52nd IEEE Conference on Decision and Control*, to be presented, 2013.

Appendix A

Reconstruction of Estimation Errors from Visual Measurements

A.1 Pinhole Camera Model

We first derive a relation between the actual and estimated visual measurements extracted by the pinhole camera model (2.5). Suppose the attitude estimation error θ_{eij} is small enough so that we can let $e^{\hat{\xi}\theta_{eij}} \approx I_3 + \mathrm{sk}(e^{\hat{\xi}\theta_{eij}})$ (see Appendix B.2.8). We then have the following relation between the actual feature point p_{ij_k} and the estimated one $\bar{p}_{ij_k}$.

$$
\begin{aligned}
p_{ij_k} - \bar{p}_{ij_k} &= p_{ij} + e^{\hat{\xi}\theta_{ij}}p_{jj_k} - \bar{p}_{ij} - e^{\hat{\bar{\xi}}\bar{\theta}_{ij}}p_{jj_k} \\
&= e^{\hat{\bar{\xi}}\bar{\theta}_{ij}}p_{eij} + e^{\hat{\bar{\xi}}\bar{\theta}_{ij}}(e^{-\hat{\bar{\xi}}\bar{\theta}_{ij}}e^{\hat{\xi}\theta_{ij}} - I_3)p_{jj_k} \quad (\because p_{eij} = e^{-\hat{\bar{\xi}}\bar{\theta}_{ij}}(p_{ij} - \bar{p}_{ij})) \\
&\approx e^{\hat{\bar{\xi}}\bar{\theta}_{ij}}p_{eij} + e^{\hat{\bar{\xi}}\bar{\theta}_{ij}}\mathrm{sk}(e^{\hat{\xi}\theta_{eij}})p_{jj_k} \quad (\because e^{\hat{\xi}\theta} \approx I_3 + \mathrm{sk}(e^{\hat{\xi}\theta})) \\
&= e^{\hat{\bar{\xi}}\bar{\theta}_{ij}}p_{eij} + (e^{\hat{\bar{\xi}}\bar{\theta}_{ij}}\mathrm{sk}(e^{\hat{\xi}\theta_{eij}})e^{-\hat{\bar{\xi}}\bar{\theta}_{ij}})e^{\hat{\bar{\xi}}\bar{\theta}_{ij}}p_{jj_k} \\
&= e^{\hat{\bar{\xi}}\bar{\theta}_{ij}}p_{eij} + (e^{\hat{\bar{\xi}}\bar{\theta}_{ij}}\mathrm{sk}(e^{\hat{\xi}\theta_{eij}})^\vee)^\wedge e^{\hat{\bar{\xi}}\bar{\theta}_{ij}}p_{jj_k} \\
&\qquad\qquad\qquad (\because e^{\hat{\xi}\theta}\hat{\omega}e^{-\hat{\xi}\theta} = (e^{\hat{\xi}\theta}\omega)^\wedge \; (\text{Appendix B.2.3})) \\
&= e^{\hat{\bar{\xi}}\bar{\theta}_{ij}}p_{eij} - (e^{\hat{\bar{\xi}}\bar{\theta}_{ij}}p_{jj_k})^\wedge e^{\hat{\bar{\xi}}\bar{\theta}_{ij}}\mathrm{sk}(e^{\hat{\xi}\theta_{eij}})^\vee \quad (\because \hat{a}b = -\hat{b}a \; (\text{Appendix B.1.2})) \\
&= e^{\hat{\bar{\xi}}\bar{\theta}_{ij}}p_{eij} - (e^{\hat{\bar{\xi}}\bar{\theta}_{ij}}\hat{p}_{jj_k}e^{-\hat{\bar{\xi}}\bar{\theta}_{ij}})e^{\hat{\bar{\xi}}\bar{\theta}_{ij}}\mathrm{sk}(e^{\hat{\xi}\theta_{eij}})^\vee \quad (\because e^{\hat{\xi}\theta}\hat{\omega}e^{-\hat{\xi}\theta} = (e^{\hat{\xi}\theta}\omega)^\wedge) \\
&= e^{\hat{\bar{\xi}}\bar{\theta}_{ij}}(p_{eij} - \hat{p}_{jj_k}\mathrm{sk}(e^{\hat{\xi}\theta_{eij}})^\vee) \\
&= e^{\hat{\bar{\xi}}\bar{\theta}_{ij}}\begin{bmatrix} I_3 & -\hat{p}_{jj_k} \end{bmatrix}\begin{bmatrix} p_{eij} \\ \mathrm{sk}(e^{\hat{\xi}\theta_{eij}})^\vee \end{bmatrix} \\
&= e^{\hat{\bar{\xi}}\bar{\theta}_{ij}}\begin{bmatrix} I_3 & -\hat{p}_{jj_k} \end{bmatrix}e_{eij}.
\end{aligned}
$$

On the other hand, by using a first-order Taylor expansion approximation, the relation

between the actual and estimated visual measurements can be expressed as

$$f_{ij_k} - \bar{f}_{ij_k} \approx \left[\frac{\partial f_{ij_k}}{\partial x_{ij_k}}|_{p_{ij_k}=\bar{p}_{ij_k}} \quad \frac{\partial f_{ij_k}}{\partial y_{ij_k}}|_{p_{ij_k}=\bar{p}_{ij_k}} \quad \frac{\partial f_{ij_k}}{\partial z_{ij_k}}|_{p_{ij_k}=\bar{p}_{ij_k}} \right] (p_{ij_k} - \bar{p}_{ij_k}).$$

Thus, the relation is given by

$$f_{ij}(g_{ij}) - \bar{f}_{ij}(\bar{g}_{ij}) = J_{ij}(\bar{g}_{ij})e_{eij},$$

where $J_{ij}(\bar{g}_{ij}) : SE(3) \rightarrow \mathbb{R}^{2s \times 6}$ is defined as

$$J_{ij}(\bar{g}_{ij}) := \begin{bmatrix} J_{ij_1}^{\mathrm{T}} & \cdots & J_{ij_s}^{\mathrm{T}} \end{bmatrix}^{\mathrm{T}},$$

$$J_{ij_k}(\bar{g}_{ij}) := \left[\frac{\partial f_{ij_k}}{\partial x_{ij_k}}|_{p_{ij_k}=\bar{p}_{ij_k}} \quad \frac{\partial f_{ij_k}}{\partial y_{ij_k}}|_{p_{ij_k}=\bar{p}_{ij_k}} \quad \frac{\partial f_{ij_k}}{\partial z_{ij_k}}|_{p_{ij_k}=\bar{p}_{ij_k}} \right] e^{\hat{\bar{\xi}}\bar{\theta}_{ij}} \begin{bmatrix} I_3 & -\hat{p}_{jj_k} \end{bmatrix}, \ k \in \{1, \cdots, s\}.$$

Suppose the matrix $J_{ij}(\bar{g}_{ij})$ is full column rank for all $\bar{g}_{ij} \in SE(3)$. Then, the relative rigid body motion can be uniquely defined by the visual measurements vector. Since this might not hold in some cases when $s = 3$, it is known that $s \geq 4$ is desirable for the full column rank of $J_{ij}(\bar{g}_{ij})$.

The above discussion shows that we can derive the estimation error vector e_{eij} from the visual measurements f_{ij} and the estimated relative pose $\bar{g}_{ij}$ as

$$e_{eij} = J_{ij}^{\dagger}(\bar{g}_{ij})(f_{ij} - \bar{f}_{ij}),$$

where † is the pseudo-inverse. Moreover, once e_{eij} is reconstructed, $e^{\hat{\xi}\theta_{eij}}$ can be calculated by $\xi\theta_{eij}$ for $\theta_{eij} \in (-\pi/2, \pi/2)$ which is derived as follows.

$$\xi\theta_{eij} = \frac{\sin^{-1} \|\mathrm{sk}(e^{\hat{\xi}\theta_{eij}})^{\vee}\|_2}{\|\mathrm{sk}(e^{\hat{\xi}\theta_{eij}})^{\vee}\|_2} \mathrm{sk}(e^{\hat{\xi}\theta_{eij}})^{\vee}.$$

A.2 Panoramic Camera Model

We next derive a relation between the actual and estimated visual measurements extracted by the panoramic camera model (2.8). Similarly to the case of the pinhole camera model, we get the following relation under the assumption that the attitude estimation error θ_{eij} is small enough so that

$$p_{m_ij_k} - \bar{p}_{m_ij_k} \approx e^{\hat{\bar{\xi}}\bar{\theta}_{m_ij}} \begin{bmatrix} I_3 & -\hat{p}_{jj_k} \end{bmatrix} e_{eij}.$$

Moreover, using a first-order Taylor expansion approximation yields

$$f_{ij_k} - \bar{f}_{ij_k} \approx \left[\frac{\partial f_{ij_k}}{\partial x_{m_ij_k}}|_{p_{m_ij_k}=\bar{p}_{m_ij_k}} \quad \frac{\partial f_{ij_k}}{\partial y_{m_ij_k}}|_{p_{m_ij_k}=\bar{p}_{m_ij_k}} \quad \frac{\partial f_{ij_k}}{\partial z_{m_ij_k}}|_{p_{m_ij_k}=\bar{p}_{m_ij_k}} \right] (p_{m_ij_k} - \bar{p}_{m_ij_k}),$$

where

$$\frac{\partial f_{ij_k}}{\partial x_{m_ij_k}} = \frac{2r_i\lambda_i\frac{\partial c(p_{m_ij_k})}{\partial x_{m_ij_k}}}{(2r_i + c(p_{m_ij_k})z_{m_ij_k})^2}\begin{bmatrix} x_{m_ij_k} \\ y_{m_ij_k} \end{bmatrix} + \frac{\lambda_i c(p_{m_ij_k})}{2r_i + c(p_{m_ij_k})z_{m_ij_k}}\begin{bmatrix} 1 \\ 0 \end{bmatrix},$$

$$\frac{\partial f_{ij_k}}{\partial y_{m_ij_k}} = \frac{2r_i\lambda_i\frac{\partial c(p_{m_ij_k})}{\partial y_{m_ij_k}}}{(2r_i + c(p_{m_ij_k})z_{m_ij_k})^2}\begin{bmatrix} x_{m_ij_k} \\ y_{m_ij_k} \end{bmatrix} + \frac{\lambda_i c(p_{m_ij_k})}{2r_i + c(p_{m_ij_k})z_{m_ij_k}}\begin{bmatrix} 0 \\ 1 \end{bmatrix},$$

$$\frac{\partial f_{ij_k}}{\partial z_{m_ij_k}} = \frac{2r_i\lambda_i\frac{\partial c(p_{m_ij_k})}{\partial z_{m_ij_k}}}{(2r_i + c(p_{m_ij_k})z_{m_ij_k})^2}\begin{bmatrix} x_{m_ij_k} \\ y_{m_ij_k} \end{bmatrix} - \frac{\lambda_i c^2(p_{m_ij_k})}{(2r_i + c(p_{m_ij_k})z_{m_ij_k})^2}\begin{bmatrix} x_{m_ij_k} \\ y_{m_ij_k} \end{bmatrix}.$$

Thus, by introducing the same image Jacobian $J_{ij}(\bar{g}_{m_ij}) : SE(3) \to \mathbb{R}^{2s\times 6}$ as that of the pinhole camera case, we get

$$e_{eij} = J_{ij}^\dagger(\bar{g}_{m_ij})(f_{ij} - \bar{f}_{ij}).$$

Appendix B

Mathematical Formulas

B.1 Formulas of '∧'

B.1.1 $\hat{a}a = 0$

Since $\hat{a}b = a \times b$ holds for any $a, b \in \mathbb{R}^3$, we get

$$\hat{a}a = a \times a = 0.$$

B.1.2 $\hat{a}b = -\hat{b}a$

Since $\hat{a}b = a \times b$ holds, we obtain

$$\hat{a}b = a \times b = -b \times a = -\hat{b}a.$$

B.1.3 $\frac{1}{2}\mathrm{tr}(\hat{a}\hat{b}) = -a^{\mathrm{T}}b$

We get from the notations $a = [a_1 \ a_2 \ a_3]^{\mathrm{T}}, \ b = [b_1 \ b_2 \ b_3]^{\mathrm{T}}$

$$
\begin{aligned}
\frac{1}{2}\mathrm{tr}(\hat{a}\hat{b}) &= \frac{1}{2}\mathrm{tr}\left(\begin{bmatrix} 0 & -a_3 & a_2 \\ a_3 & 0 & -a_1 \\ -a_2 & a_1 & 0 \end{bmatrix}\begin{bmatrix} 0 & -b_3 & b_2 \\ b_3 & 0 & -b_1 \\ -b_2 & b_1 & 0 \end{bmatrix}\right) \\
&= \frac{1}{2}\mathrm{tr}\left(\begin{bmatrix} -a_2b_2 - a_3b_3 & * & * \\ * & -a_3b_3 - a_1b_1 & * \\ * & * & -a_1b_1 - a_2b_2 \end{bmatrix}\right) \\
&= -(a_1b_1 + a_2b_2 + a_3b_3) \\
&= -a^{\mathrm{T}}b.
\end{aligned}
$$

B.1.4 $\hat{a}^2 = aa^{\mathrm{T}} - \|a\|_2^2 I_3$

The direct calculation of $\hat{a}^2$ yields

$$
\begin{aligned}
\hat{a}^2 &= \begin{bmatrix} 0 & -a_3 & a_2 \\ a_3 & 0 & -a_1 \\ -a_2 & a_1 & 0 \end{bmatrix} \begin{bmatrix} 0 & -a_3 & a_2 \\ a_3 & 0 & -a_1 \\ -a_2 & a_1 & 0 \end{bmatrix} \\
&= \begin{bmatrix} -a_2^2 - a_3^2 & a_1 a_2 & a_3 a_1 \\ a_1 a_2 & -a_3^2 - a_1^2 & a_2 a_3 \\ a_3 a_1 & a_2 a_3 & -a_1^2 - a_2^2 \end{bmatrix} \\
&= \begin{bmatrix} a_1^2 & a_1 a_2 & a_3 a_1 \\ a_1 a_2 & a_2^2 & a_2 a_3 \\ a_3 a_1 & a_2 a_3 & a_3^2 \end{bmatrix} - \begin{bmatrix} a_1^2 + a_2^2 + a_3^2 & 0 & 0 \\ 0 & a_1^2 + a_2^2 + a_3^2 & 0 \\ 0 & 0 & a_1^2 + a_2^2 + a_3^2 \end{bmatrix} \\
&= aa^{\mathrm{T}} - \|a\|_2^2 I_3.
\end{aligned}
$$

B.1.5 $\hat{a}^3 = -\|a\|_2^2 \hat{a}$

We get from Appendices B.1.1 and B.1.4

$$
\hat{a}^3 \;=\; \hat{a}(\hat{a})^2 = \hat{a}(aa^{\mathrm{T}} - \|a\|_2^2 I_3) = \hat{a}aa^{\mathrm{T}} - \|a\|_2^2 \hat{a} = -\|a\|_2^2 \hat{a}.
$$

B.2   Formulas of $e^{\hat{\xi}\theta}$

B.2.1   Rodrigues' Formula

For any $e^{\hat{\xi}\theta} \in SO(3)$, Rodrigues' formula is given as follows [82]

$$
e^{\hat{\xi}\theta} = I_3 + \hat{\xi}\sin\theta + \hat{\xi}^2(1 - \cos\theta). \tag{B.1}
$$

This formula is derived from the definition of $e^{\hat{\xi}\theta}$ and Appendix B.1.5 as follows.

$$
\begin{aligned}
e^{\hat{\xi}\theta} &= I_3 + \hat{\xi}\theta + \frac{1}{2!}\hat{\xi}^2\theta^2 + \frac{1}{3!}\hat{\xi}^3\theta^3 + \cdots \\
&= I_3 + \hat{\xi}\left(\theta - \frac{1}{3!}\theta^3 + \cdots\right) + \hat{\xi}^2\left(\frac{1}{2!}\theta^2 - \frac{1}{4!}\theta^4 + \cdots\right) \quad (\because \hat{\xi}^3 = -\|\xi\|_2^2\hat{\xi} = -\hat{\xi}) \\
&= I_3 + \hat{\xi}\sin\theta + \hat{\xi}^2(1 - \cos\theta).
\end{aligned}
$$

B.2.2   Positive Definiteness of $e^{\hat{\xi}\theta}$

A rotation matrix $e^{\hat{\xi}\theta}$ is positive definite if and only if θ satisfies $\theta \in (-\pi/2, \pi/2)$, where θ is defined in $(-\pi, \pi]$. This property can be proved as follows.

Sufficiency: For any $x \in \mathbb{R}^3$, we get from Rodrigues' formula (B.1) and Appendix B.1.4

$$
\begin{aligned}
x^\mathrm{T} e^{\hat{\xi}\theta} x &= x^\mathrm{T}\left(I_3 + \hat{\xi}\sin\theta + \hat{\xi}^2(1 - \cos\theta)\right)x \\
&= x^\mathrm{T}x + x^\mathrm{T}\hat{\xi}^2(1 - \cos\theta)x \quad (\because x^\mathrm{T}\hat{\xi}x = 0) \\
&= x^\mathrm{T}x + x^\mathrm{T}(\xi\xi^\mathrm{T} - I_3)(1 - \cos\theta)x \quad (\because \hat{\xi}^2 = \xi\xi^\mathrm{T} - \|\xi\|_2^2 I_3) \\
&= (1 - \cos\theta)x^\mathrm{T}\xi\xi^\mathrm{T}x + \cos\theta x^\mathrm{T}x.
\end{aligned}
$$

Therefore, if $\theta \in (-\pi/2, \pi/2)$ holds, then the rotation matrix $e^{\hat{\xi}\theta}$ is positive definite. □

Necessity: We prove the necessity by using the contraposition. Namely, we show that if $\theta \notin (-\pi/2, \pi/2)$ holds, then the rotation matrix $e^{\hat{\xi}\theta}$ is not positive definite. Here, note that it is sufficient to show that $\exists x \neq 0$ s.t. $x^\mathrm{T}Ax \leq 0$, $x \in \mathbb{R}^3$ in order to prove that a matrix $A \in \mathbb{R}^{3\times3}$ is not positive definite. Let us now consider a vector x such that $\xi^\mathrm{T}x = 0$ and $x \neq 0$. Then, the quadratic form of $e^{\hat{\xi}\theta}$ is given by

$$
\begin{aligned}
x^\mathrm{T} e^{\hat{\xi}\theta} x &= (1 - \cos\theta)x^\mathrm{T}\xi\xi^\mathrm{T}x + \cos\theta x^\mathrm{T}x \\
&= \cos\theta x^\mathrm{T}x \quad (\because \xi^\mathrm{T}x = 0).
\end{aligned}
$$

Note that this quadratic form becomes non-positive when $\theta \notin (-\pi/2, \pi/2)$ holds. This completes the proof. □

B.2.3 $\quad e^{\hat{\xi}\theta}\hat{\omega}e^{-\hat{\xi}\theta} = (e^{\hat{\xi}\theta}\omega)^\wedge$

For any $\omega, v \in \mathbb{R}^3$, we get

$$
\begin{aligned}
e^{\hat{\xi}\theta}\hat{\omega}e^{-\hat{\xi}\theta}v &= e^{\hat{\xi}\theta}\hat{\omega}(e^{-\hat{\xi}\theta}v) \\
&= e^{\hat{\xi}\theta}\left(\omega \times (e^{-\hat{\xi}\theta}v)\right) \quad (\because \hat{a}b = a \times b) \\
&= (e^{\hat{\xi}\theta}\omega) \times (e^{\hat{\xi}\theta}e^{-\hat{\xi}\theta}v) \\
&= (e^{\hat{\xi}\theta}\omega) \times v \\
&= (e^{\hat{\xi}\theta}\omega)^\wedge v \quad (\because \hat{a}b = a \times b).
\end{aligned}
$$

Therefore, we obtain $e^{\hat{\xi}\theta}\hat{\omega}e^{-\hat{\xi}\theta} = (e^{\hat{\xi}\theta}\omega)^\wedge$.

B.2.4 $\quad e^{\hat{\xi}\theta}(e^{-\hat{\xi}\theta}\dot{e}^{\hat{\xi}\theta})^\vee = (\dot{e}^{\hat{\xi}\theta}e^{-\hat{\xi}\theta})^\vee$

The direct calculation of $e^{\hat{\xi}\theta}(e^{-\hat{\xi}\theta}\dot{e}^{\hat{\xi}\theta})^\vee$ yields

$$
\begin{aligned}
e^{\hat{\xi}\theta}(e^{-\hat{\xi}\theta}\dot{e}^{\hat{\xi}\theta})^\vee &= \left(\left(e^{\hat{\xi}\theta}(e^{-\hat{\xi}\theta}\dot{e}^{\hat{\xi}\theta})^\vee\right)^\wedge\right)^\vee \\
&= (e^{\hat{\xi}\theta}e^{-\hat{\xi}\theta}\dot{e}^{\hat{\xi}\theta}e^{-\hat{\xi}\theta})^\vee \quad (\because \text{Appendix B.2.3}) \\
&= (\dot{e}^{\hat{\xi}\theta}e^{-\hat{\xi}\theta})^\vee.
\end{aligned}
$$

B.2.5   Skew-symmetric Property of $\dot{e}^{\hat{\xi}\theta}e^{-\hat{\xi}\theta}$

The time derivative of the both sides of $e^{\hat{\xi}\theta}e^{-\hat{\xi}\theta} = I_3$ yields

$$\dot{e}^{\hat{\xi}\theta}e^{-\hat{\xi}\theta} + e^{\hat{\xi}\theta}\dot{e}^{-\hat{\xi}\theta} = 0.$$

Then, from this equality and the property that $(e^{\hat{\xi}\theta})^{\mathrm{T}} = e^{-\hat{\xi}\theta}$, we obtain

$$\dot{e}^{\hat{\xi}\theta}e^{-\hat{\xi}\theta} = -e^{\hat{\xi}\theta}\dot{e}^{-\hat{\xi}\theta} = -e^{\hat{\xi}\theta}(\dot{e}^{\hat{\xi}\theta})^{\mathrm{T}} = -(\dot{e}^{\hat{\xi}\theta}e^{-\hat{\xi}\theta})^{\mathrm{T}}.$$

This means that $\dot{e}^{\hat{\xi}\theta}e^{-\hat{\xi}\theta}$ is skew-symmetric.

B.2.6 $\mathrm{sk}(e^{\hat{\xi}\theta}) = \hat{\xi}\sin\theta$

We get from Rodrigues' formula (B.1)

$$\begin{aligned}
\mathrm{sk}(e^{\hat{\xi}\theta}) &= \frac{1}{2}(e^{\hat{\xi}\theta} - e^{-\hat{\xi}\theta}) \\
&= \frac{1}{2}\left(I_3 + \hat{\xi}\sin\theta + \hat{\xi}^2(1 - \cos\theta) - \left(I_3 + \hat{\xi}\sin(-\theta) + \hat{\xi}^2(1 - \cos(-\theta))\right)\right) \\
&= \frac{1}{2}\left(I_3 + \hat{\xi}\sin\theta + \hat{\xi}^2(1 - \cos\theta) - \left(I_3 - \hat{\xi}\sin\theta + \hat{\xi}^2(1 - \cos\theta)\right)\right) \\
&= \hat{\xi}\sin\theta.
\end{aligned}$$

B.2.7 $e^{\hat{\xi}\theta}\mathrm{sk}(e^{\hat{\xi}\theta})^{\vee} = \mathrm{sk}(e^{\hat{\xi}\theta})^{\vee}$

Since '$\vee$' is the inverse operator to '$\wedge$', we obtain

$$\begin{aligned}
e^{\hat{\xi}\theta}\mathrm{sk}(e^{\hat{\xi}\theta})^{\vee} &= \left(\left(e^{\hat{\xi}\theta}\mathrm{sk}(e^{\hat{\xi}\theta})^{\vee}\right)^{\wedge}\right)^{\vee} \\
&= \left(e^{\hat{\xi}\theta}\mathrm{sk}(e^{\hat{\xi}\theta})e^{-\hat{\xi}\theta}\right)^{\vee} \quad (\because \text{Appendix B.2.3}) \\
&= \left(e^{\hat{\xi}\theta}\frac{1}{2}(e^{\hat{\xi}\theta} - e^{-\hat{\xi}\theta})e^{-\hat{\xi}\theta}\right)^{\vee} \\
&= \left(\frac{1}{2}(e^{\hat{\xi}\theta} - e^{-\hat{\xi}\theta})\right)^{\vee} \\
&= \mathrm{sk}(e^{\hat{\xi}\theta})^{\vee}.
\end{aligned}$$

Similarly, we get $e^{-\hat{\xi}\theta}\mathrm{sk}(e^{\hat{\xi}\theta})^{\vee} = \mathrm{sk}(e^{\hat{\xi}\theta})^{\vee}$.

B.2.8 $e^{\hat{\xi}\theta} \approx I_3 + \mathrm{sk}(e^{\hat{\xi}\theta})$ for $|\theta| << 1$

Since $\mathrm{sk}(e^{\hat{\xi}\theta}) = \hat{\xi}\sin\theta$ holds (Appendix B.2.6), Rodrigues' formula (B.1) can be given by

$$e^{\hat{\xi}\theta} = I_3 + \mathrm{sk}(e^{\hat{\xi}\theta}) + \hat{\xi}^2(1 - \cos\theta).$$

Thus, when $|\theta| << 1$ (i.e. $\cos\theta \approx 1$) holds, we obtain $e^{\hat{\xi}\theta} \approx I_3 + \mathrm{sk}(e^{\hat{\xi}\theta})$.

B.3 Formulas of $\phi(e^{\hat{\xi}\theta})$

Consider the potential function $\phi(e^{\hat{\xi}\theta}) \in \mathbb{R}$ defined as

$$\phi(e^{\hat{\xi}\theta}) := \frac{1}{4}\|I_3 - e^{\hat{\xi}\theta}\|_F^2 = \frac{1}{2}\mathrm{tr}(I_3 - e^{\hat{\xi}\theta}).$$

Then, from the definition of the Frobenius norm, $\phi(e^{\hat{\xi}\theta})$ has the properties that $\phi(e^{\hat{\xi}\theta}) \geq 0$ and $\phi(e^{\hat{\xi}\theta}) = 0$ if and only if $e^{\hat{\xi}\theta} = I_3$.

B.3.1 $\phi(e^{\hat{\xi}\theta}) = 1 - \cos\theta$

The direct calculation of $\phi(e^{\hat{\xi}\theta})$ with Rodrigues' formula (B.1) yields

$$
\begin{aligned}
\phi(e^{\hat{\xi}\theta}) &= \frac{1}{2}\mathrm{tr}(I_3 - e^{\hat{\xi}\theta}) \\
&= \frac{1}{2}\mathrm{tr}\left(-\hat{\xi}\sin\theta - \hat{\xi}^2(1 - \cos\theta)\right) \\
&= -\frac{1}{2}\mathrm{tr}(\hat{\xi}^2)(1 - \cos\theta) \quad (\because \mathrm{tr}(\hat{\xi}) = 0) \\
&= \xi^T\xi(1 - \cos\theta) \quad (\because \text{Appendix B.1.3}) \\
&= 1 - \cos\theta. \quad (\because \xi^T\xi = 1)
\end{aligned}
$$

B.3.2 $\dot{\phi}(e^{\hat{\xi}\theta}) = (\mathrm{sk}(e^{\hat{\xi}\theta})^\vee)^T\omega^b$

The time derivative of $\phi(e^{\hat{\xi}\theta})$ yields

$$
\begin{aligned}
\dot{\phi}(e^{\hat{\xi}\theta}) &= -\frac{1}{2}\mathrm{tr}(\dot{e}^{\hat{\xi}\theta}) \\
&= -\frac{1}{2}\mathrm{tr}(\dot{e}^{\hat{\xi}\theta}e^{-\hat{\xi}\theta}e^{\hat{\xi}\theta}) \\
&= -\frac{1}{2}\mathrm{tr}\left(\dot{e}^{\hat{\xi}\theta}e^{-\hat{\xi}\theta}\mathrm{sk}(e^{\hat{\xi}\theta})\right) - \frac{1}{2}\mathrm{tr}\left(\dot{e}^{\hat{\xi}\theta}e^{-\hat{\xi}\theta}\mathrm{sym}(e^{\hat{\xi}\theta})\right) \qquad \text{(B.2)}
\end{aligned}
$$

Here, $\mathrm{sym}(e^{\hat{\xi}\theta}) \in \mathbb{R}^{3\times 3}$ is the symmetric component of $e^{\hat{\xi}\theta}$ defined as $\mathrm{sym}(e^{\hat{\xi}\theta}) := (1/2)(e^{\hat{\xi}\theta} + e^{-\hat{\xi}\theta})$, and we use the property that $A = \mathrm{sym}(A) + \mathrm{sk}(A)$ holds for any $A \in \mathbb{R}^{n\times n}$. Then, since $\dot{e}^{\hat{\xi}\theta}e^{-\hat{\xi}\theta}$ is skew-symmetric (Appendix B.2.5), we obtain

$$
\begin{aligned}
\mathrm{tr}\left(\dot{e}^{\hat{\xi}\theta}e^{-\hat{\xi}\theta}\mathrm{sym}(e^{\hat{\xi}\theta})\right) &= \mathrm{tr}\left(\left(\dot{e}^{\hat{\xi}\theta}e^{-\hat{\xi}\theta}\mathrm{sym}(e^{\hat{\xi}\theta})\right)^{\mathrm{T}}\right) \quad (\because \mathrm{tr}(A) = \mathrm{tr}(A^{\mathrm{T}})) \\
&= \mathrm{tr}\left(\mathrm{sym}(e^{\hat{\xi}\theta})^{\mathrm{T}}\left(\dot{e}^{\hat{\xi}\theta}e^{-\hat{\xi}\theta}\right)^{\mathrm{T}}\right) \\
&= \mathrm{tr}\left(\mathrm{sym}(e^{\hat{\xi}\theta})\left(-\dot{e}^{\hat{\xi}\theta}e^{-\hat{\xi}\theta}\right)\right) \quad (\because \text{Appendix B.2.5}) \\
&= -\mathrm{tr}\left(\dot{e}^{\hat{\xi}\theta}e^{-\hat{\xi}\theta}\mathrm{sym}(e^{\hat{\xi}\theta})\right) \quad (\because \mathrm{tr}(AB) = \mathrm{tr}(BA))
\end{aligned}
$$

We thus get $\mathrm{tr}\left(\dot{e}^{\hat{\xi}\theta}e^{-\hat{\xi}\theta}\mathrm{sym}(e^{\hat{\xi}\theta})\right) = 0$. Finally, substituting this equation into (B.2) yields

$$
\begin{aligned}
\dot{\phi}(e^{\hat{\xi}\theta}) &= -\frac{1}{2}\mathrm{tr}\left(\dot{e}^{\hat{\xi}\theta}e^{-\hat{\xi}\theta}\mathrm{sk}(e^{\hat{\xi}\theta})\right) \\
&= -\frac{1}{2}\mathrm{tr}\left(\left((\dot{e}^{\hat{\xi}\theta}e^{-\hat{\xi}\theta})^{\vee}\right)^{\wedge}\left(\mathrm{sk}(e^{\hat{\xi}\theta})^{\vee}\right)^{\wedge}\right) \\
&= \left((\dot{e}^{\hat{\xi}\theta}e^{-\hat{\xi}\theta})^{\vee}\right)^{\mathrm{T}}\mathrm{sk}(e^{\hat{\xi}\theta})^{\vee} \quad (\because \text{Appendix B.1.3}) \\
&= \left(\mathrm{sk}(e^{\hat{\xi}\theta})^{\vee}\right)^{\mathrm{T}}(\dot{e}^{\hat{\xi}\theta}e^{-\hat{\xi}\theta})^{\vee} \\
&= \left(\mathrm{sk}(e^{\hat{\xi}\theta})^{\vee}\right)^{\mathrm{T}}e^{\hat{\xi}\theta}e^{-\hat{\xi}\theta}(\dot{e}^{\hat{\xi}\theta}e^{-\hat{\xi}\theta})^{\vee} \\
&= \left(\mathrm{sk}(e^{\hat{\xi}\theta})^{\vee}\right)^{\mathrm{T}}e^{\hat{\xi}\theta}e^{-\hat{\xi}\theta}(e^{\hat{\xi}\theta}\hat{\omega}^{b}e^{-\hat{\xi}\theta})^{\vee} \quad (\because \hat{\omega}^{b} = e^{-\hat{\xi}\theta}\dot{e}^{\hat{\xi}\theta}) \\
&= \left(\mathrm{sk}(e^{\hat{\xi}\theta})^{\vee}\right)^{\mathrm{T}}e^{\hat{\xi}\theta}e^{-\hat{\xi}\theta}e^{\hat{\xi}\theta}\omega^{b} \quad (\because \text{Appendix B.2.3}) \\
&= \left(\mathrm{sk}(e^{\hat{\xi}\theta})^{\vee}\right)^{\mathrm{T}}e^{\hat{\xi}\theta}\omega^{b} \\
&= \left(\mathrm{sk}(e^{\hat{\xi}\theta})^{\vee}\right)^{\mathrm{T}}\omega^{b}. \quad (\because \text{Appendix B.2.7})
\end{aligned}
$$

B.3.3 $\quad \phi(e^{\hat{\xi}\theta}) \leq \|\mathrm{sk}(e^{\hat{\xi}\theta})^{\vee}\|_{2}^{2}$ for $\theta \in (-\pi/2, \pi/2)$

Since $\mathrm{sk}(e^{\hat{\xi}\theta})^{\vee} = \xi\sin\theta$, $\|\xi\|_{2} = 1$ and $\phi(e^{\hat{\xi}\theta}) = 1 - \cos\theta$ hold, we get for $\theta \in (-\pi/2, \pi/2)$

$$
\|\mathrm{sk}(e^{\hat{\xi}\theta})^{\vee}\|_{2}^{2} = \|\xi\sin\theta\|_{2}^{2} = \sin^{2}\theta = 1 - \cos^{2}\theta \geq 1 - \cos\theta = \phi(e^{\hat{\xi}\theta}). \quad (\because \cos\theta > 0)
$$